Report 14354-Q-3

HYDROGEN-OXYGEN HIGH P_c APS ENGINES

NAS 3-14354

Period Ending 31 March 1971

L. Schoenman and A. A. Oare

14 April 1971

Engine Components Department
Aerojet Liquid Rocket Company
Sacramento, California

Prepared for
NASA-Lewis Research Center
Cleveland, Ohio 44135

AEROJET LIQUID ROCKET COMPANY

SACRAMENTO, CALIFORNIA • A DIVISION OF AEROJET-GENERAL

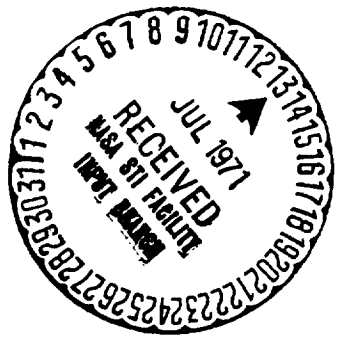

FOREWORD

This is the third quarterly report for Contract NAS 3-14354. The purpose of this contract is the development of a comprehensive technology base for high performance, long life, gaseous hydrogen - gaseous oxygen rocket engines suitable for the Space Shuttle APS. Significant goals in thruster design are a 50-hour firing life over a 10-year period, with up to 10^6 restarts, and single firings up to 1000 sec.

The program was initially structured as two parallel efforts: one directed toward high pressure (100 to 500 psia) systems and the other toward low pressure (10 to 20 psia) systems. Nominal engine thrust in each case is 1500 lb. Initial program tasks were devoted to the analytical evaluation and screening of injector and cooled thrust chamber concepts for both pressure levels. This was followed by closely paralleled but separate experimental evaluations of low and high pressure injectors and ignition devices. Recommendations of specific injector and igniter designs have been made for both pressure levels as a result of these tests.

As these parallel efforts were about to enter the cooled chamber fabrication phase, the program was redirected to apply additional emphasis on the high P_c technology with a revised schedule on propellant inlet temperatures. Activities on the low pressure phase were terminated by a stop work order, which eliminated the requirements for a portion of the injector testing and all of the low P_c cooled chamber fabrication, durability and pulse testing. The program's resources originally planned for these activities are being reallocated, via a new cost proposal, to expand design and test efforts related to the lower temperature gaseous propellants.

The program management consists of separate project managers for the low and high pressure efforts reporting to a single program manager. Mr. L. Schoenman is project manager for the high pressure phase, while Mr. A. A. Oare is project manager for the low pressure phase. They report to Dr. R. J. LaBotz, who is program manager of all ALRC APS thruster programs. The NASA Lewis Research Center program manager is Mr. J. Gregory.

TABLE OF CONTENTS

TABLE LIST

FIGURE LIST

FIGURE LIST (cont.)

I. PROGRAM OBJECTIVES

The primary objective of this contract is to generate a comprehensive technology base for high performance gaseous hydrogen-gaseous oxygen rocket engines suitable for the Space Shuttle Auxiliary Propulsion System (APS). Durability requirements include injector and thrust chamber designs capable of 50 hours of firing life over a 10-year period with up to 10^6 pulses and single firings up to 1000 sec. These technical objectives are being accomplished and reported upon in a twenty-one task program summarized below. The first ten tasks relate to high pressure APS engines, parallel tasks eleven through twenty relate to low pressure APS engines, and task twenty-one is a common reporting task.

Task Titles	High P_c Task	Low P_c Task
Injector analysis and design	I	XI
Injector fabrication	II	XII *
Thrust chamber analysis and design	III	XIII *
Thrust chamber fabrication	IV	XIV *
Ignition system analysis and design	V	XV
Ignition system fabrication and checkout	VI	XVI
Propellant valves preparation	VII	XVII
Injector tests	VIII	XVIII *
Thrust chamber cooling tests	IX	XIX *
Pulsing tests	X	XX *

Common Task

Reporting requirements XXI

* During this report period, the program objectives were redirected toward providing an expanded high pressure program which would analytically and experimentally investigate the impact of lower temperature propellants (fuel = 150 to 600°R, oxidizer = 300 to 600°R). Work on Tasks XIV, XIX, and XX was halted by a

I, Program Objectives (cont.)

stop work order dated 11 February 1971, while the scope of work on Tasks XII, XIII, XVII, and XVIII was reduced to that compatible with closing out Low P_c activities in an orderly and documented manner.

The new High P_c tasks being proposed specifically to investigate the low temperature propellants include:

Task	
XXII	Injector analysis and design
XXIII	Injector fabrication
XXIV	Thrust chamber analysis and design
XXV	Thrust chamber fabrication
XXVI	Injector tests
XXVII	Thrust chamber cooling tests
XXVIII	Pulsing tests

Section III of this report provides a review of the progress in the third quarter on the high pressure engine technology portion of this contract. Low pressure engine technical progress and closeout is covered in Section IV.

II. SUMMARY OF ACCOMPLISHMENTS

A. HIGH PRESSURE TECHNOLOGY

The major accomplishments during the report quarter were in the areas of injector and ignition tests and in cooled thrust chamber fabrication. A total of 90 hot fire injector checkout tests were conducted on this program. Of these, 81 were heat transfer and performance tests, four were streak chamber compatibility tests, four were combustion stability tests with low temperature propellants, and one was a pulse test series. The maximum test duration was 10 sec. The test matrix for the two injector concepts being evaluated (72-element impinging coaxial and 42-element coaxial tube) included chamber pressures from 100 to 500 psia, mixture ratios from 3 to 6, film cooling flow rates from 0 to 30%, and various combinations of propellant temperatures.

All of the injector designs tested provided data which suggested that the 10^6 restart requirements could probably be attained with little or no modification to the basic concepts. This includes impinging coaxial designs with nickel face plates and the coaxial tube design with either copper or aluminum face plates. The impinging coaxial element design is being recommended over the coaxial tube design because test data indicate it develops a higher (in excess of program objectives) combustion efficiency at any given chamber length while at the same time providing a more compatible, lower heat flux environment at the chamber wall. The ability of the recommended design to operate stably and without loss in performance at the lower range of propellant temperatures was also demonstrated.

Checkout and limit evaluation tests with the spark and catalytic ignition systems showed the spark energy source to be a more reliable approach. The three-stage ignition concept, which features a spark discharging into a highly oxidizer-rich mixture in the first stage, was demonstrated to be reliable and rapid over a wide range of pressures, mixture ratios, and propellant temperatures to saturated vapor on oxygen and 175°R on the fuel with power levels as low as 1 millijoule.

II, A, High Pressure Technology (cont.)

Durability and reliability testing of the recommended injector and igniter was accomplished in a 2500-pulse test series with a sea level film cooled chamber. The duty cycle involving 0.050 sec on, 0.150 sec off was conducted in several groupings. The longest grouping contained 1110 consecutive restarts. The system, including valves, ignition equipment, injectors and chamber, responded flawlessly and reproducible to each of the 2500 computerized fire signals.

Fabrication of four cooled thrust chambers has proceeded reasonably well in that only the usual minor and no major fabrication difficulties have been encountered. Delivery of the first film-cooled chamber remains compatible with the targeted date for the initiation of altitude testing. Subsequent chambers are scheduled for delivery at two-week intervals.

II, Summary of Accomplishments (cont.)

B. LOW PRESSURE TECHNOLOGY

During this reporting period, a reduced scope injector test series and the catalytic igniter test series were completed. Data reduction and analysis have been initiated in preparation for final program documentation.

Twenty-four engine tests were conducted in the J-Zone altitude test facility for performance and heat transfer data. These tests were conducted using a 200-element coaxial element injector, a workhorse chamber, and a film coolant ring designed to introduce hydrogen coolant at various velocities and axial positions. All tests were conducted at simulated altitude conditions.

The parameters evaluated are shown below:

P_c	10 to 20 psia
Mixture ratio	2 to 4
L*	16 and 26 in.
Film coolant	0 to 30% (of the hydrogen)
Coolant sleeve length	0.5 to 2.78

Preliminary data analysis indicates that specific impulse performance for all tests exceeded the 375-sec contract goal, including tests with 30% film coolant. Thermal data indicate that the film-cooled chamber design can operate successfully with 11% hydrogen coolant at a 1500°F maximum wall temperature. Demonstrated performance at this condition is 399 sec.

Over 200 tests were conducted with a catalytic igniter at simulated altitude conditions. The design employs a small catalyst bed for primary reaction with additional (secondary) oxygen added to the bed effluent to increase the heat output of the assembly.

II, B, Low Pressure Technology (cont.)

The shortest times to the reaction of the secondary oxygen with the effluent ranged from 0.03 sec for a hot bed restart with ambient propellants to 0.075 sec with ambient temperature bed and propellants. Successful ignitions were achieved with both the propellant and bed temperatures at a nominal 290°R. Operation was found to be somewhat unpredictable at all temperatures in that tests at identical conditions resulted in different response characteristics.

Relatively fast response of a catalytic ignition system for oxygen-hydrogen was demonstrated. Additional effort is required to improve operating reproducibility.

Future program activities will be limited to data analysis and documentation for inclusion in the program final report.

III. HIGH PRESSURE ENGINE TECHNOLOGY

A. PROGRAM PROGRESS (BY TASK)

1. Task I - Injector Analysis and Design

No activity on this task.

2. Task II - Injector Fabrication

Because of the good injector durability demonstrated in Task VIII, it was found unnecessary to complete fabrication of all of the injectors planned for this program.

During the past three-month report period, the SN 2 impinging coaxial element injector body was converted to the "I" configuration by machining off the triplet pattern face plate and bonding on the "I" plate pattern. The manifolding on this body was also modified (as shown in Figure III-43 of Quarterly Report No. 2) to improve oxidizer flow distribution. The face plate of SN 3 impinging coaxial design was modified to unbalance the fuel momentum which provides an 8-degree inboard from the axial deflection of the oxidizer flow. The 8-degree deflection avoids possible impingement of the oxidizer stream on the wall, thus ensuring better compatibility.

Modification of the removable face plate of the coaxial tube injector was completed to provide 5% additional fuel to the outer quadrant of the outer row of elements to improve compatibility. A lightweight aluminum face plate, providing an 0.080-in. tip recess, was also completed.

Machining, pattern drilling of the body, and fabrication of a set of nickel elements (tubes) for the SN 2 coaxial design was completed during this report period. This hardware will be held in a disassembled state since the impinging element design has been selected as the final injector configuration for cooled chamber testing.

III, A, Program Progress (By Task) (cont.)

The injectors employed in Task VIII testing are being modified for use with cooled chambers in Task IX testing. This modification allows the injector fuel manifold to feed directly from the chambers.

The residual funding from this task has been employed in Task VIII to conduct 15 more injector checkout tests than were originally planned and funded in the program.

3. Task III - Chamber Analysis and Design

The major effort on this task has been directed toward evaluating the thermal data which were derived from Task VIII testing in order to obtain a better understanding of the heat transfer characteristics of the APS thrusters. Three factors of major interest were: (1) the influence of P_c and mixture ratio on heat flux, (2) the influence of film cooling on heat flux and heat transfer coefficients, and (3) evaluation of the film cooling effectiveness in relationship to the original design predictions and the method of analyzing the injection geometry.

The sources of thermal data, as discussed in Quarterly Reports No. 1 and 2, consist of (1) a thick-wall copper heat sink chamber providing gas-side wall temperature measurements, (2) adiabatic wall probes positioned at the gas-side surface but insulated from the cooled wall in film cooling tests, and (3) transient and steady-state backside wall temperature measurements from a 0.040-in.-wall stainless steel chamber. Table III-1 summarizes the tests and test conditions evaluated in this phase of the program.

a. Analysis of Thermal Data, No Film Cooling

Earlier program reports presented heat flux vs axial distance profiles for various L* chambers and injectors. For consistency, heat fluxes were quoted at the point in time at which the internal wall temperature

TABLE III-1

SUMMARY OF TEST CONDITIONS IN THERMAL ANALYSES

Run	L*, in.	Chamber/Injector	P_c, psia	TCA MR	% FC	Ring Length, in.	V/R* Coolant to Core Velocity Ratio
2K8-131	15	FFC/SN 3	320	2.73	30	2.5	1.1
2K8-157	15	FFC/SN 5	321	3.47	30	2.5	0.99
2K8-163	20	FFC/SN 5	331	3.45	30	2.5	1.05
2K8-166	20	FFC/SN 5	473	3.52	30	2.5	1.0
2K8-173	20	Cu/SN 5	301	3.34	30	2.5	1.56
2K6-113	15	Cu/SN 1	293	4.86	0	--	--
2K9-103	15	Cu/SN 3	309	5.01	0	--	--
2K9-106	15	Cu/SN 3	299	5.02	0	--	--
2K8-112	25	Cu/Swirler Coax	99	4.92	0	--	--
2K8-115	25	Cu/Swirler Coax	469	4.63	0	--	--
2K6-111	15	Cu/SN 1	294	3.90	0	--	--
2K6-112	15	Cu/SN 1	297	2.90	0	--	--

*Based on injection velocity

III, A, Program Progress (By Task) (cont.)

reached 500°F. Figure III-1 shows the complete flux vs wall temperature curves derived from the copper chamber surface temperatures for 300 psia operation at nominal mixture ratios of 3, 4 and 5. Both heat transfer coefficients and recovery temperatures can be obtained from the slopes and intercept of these curves. Variation of the throat flux and heat transfer coefficient with mixture ratio is seen to be small (less than 15%).

The experimental variation of heat flux as the wall heated during a test lasting 2 sec has now been employed to calculate local heat transfer coefficients as they varied both with wall temperature, peripheral and axial positions in the chamber. For the condition where there is no film cooling, the recovery temperature (T_r) is assumed to be equal to $T_o * \eta^2$, where T_o is the theoretical combustion temperature and η is the energy release efficiency. This approach is in good agreement with the recovery temperatures determined by the slope and intercept method. The coefficients calculated in this manner are shown in Figure III-2. Data for two peripheral and four axial stations are shown as the wall heats from ambient to about 1000°F. Also shown in this figure are the predicted heat transfer coefficients for these test conditions and the equation from which they were calculated. The following points are to be noted about the information presented in Figure III-2:

(1) The heat flux and resulting heat transfer coefficients are consistent and reproducible at peripheral stations D, G and K which are 90° apart.

(2) The simplified Bartz equation (a pipe flow equation) having a C_g of 0.026, when used with properties evaluated at a film temperature which is the average of the recovery and wall temperature, adequately predicts both the magnitude of the local heat transfer coefficients and variation with wall temperature at the low Mach number stations.

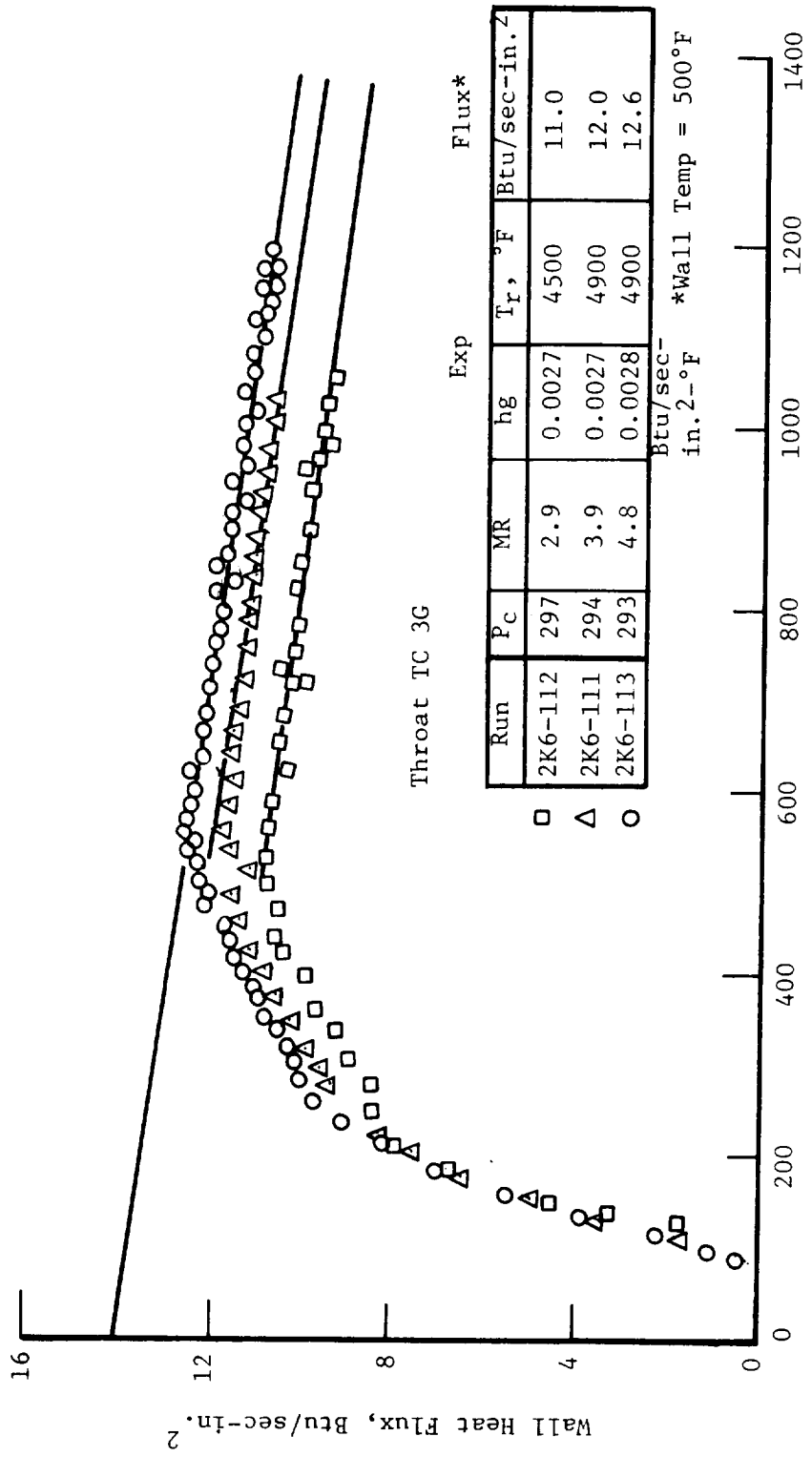

Throat Heat Flux vs Wall Temperature

Figure III-1

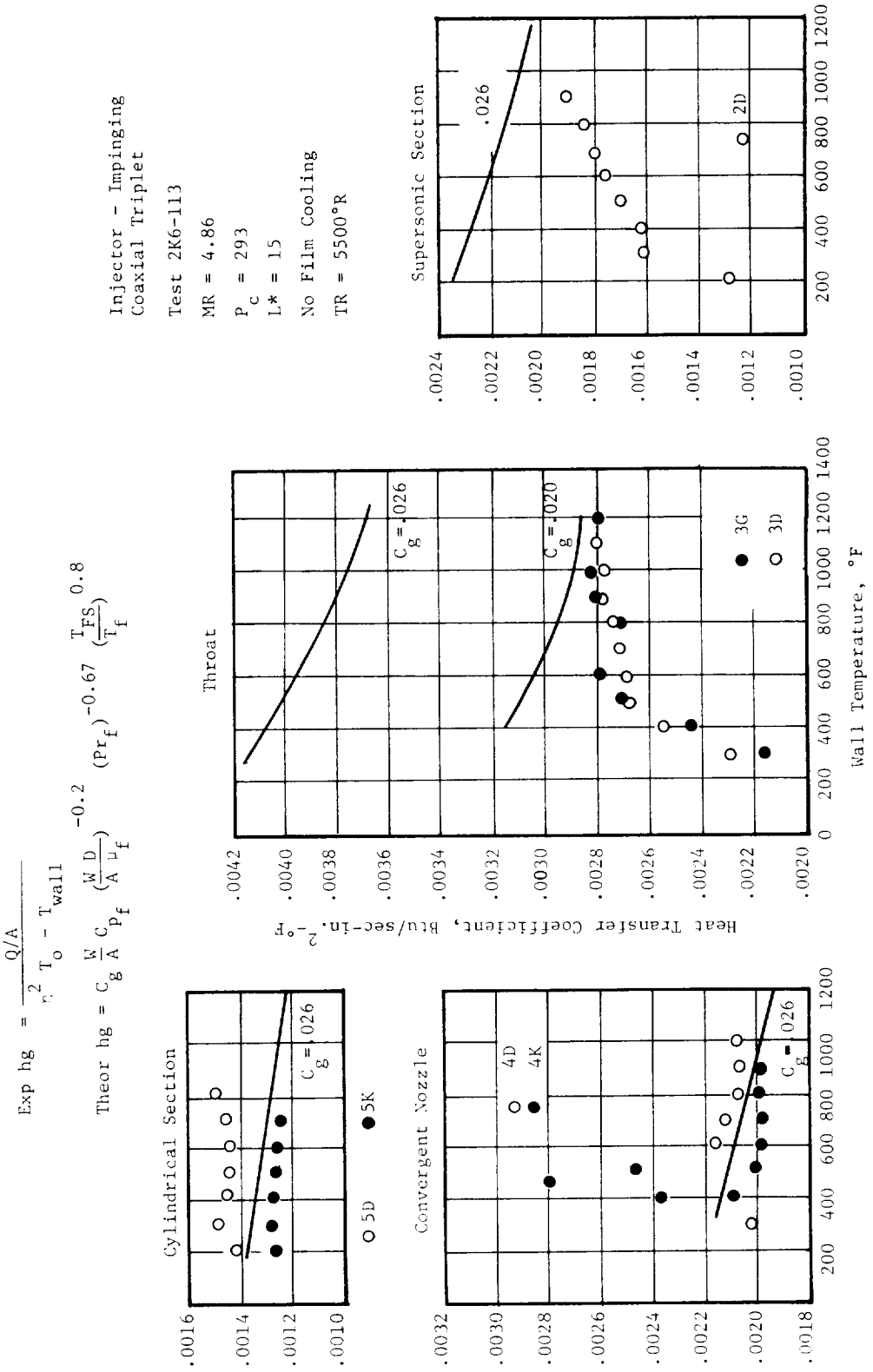

No Film Cooling Heat Transfer Coefficients

Figure III-2

III, A, Program Progress (By Task) (cont.)

(3) As the flow approaches the throat and pressure gradients become significant, the familiar phenomenon (Ref 1,2) of having lower than predicted coefficients is once again observed. This is accounted for analytically by altering the correlating constant "C_g" as noted. This aspect is discussed in the following sections.

(4) The shape of the experimental coefficient vs temperature curves does not match the predicted curves at the throat and supersonic stations. This could be due either to axial conduction effects not taken into account in the data reduction or to alteration of the nature of the boundary layer as the wall cooling effects on the boundary layer diminish or a combination of both effects. The latter is highly suspect as the test conditions are in a region that has been characterized (Ref 3,4,5) as transitional between fully turbulent and relaminarized, in which wall cooling is an important parameter. Additional analysis of the sonic and supersonic flow conditions is warranted.

Figure III-3 shows the same type of analysis for the throat station at three chamber pressures. Note two different injectors have been employed. The point of interest is that the same C_g can be employed to predict the 300 and 500 psia data, while the C_g which matches the 100 psia run is a factor of 2 lower. Earlier observations of similar effects in small nozzles (Ref 1,3,5) have led to the conclusion that the lower than expected throat heat transfer coefficients result from flow acceleration, which at low Reynolds numbers can result in relaminarization of a turbulent boundary layer.

Referring to Figure III-4, one observes that, at throat Reynolds numbers greater than 10^6, throat Stanton*Prandtl number products are satisfactorily estimated by turbulent boundary layer equations with a Reynolds number coefficient of 0.016. At Reynolds numbers less than 2.0, 10^5 throat boundary layers appear laminar while the intermediate Reynolds number range

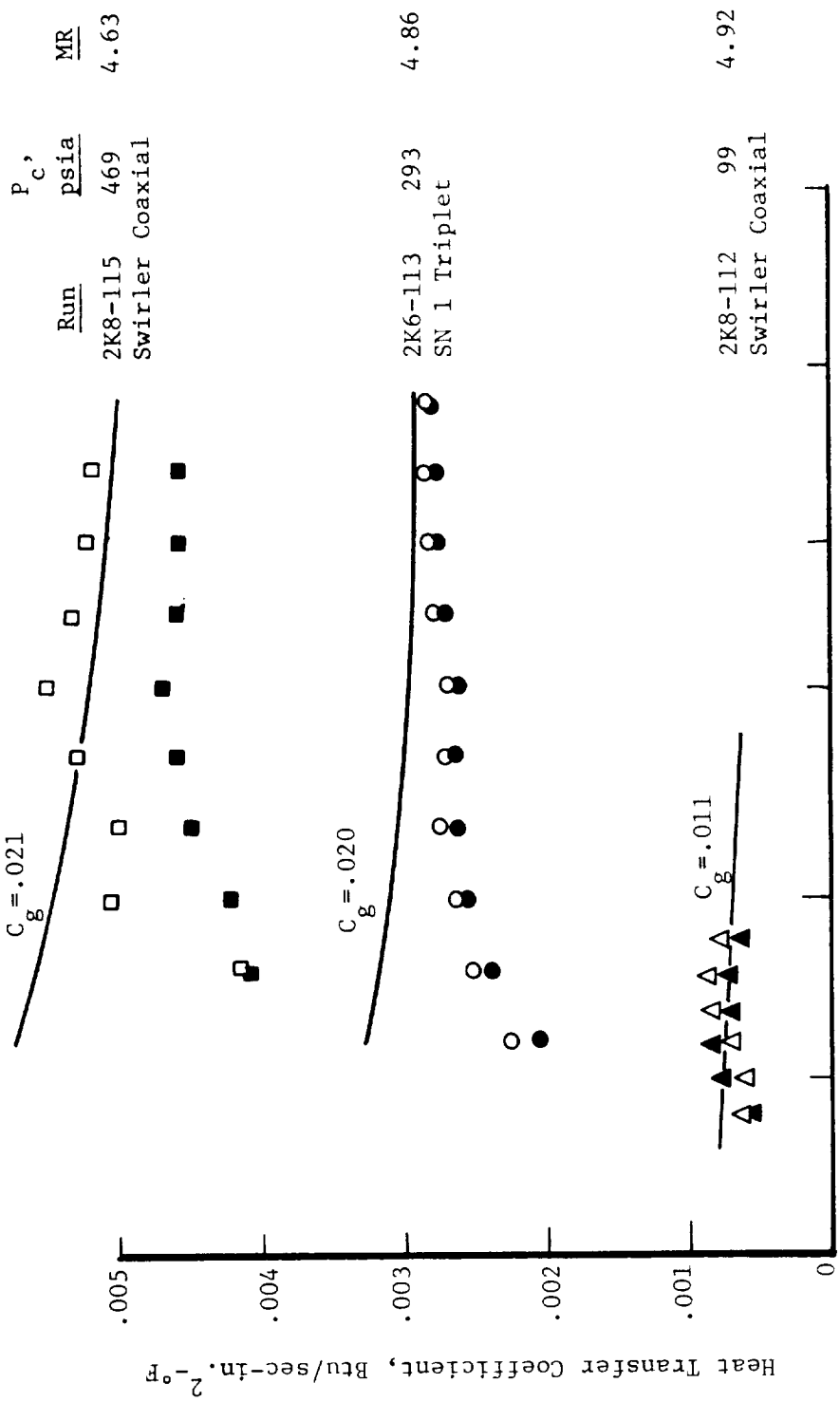

Throat Heat Transfer Coefficients with Chamber Pressure as a Parameter

Figure III-3

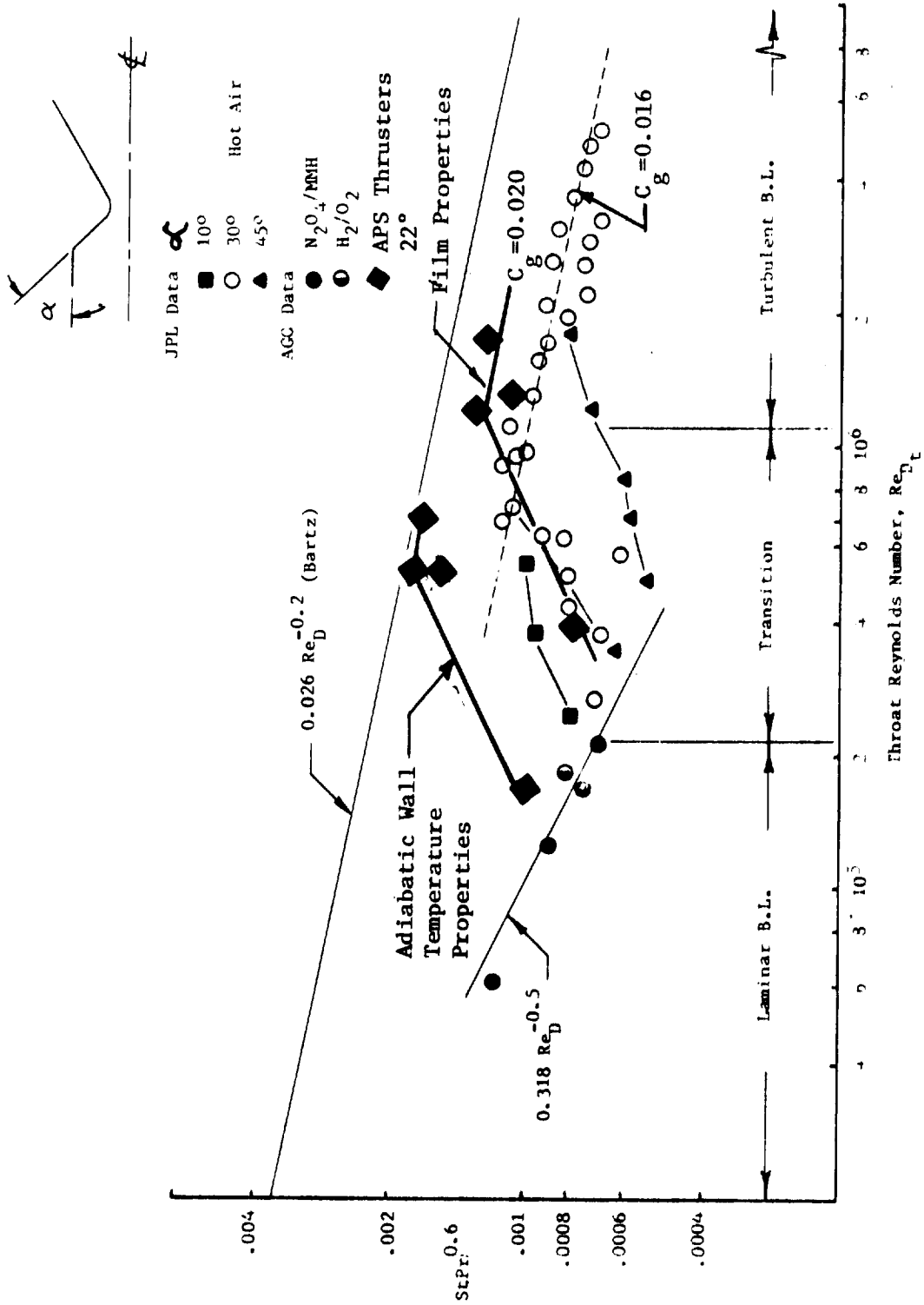

Nozzle Throat Heat Transfer Characteristics

Figure III-4

III, A, Program Progress (By Task) (cont.)

may be either laminar, turbulent, or transitional. The heat transfer coefficients which materialize in the transitional range are dependent on nozzle contraction ratios, angles, throat curvature, and wall-to-stream temperature ratios. Data from the reference sources was correlated with adiabatic wall temperature properties. This contrasts to the film temperature properties, which appear more appropriate for the APS data obtained. APS thruster heat transfer coefficients converted to dimensionless Stanton numbers for 100, 300 and 500 psia have therefore been superimposed on existing data (large diamonds) using both adiabatic wall and film reference temperatures. This thermal behavior of the nozzle throat should be considered in the system, thrust and chamber pressure optimization and in the selection of nozzle contours for future designs.

b. Analysis of Film-Cooled Chamber Data

The analysis in the previous section defined the thermal characteristics of the APS thrusters without film cooling. The addition of fuel film cooling to extend the chamber life alters the thermal characteristics by reducing the recovery temperature and making the boundary layer considerably more fuel rich, which in turn alters the heat transfer coefficients. Figure III-5 presents throat heat flux and recovery temperature data derived from the following sources: (1) thick-wall copper chamber containing both brazed-in surface temperature measuring thermocouples and adiabatic wall probes (insulated from the copper wall) and (2) a thin-wall stainless steel chamber of the same contour with spot welded backside thermocouples. Both chambers were tested at approximately the same conditions.

Recovery temperature can be obtained in three ways: from steady-state operation of the thin-wall chamber, direct readings of the adiabatic wall probes, and extrapolation of the flux vs gas-side surface temperature measurements from the thick-wall copper chamber. The most reliable is considered

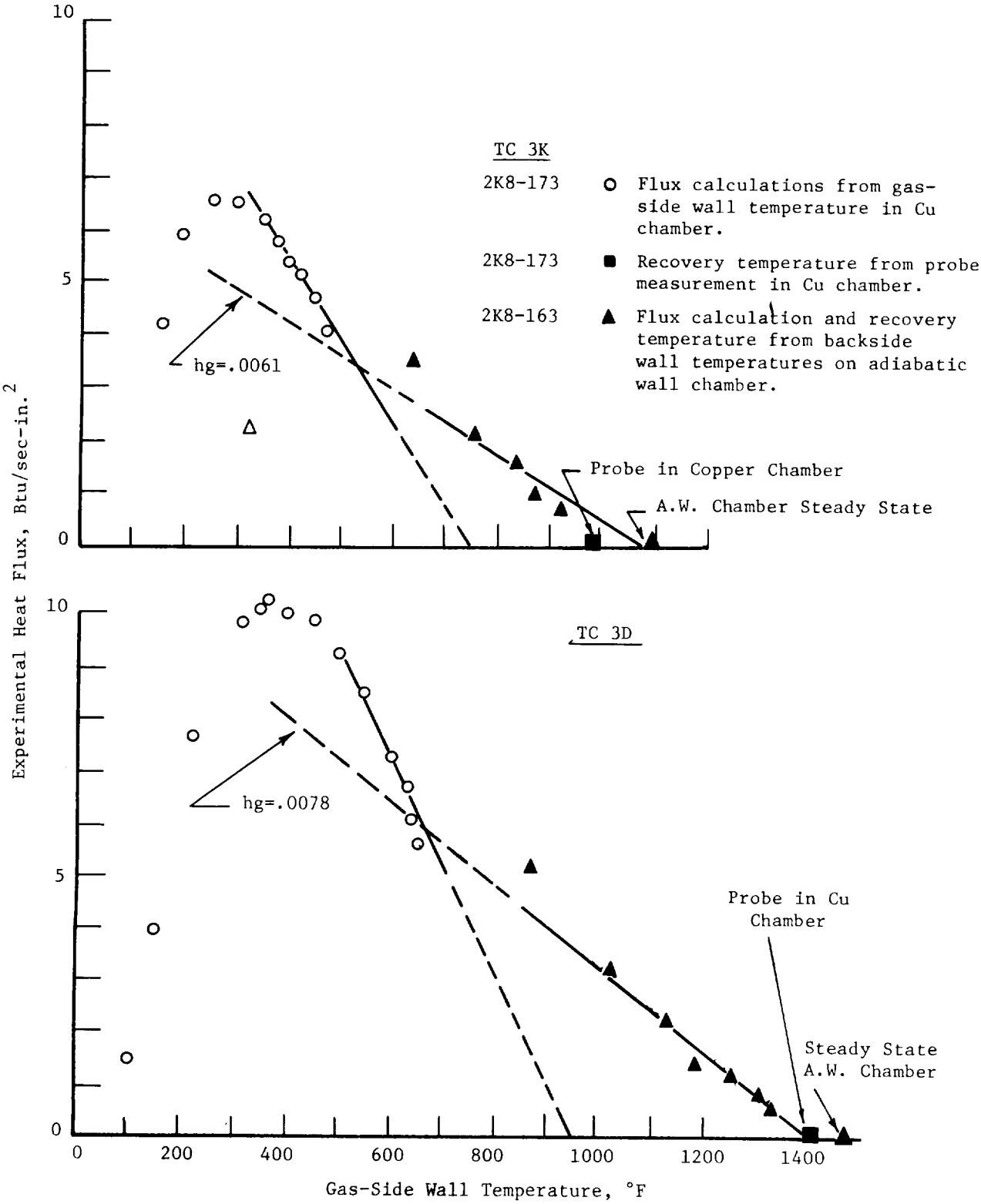

Throat Heat Flux Data for Film-Cooled Chambers

Figure III-5

III, A, Program Progress (By Task) (cont.)

to be the steady-state operating temperature of the thin-wall chamber. The recovery temperatures as determined from the probe data, by extrapolating to zero flux the heat flux vs wall temperature data from the copper chamber, and the steady-state adiabatic wall measurements are compared in the following table:

	2K8-163				2K8-173				
	SS-AW				Probe		Copper Wall		
Peripheral Station:	A	D	G	K	D	K	A	D	K
Axial Distance, in.									
-1.5	956	1149	--	--	950	900	650	670	540
Throat 0	1313	1462	1087	1056	1400	1000	850	950	750
1.1	1379	1669	1225	--	1200	800			900
2.2	1466	1902	1243	1115					

Comparison of the data presented in the above table shows that:

(1) The steady-state wall temperatures recorded from the backside of the thin-wall steel chamber at subsonic and sonic conditions are in reasonable agreement with the adiabatic wall probe measurements obtained from the copper chamber at the same test conditions. The fact that the probes have consistently underpredicted the recovery temperature in the supersonic flow was first noted in the second quarterly report.

(2) Extrapolation of the heat flux vs wall temperature curve from the copper chamber results in a much lower recovery temperature.

Figure III-5 displays these data and recovery temperatures derived from the various experimental techniques for two typical throat thermocouple stations. The open circles, representing the heat flux from copper chamber, indicate a high flux at low temperatures, which decreases rapidly as the wall heats. The flux data derived from the steel adiabatic wall chamber, depicted

III, A, Program Progress (By Task) (cont.)

by triangles, suggests a lower flux at the lower wall temperatures, which then diminishes less rapidly as the wall heats. The heat flux data profiles and tabulations provided in earlier reports were obtained from the copper chamber at a wall temperature of 500°F, which in most cases is a more conservative value than the backside steel data. The lower recovery temperature and steeper slope of the copper chamber data suggest a much higher heat transfer coefficient.

The shapes of these data curves, or rather the changes in shapes, are of considerable interest in that they represent a flux vs wall temperature history from P_c rise to steady-state thermal conditions. The initial rise of flux with wall temperature represents the first 0.1 sec after P_c rise, which is accomplished in 0.01 sec. A major portion of the hump corresponds to the next few tenths of seconds and the remainder of the data to about 10 sec of firing. Figure III-6 compares the similarities of the shape of high and low P_c data with and without the use of film cooling. The hump in the flux curve at low wall temperatures consistently develops whenever film cooling is employed. The magnitude of the hump increases either as additional film cooling or higher injection velocities are employed. Additional analyses are being conducted to determine if these indicated high heat fluxes at the low wall temperatures are real transient thermal affects, a phenomenon which is being generated by the instrumentation technique, a data reduction method, or a result of the engine start sequence being employed. These high early time fluxes, if real, are detrimental to chamber life.

The heat flux vs wall temperature data shown for the two throat thermocouple stations in Figure III-5 were employed to calculate the heat transfer coefficients. These are plotted vs gas-side wall temperature in Figure III-7 along with theoretical predictions using film mixture ratio and temperature properties. These coefficients have been calculated using the indicated heat flux and steady-state adiabatic wall temperature from the thin-wall steel chamber. The deviation between the copper wall data and theoretical, with a C_g of 0.026, is about 25% at a wall temperature of 500°F. The difference is

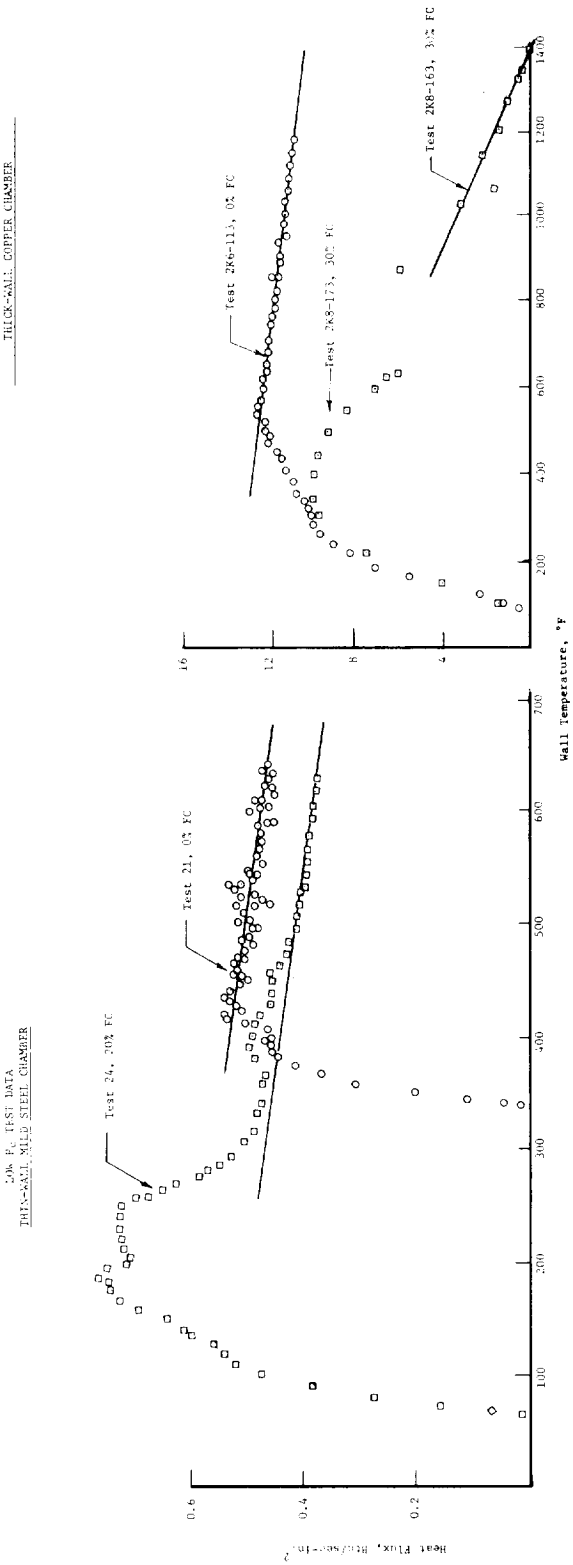

Comparison of Throat Flux vs Wall Temperature Profiles With and Without Film Cooling

Figure III-6

CONVERGENT NOZZLE

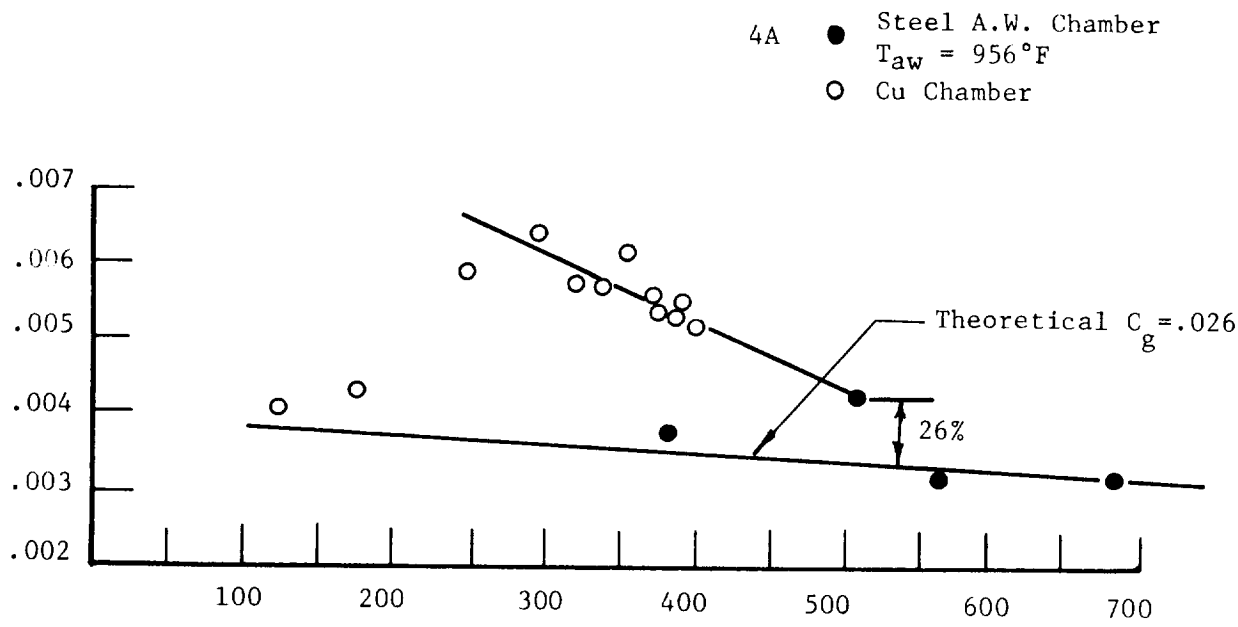

THROAT STATION

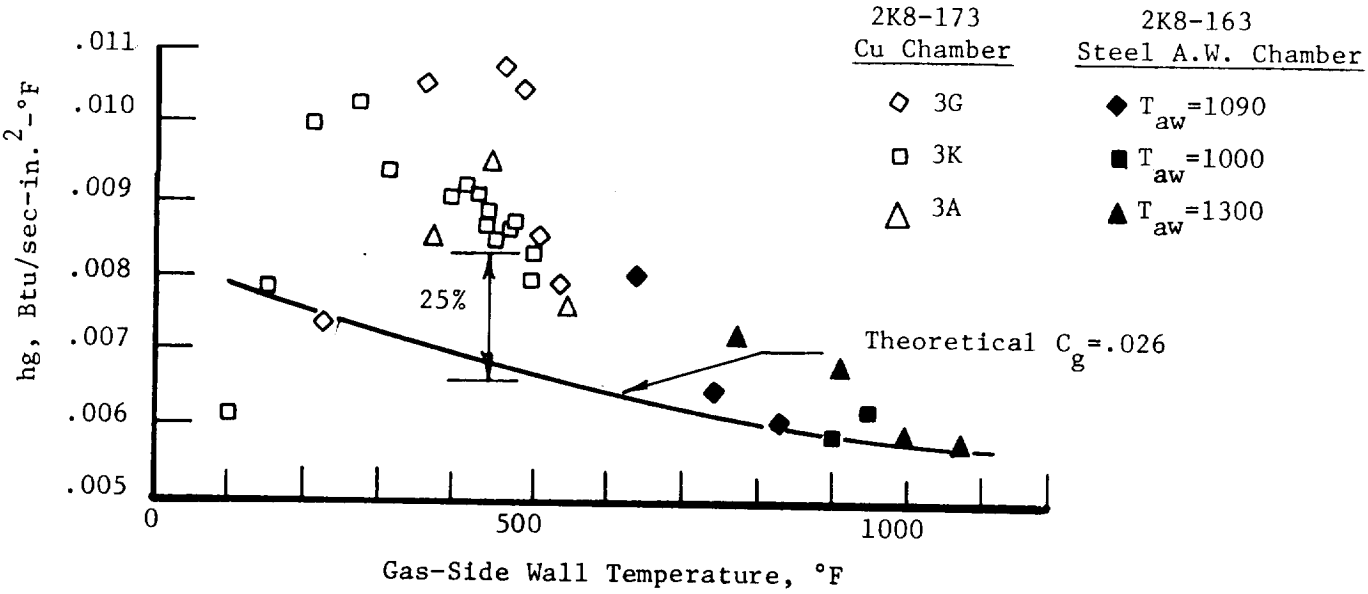

Heat Transfer Coefficients with Film Cooling vs Wall Temperature

Figure III-7

III, A, Program Progress (By Task) (cont.)

greater at lower wall temperatures. The apparent continuity of the coefficient between copper wall data and steel wall data suggests a real thermodynamic phenomenon may be involved and that further investigation is justified.

Figure III-8 provides a comparison of axial heat transfer coefficient profiles for a film- and several nonfilm-cooled tests. The nonfilm-cooled test coefficients are for a 500°F wall temperature, while the film-cooled coefficients are for the higher 1000°F wall temperatures, where the predictions and data agree. Throat heat transfer coefficients with film cooling in this comparison are about twice the nonfilm cooling experimental values - 0.006 vs 0.003 Btu/sec-in.^{2}-°F. If the comparison were made at a 500°F wall temperature, the coefficient with film cooling would be 0.007 to 0.008 Btu/sec-in.^{2}-°F.

c. Film Cooling Effectiveness

The model employed in the film cooling analysis is essentially a boundary layer mixing model which relates, via an entrainment factor, the mass transfer normal to the flow direction to the local core mass velocity in the flow direction. The local film coolant mixture ratio and enthalpy is calculated, as the flow proceeds along the wall and through the nozzle, by integration of the entrainment mass flux area product. The entrainment factor derived from plane unaccelerated flow using laboratory data accounts for initial shear mixing via an empirical function of the coolant injection velocity, density, and slot height. The entrainment factor also provides for (1) alteration due to flow acceleration, (2) additional empirical multiplying factors which allow the inclusion of combustion effects associated with specific injectors, and (3) turning effects due to specific nozzle contours.

The basic analytical approach and a schematic drawing defining the experimental film cooling parameters are summarized in Figure III-9. A more complete discussion of this model will be published in the final report to Contract NAS 3-14343.

	Run	P_c, psia	MR	% FFC	T_r, °R
▲	8-163	331	4.89/3.45	30	
■	9-103	309	5.01	0	5800
□	9-106	299	5.02	0	5800
●	6-113	293	4.86	0	5500

Predicted Coefficients

$$hg = \frac{0.026 \left(\frac{W}{A}\right) C_{P_f}}{\left(\frac{\frac{W}{A} D_e}{\mu_f}\right)^{0.2} Pr_f^{0.67}} \left(\frac{T_{fs}}{T_f} \frac{MW_f}{MW_{fs}}\right)^{0.8}$$

$$T_f = \frac{T_{aw} + T_w}{2}$$

Film properties @ local wall MR

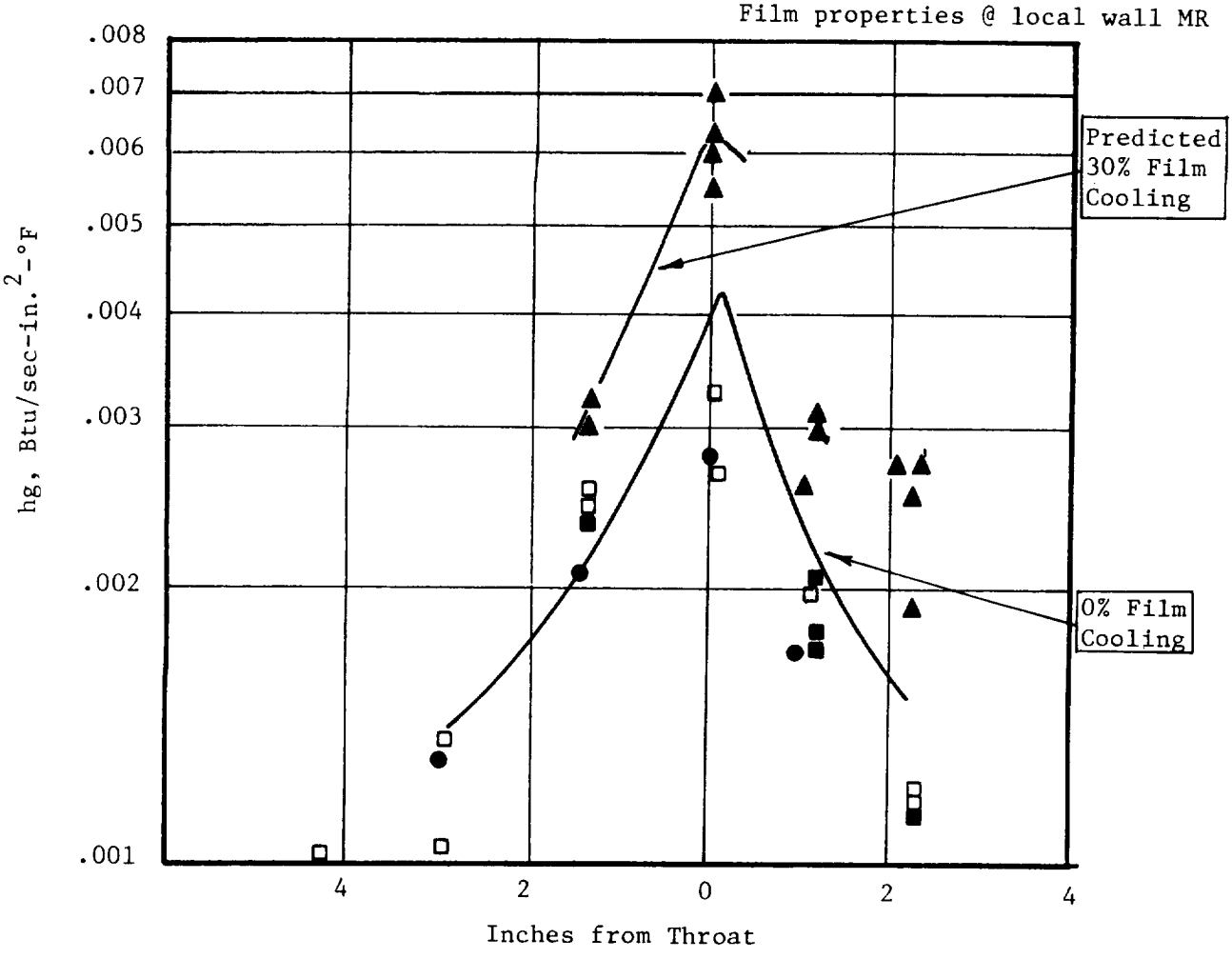

Influence of Film Cooling on Gas-Side Heat Transfer Coefficient

Figure III-8

enthalpy effectiveness

$$\eta = \frac{H_e - H_{aw}}{H_e - H_{in}} = \frac{1}{MR_e}\left(\frac{1 + MR_e}{1 + MR_w} - 1\right)$$

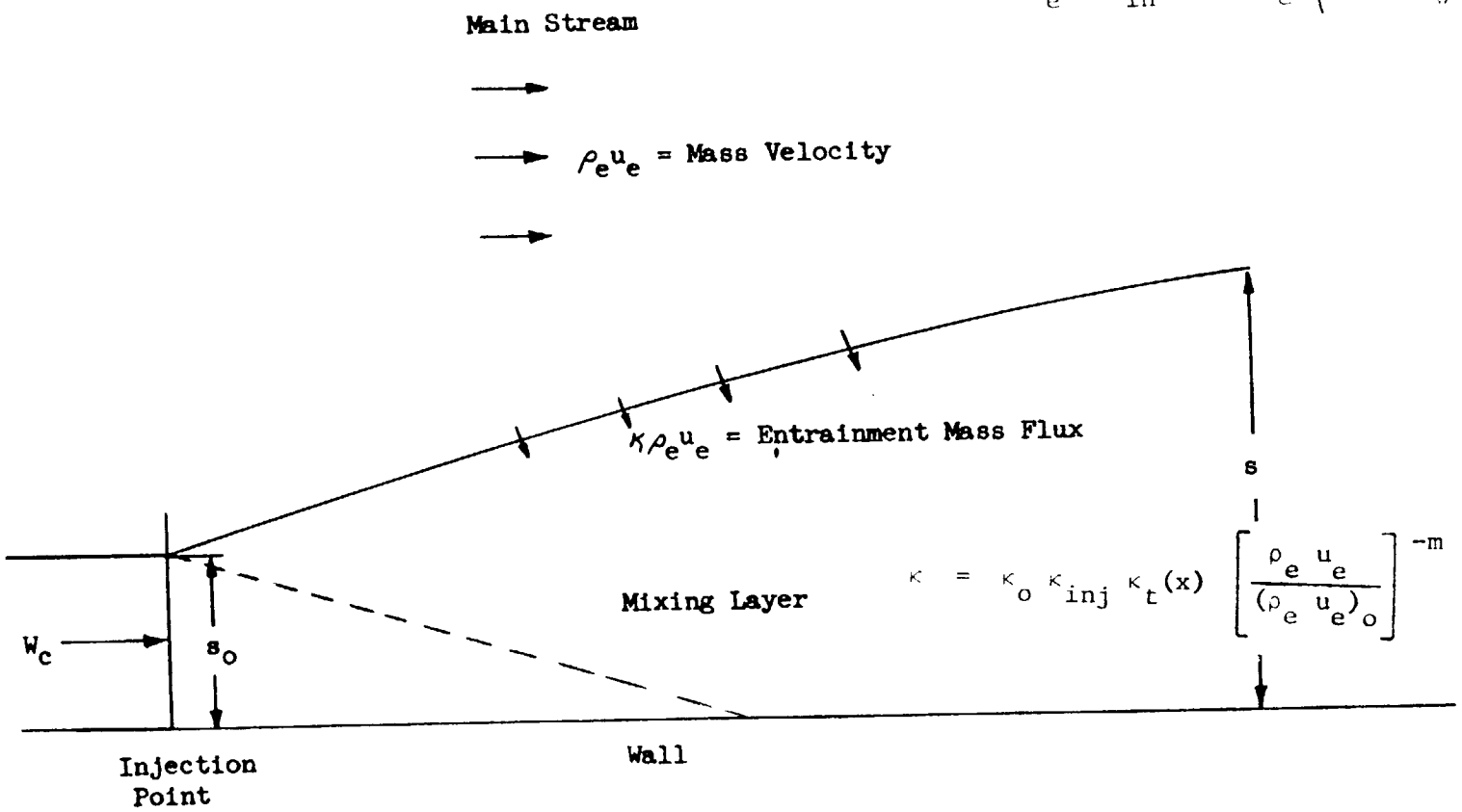

Figure III-9

in which κ_o is the entrainment fraction with laboratory conditions and no turning or flow acceleration, κ_{inj} accounts for increased freestream turbulence and other effects associated with liquid rocket injectors and $\kappa_t(x)$ represents the turning effects near the start of convergence. The bracketed term accounts for flow acceleration

Film Cooling Entrainment Model

III, A, Program Progress (By Task) (cont.)

An uncertainty in using the model in the APS applications arises from the utilization of an injection device which is suitable for sustaining rocket heat flux levels for 10^6 restarts. This rocket configuration provides a discharge geometry consisting of discrete channels separated by structural ribs and a finite thickness lip which separates the coolant from core flow. This is in contrast to available laboratory gas film cooling experimental data, which almost universally employ a continuous annular injection slot and knife edge on the separating lip. The geometry of the lip and experimental data are defined in Figure III-10, III-11, and III-12 for several chamber geometries and mixture ratios. The experimental entrainment parameter, κ_e, is a multiplying factor which must be employed at each axial station to make the model match the experimental results; i.e., the product of κ_{inj} and $\kappa_t(x)$ in Figure III-9. In these data reduction analyses, the downstream coolant injector configuration is viewed in three ways:

(1) Coolant expands and slows to fill step height A

(2) Coolant expands and slows to fill step height B

(3) Coolant effective injection area is converted to an equivalent continuous annular gap and actual ribs and step height are neglected.

The data suggest that, for case 3 above, the entrainment multiplying factor should be varied between 3 to 1.5 along the contour length. If case 1, the step height is used and the variation should generally be between 2 and 1. The multiplying factor employed in the design analyses was 1.5, based on case 3. The high degree of coolant mixing that is sometimes observed and other times lacking in the areas where the flow turns is believed to be dependent on the ratio of core to film density.

Figure III-13 provides a comparison of the film cooling effectiveness and entrainment multiplying factor for several geometries and mixture ratios.

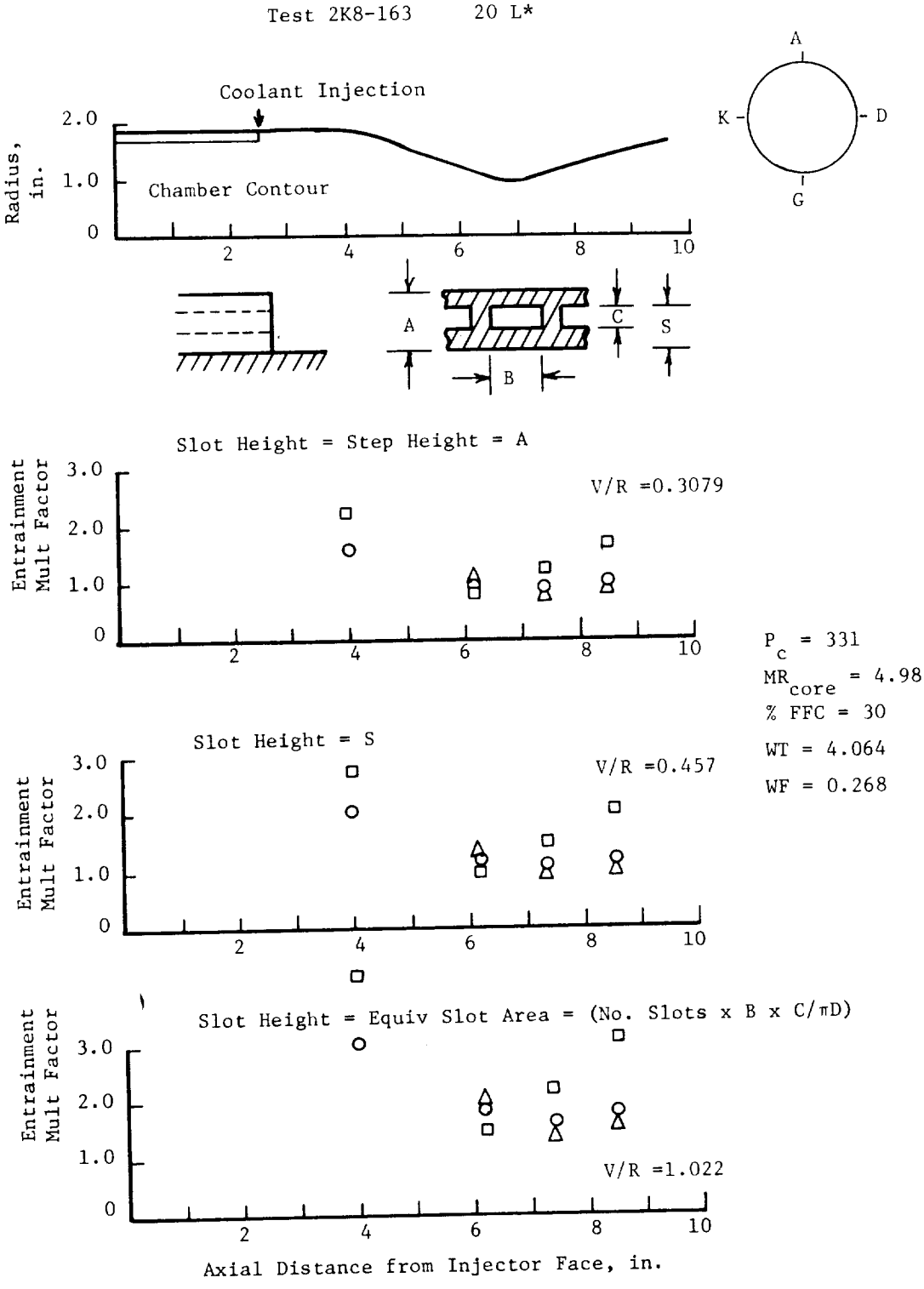

Film Cooling Entrainment Multiplying Factors - Test 2K8-163, 20 L*

Figure III-10

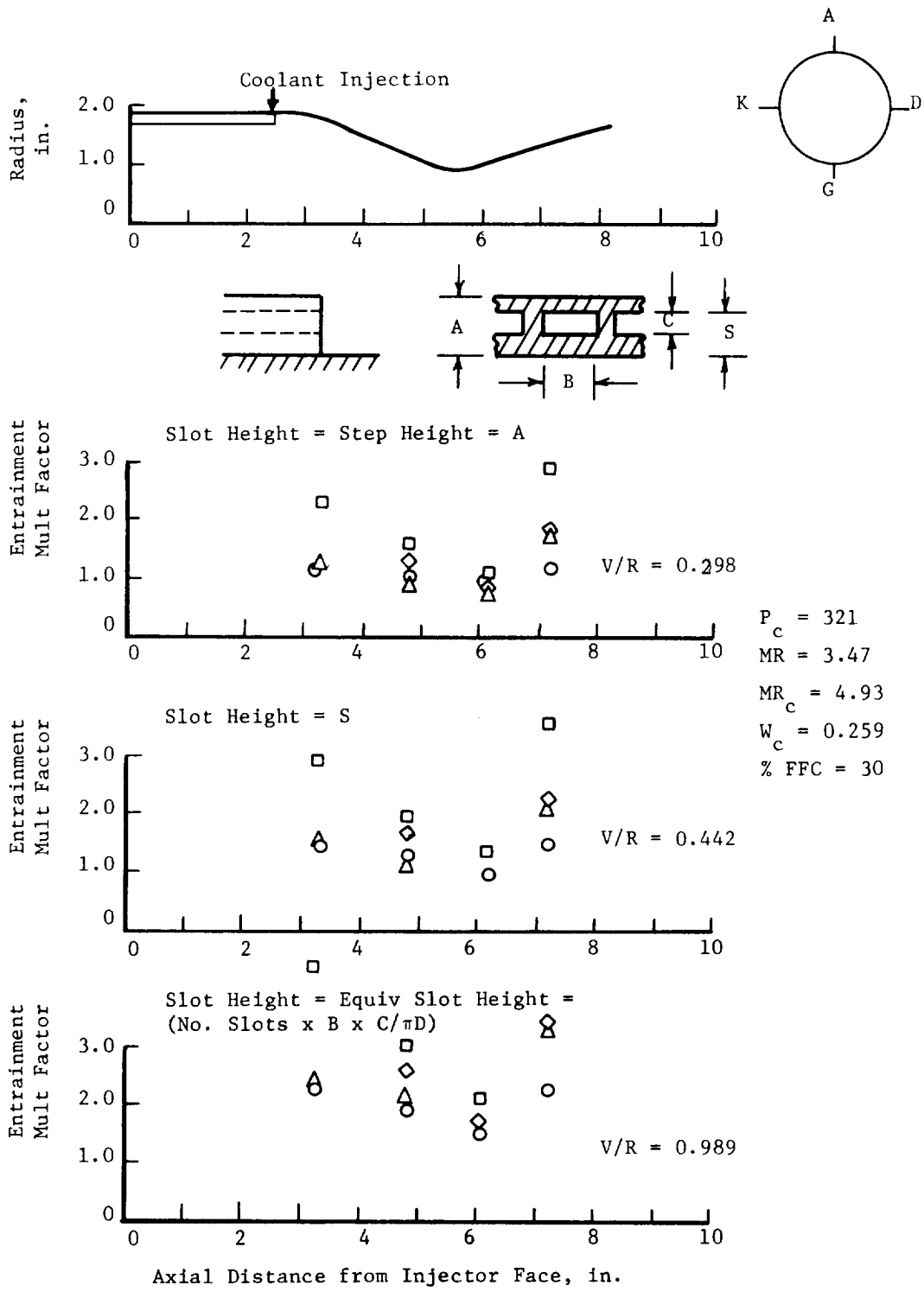

Film Cooling Entrainment Multiplying Factors - Test 2K8-157, 15 L*

Figure III-11

Test 2K8-131 15 L*

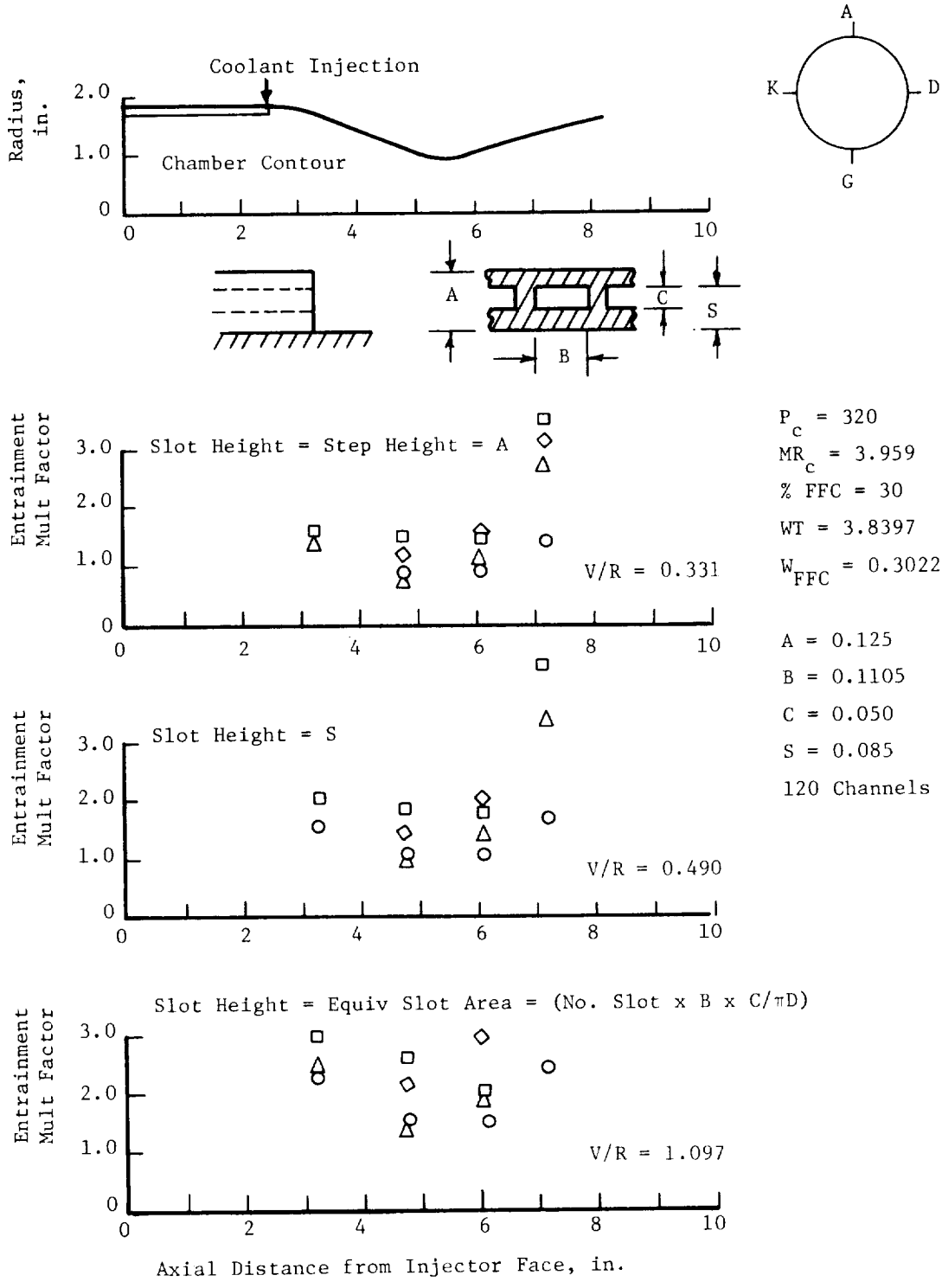

P_c = 320
MR_c = 3.959
% FFC = 30
WT = 3.8397
W_{FFC} = 0.3022

A = 0.125
B = 0.1105
C = 0.050
S = 0.085
120 Channels

Film Cooling Entrainment Multiplying Factors - Test 2K8-131, 15 L*

Figure III-12

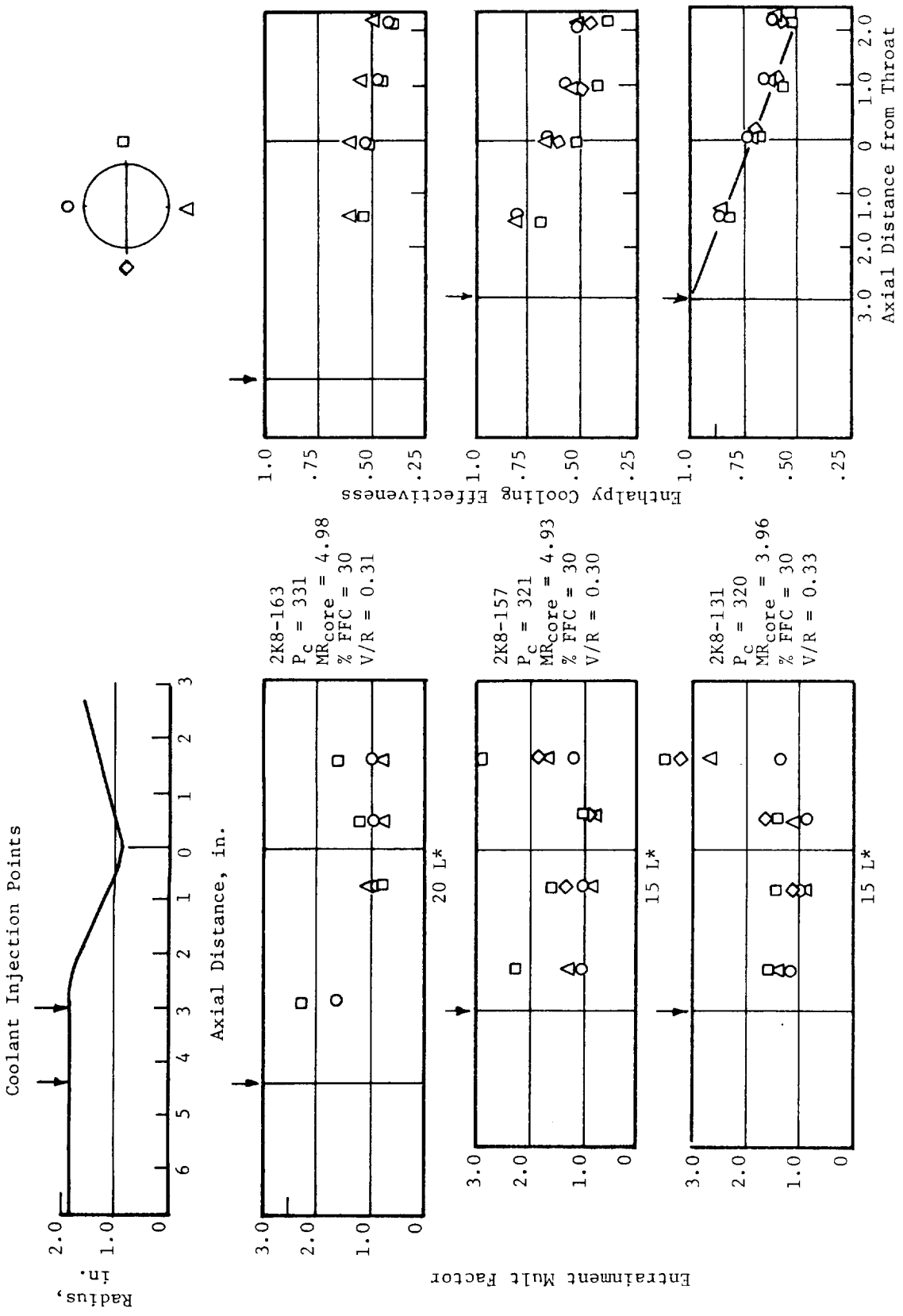

Film Cooling Entrainment Multiplying Factor and Effectiveness

Figure III-13

III, A, Program Progress (By Task) (cont.)

d. Impact of Data on Designs

Because of the lower than expected cooling effectiveness and higher heat transfer coefficients, the coolant injection station on the film-cooled chamber was moved from the end of the cylindrical section of the chamber to a location on the conical nozzle 1.25 in. upstream of the throat, the projected area of the lip decreased from 0.040 to 0.020 in., and the open channels made a larger percentage of the projected area.

The ability of small amounts of film cooling to significantly lower the throat wall temperatures on the regeneratively cooled chamber must now be questioned. Several film coolant injection rings, consisting of various lengths and velocity ratios, are available for use on this design. Additional data from Task VIII testing are being reviewed to determine the optimum injection configuration.

Design of the film cooling injector ring required for film cooling the area ratio 8:1 to 40:1 skirt of the regeneratively cooled chamber was completed during this report quarter. The film coolant will be injected at supersonic velocity (Mach No. 2.6) through a series of 100 one-dimensional convergent-divergent nozzles. Supersonic injection is considered to be more efficient than subsonic injection. The nozzles have been optimized to match the coolant injection pressure with the local nozzle free-stream pressure. When 7% of the fuel is employed as film cooling, the design will be capable of adjusting the flow from 3 to 21%. The film cooling injection nozzle configuration is shown in Figure III-14. Fabrication of these parts is covered in the next section and the data employed in the flow rate selection are shown in Figure III-15. There is an obvious broad range in the quantities of coolant projected (3 to 13%) to achieve the 0.4 effectiveness at the downstream tip of the skirt. The test program will therefore be structured to back down on this coolant flow until the desired effectiveness is attained, thus supplying valuable new data to the analysis of film cooling in supersonic flow.

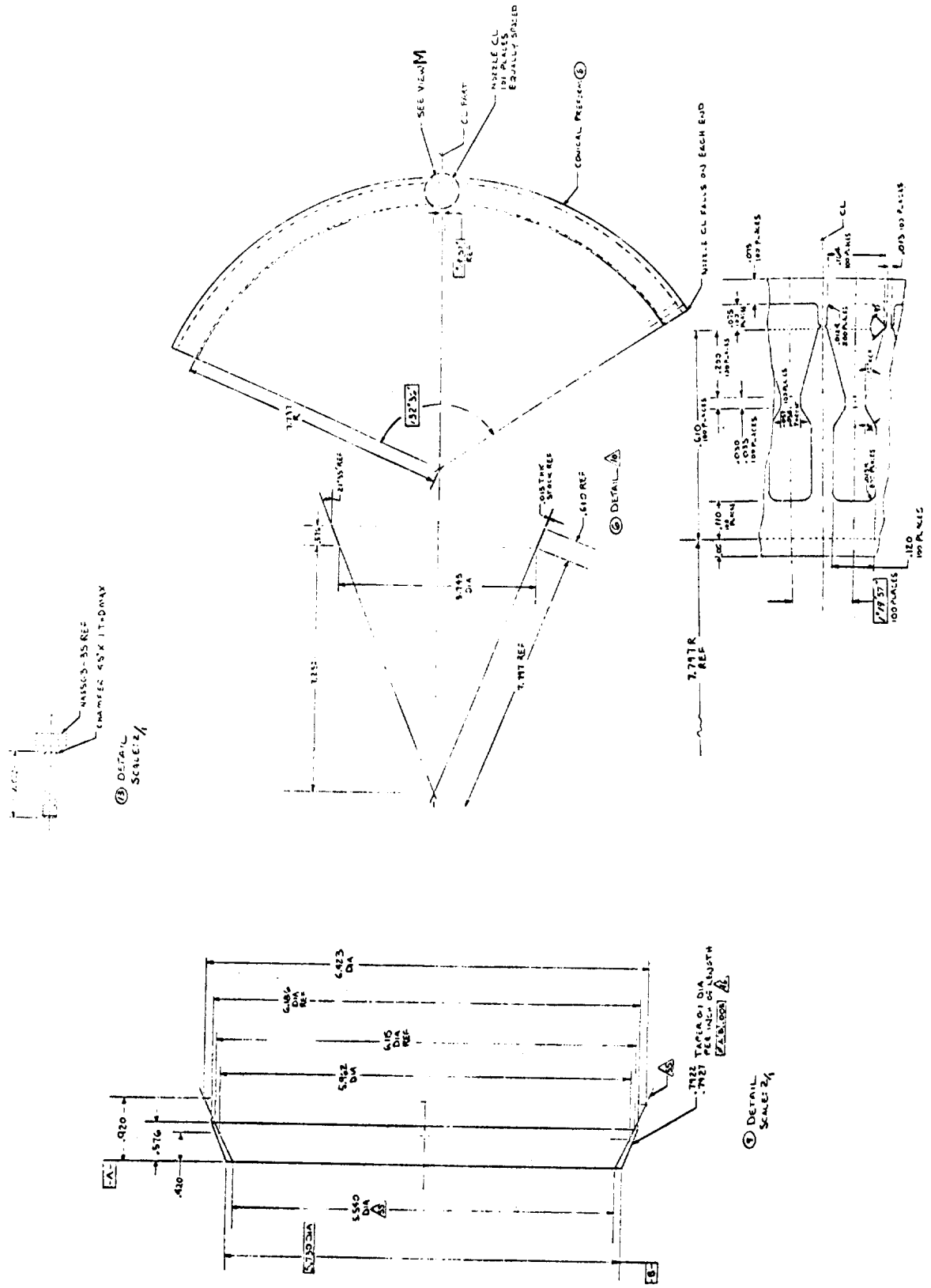

Supersonic Film Coolant Injector Design

Figure III-14

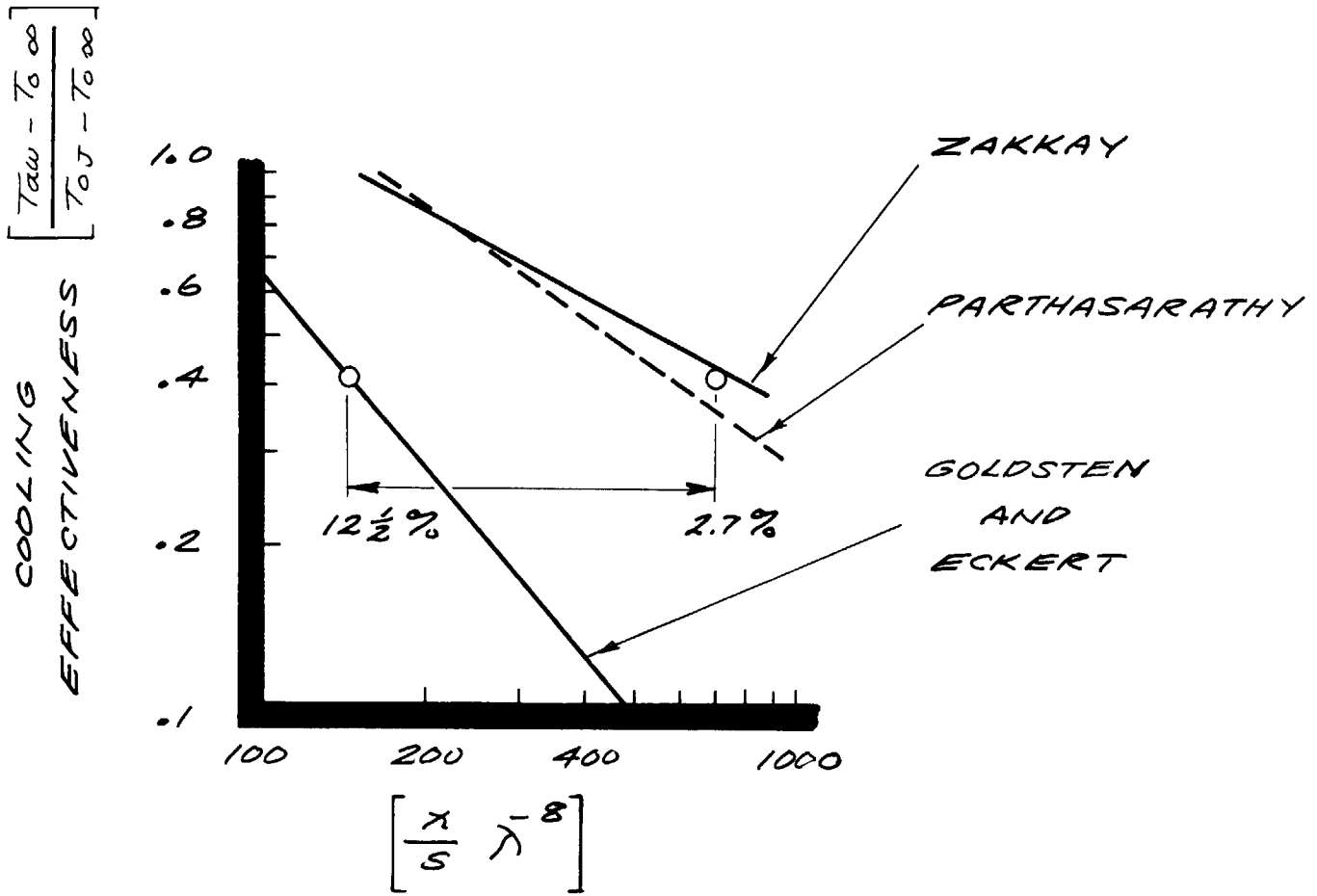

1. V. Zakkay, L. Sakell, and K. Parthasarathy, "An Experimental Investigation of Supersonic Slot Cooling," from Proceedings of the 1970 Heat Transfer and Fluid Mechanics Institute, Naval Postgrad School, Monterey, Calif, June 1970, ed. by Turgut Sarpkaya, Stanford University Press.
2. R. Goldstein, E. Eckert, F. Taou, and A. Haji-Sheikh, "Film Cooling with Air and Helium Injection Through a Rearward-Facing Slot into a Supersonic Air Flow," University of Minnesota, Heat Transfer Laboratory, HTL TR No. 60, February 1965.
3. K. Parthasarathy and V. Zakkay, "Turbulent Slot Injection Studies at Mach 6," ARL 69-0066, April 1969.

Supersonic Injection Effectiveness Correlations

III, A, Program Progress (By Task) (cont.)

4. Task IV - Cooled Chamber Fabrication

During this report quarter, considerable progress has been made in fabrication of cooled thrust chambers. A total of four cooled chambers, two of each design as discussed in Report 14354-Q-2, are being fabricated in the ALRC Research and Advanced Technology Shop.

a. Film Cooled Chamber Fabrication, PN 1160334-1 and -2

Figure III-16 shows the fabrication schedule for the two chambers of this design. All functions or operations indicated by the heavier bars have been accomplished. Delivery of the first cooled chamber assembly is scheduled for mid-April. The chamber, as delivered, contains all brazed-in thermocouples for measuring gas-side wall temperatures. Delivery of the second unit is scheduled for the first week in May. This chamber design consists of five major and two secondary components as shown in the photograph in Figure III-17.

Rolling and welding of conical preforms for the Haynes 188 throats from 0.050-in. sheet material was completed. Welding was accomplished with Haynes 188 weld rod material to provide a maximum strength joint. Spinning of these preforms into the convergent-divergent throat section proceeded satisfactorily but was more time consuming than had been anticipated. The difficulties were that this material work hardens easily and therefore requires frequent annealing and quenching cycles (five heat treatments per part). The quenching operation produces an extremely tenacious surface oxide, involving the cobalt base and rare earth alloying constituents, which has been found to be resistant to all available pickling and etching solutions. This oxide must therefore be removed mechanically by a hydrohoning operation followed by pickling prior to each spin operation. (The outstanding capability of this material to withstand chemical attack and its high strength were, of course, the main reason for its selection.) Two Haynes 188 throat sections, including a 304L film cooling

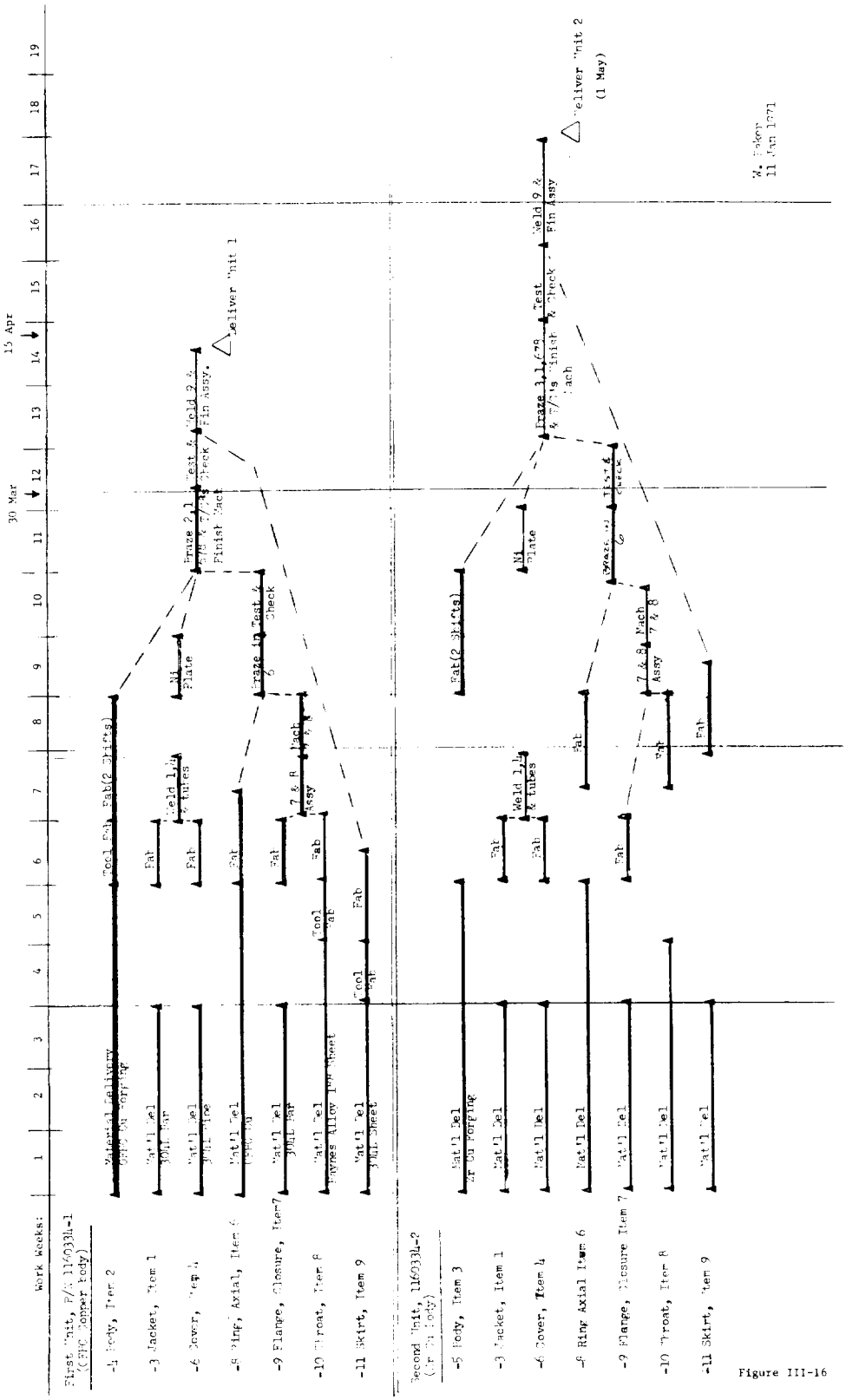

Figure III-16

Film-Cooled Chamber Fabrication Schedule

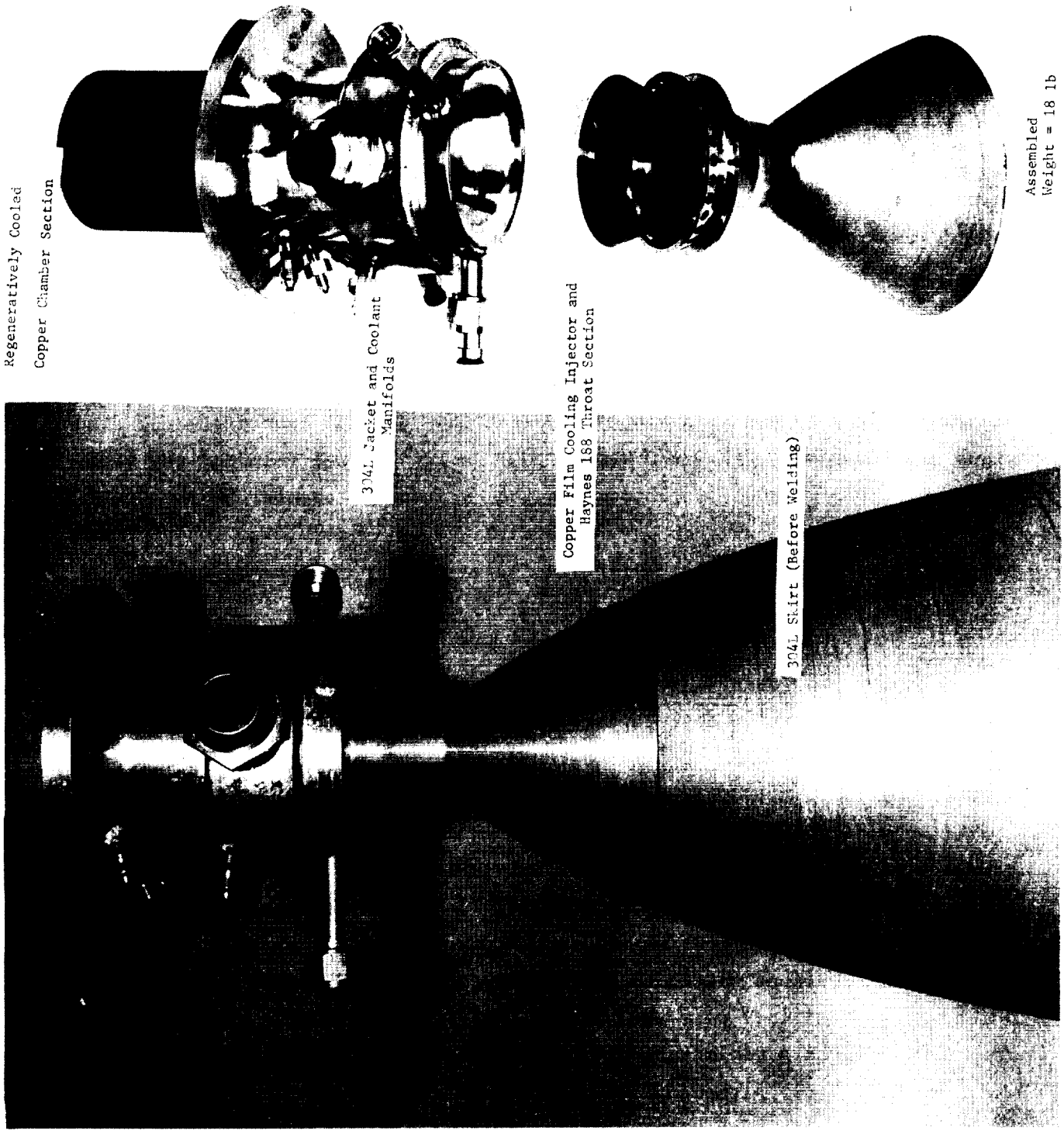

Film-Cooled Chamber Before and After Assembly

Figure III-17

III, A, Program Progress (By Task) (cont.)

manifold, were completed to design specifications (uniform 0.040 to 0.050 in. wall thickness) and were made available for the next assembly, which involves bonding of the copper film cooling injection ring.

A parallel fabrication sequence on copper parts was initiated by rough turning the copper forgings and ultrasonically inspecting for internal voids. All materials were found to be free of voids larger than 0.015 in. The inside diameter of copper parts which will contain cooling channels was bored, leaving extra stock on the ID, while the OD was machined to print dimensions. The conical film cooling injection ring is match machined to the ID of the Haynes 188 throat section. Axial coolant channels were then machined in the copper in a slotting operation. Nominal quantities and dimensions are 120 slots, 0.040 x 0.040 $\pm$ 0.001 in the conical film cooling ring; 80 slots, 0.050 $\pm$ 0.001, 0.180 deep in the cylindrical chamber body. One film cooling ring and one chamber body were satisfactorily completed to specified dimensions and tolerances. Deviations in the other parts are as follows:

Slots in the film cooling ring were 0.036 to 0.037 in. wide and 0.043 in. deep, which results in approximately the same flow area as the nominal fabrication objectives.

Slots in the zirconium copper body differed from the specified widths and depths due mainly to undetected dulling and subsequent breakage of the slotting tools. Data available from the single part is insufficient to determine if the small zirconium content in this material is a contributing factor in tool wear and breakage. The major deviation from fabrication specifications was in channel widths due to deflections of the ribs, which accompanied tool wear and breakage. A few channel sizes varied locally from 0.044 in. as a minimum to 0.058 in. as a maximum. The nominal channel width is 0.050 in. Although these deviations are not expected to have significant impact on this technology program, they will certainly play a role in

III, A, Program Progress (By Task) (cont.)

determining the ultimate life capabilities of the thrusters. The ALRC R&AT shop has therefore initiated, under its own process development resources, a modest program to develop a better understanding of the variable involved in slotting deep, narrow coolant channels in copper and copper alloys.

Fabrication of two CRES 304L jackets containing the manifold and inlet lines was accomplished routinely by machining from bar stock and welding on indicated lines and instrumentation bosses.

The first assembly operation involves the bonding of the matched machined film cooling ring into the throat section. Prior to this operation, several test specimens were run to determine the potential bond strengths. The first specimen was brazed very lightly weighted in a hydrogen atmosphere. The second specimen was diffusion bonded with a very high load and in a hard vacuum. Both test specimens were plated with a minute quantity of an Aerojet-formulated nickel alloy. The diffusion bonding process was conducted at temperatures, pressures, and times and plating thicknesses which were optimized in early company-funded programs. The diffusion bonding process provided a superior joint, the strength of which exceeded the parent materials in peel, bend, and chisel tests.

Two assemblies were successfully joined by the diffusion bonding procedure. The first assembly is shown in Figure III-18. Manifold cold flow and visual inspections showed all channels to be open and flowing properly. An ultrasonic inspection of the bond line subsequently indicated that all 120 copper ribs were successfully bonded to the conical steel pressure vessel. The record of this inspection (shown in Figure III-18) reveals the dark stripes as bonded ribs and the light areas as the channel position.

The next assembly operation involves shrink fitting the matched machined, slotted copper chamber and the throat subassembly into the

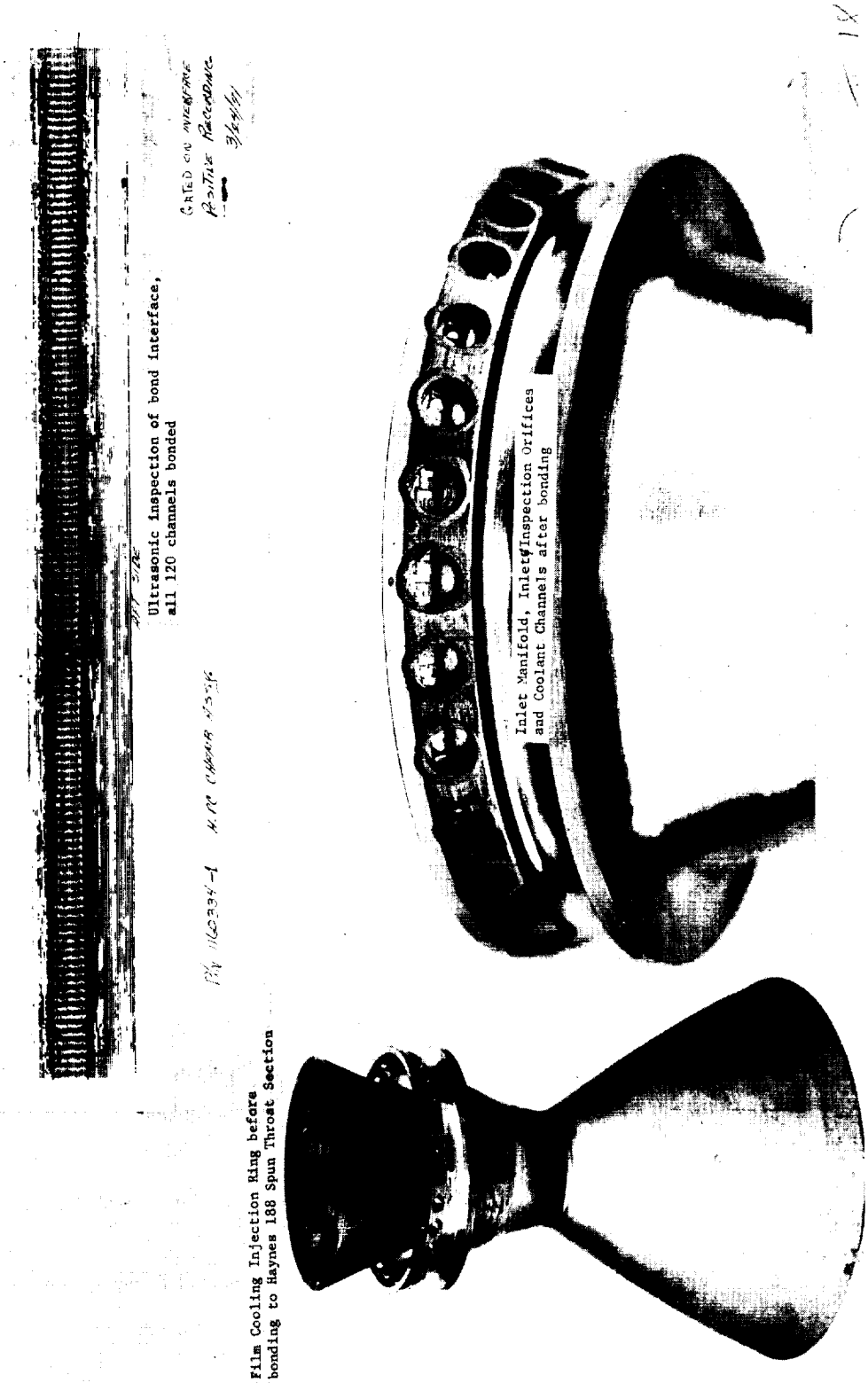

Assembly and Inspection of Film-Cooled Throat

Figure III-18

III, A, Program Progress (By Task) (cont.)

jacket as shown in Figure III-17 and brazing. This is followed by final machining the chamber ID and installing the gas-side thermocouples in a second brazing operation.

At the close of the report period, the first unit was at the point of having the thermocouples installed. The second was at the chamber assembly stage. The final assembly operation is to weld the spun 304L skirt to the Haynes 188 nozzle, clean the weld, and respin the joint. Figure III-19 is a photograph of the finished skirt prior to welding.

b. Regeneratively Cooled Chamber Fabrication, PN 1160313-1 and -2

The two chambers of this type which are being fabricated are shown in Figure III-20. The major difference between the two chambers is that the first has an OFHC copper body and the second has a body fabricated from zirconium copper.

The fabrication status of the two major and three lesser components is detailed in the status chart of Figure III-21. Delivery of the first chamber is expected during the last week of April. The second unit is to be delivered the last week in May.

As of this report date, fabrication of all components had been completed up to final machining for fit with the exception of the slotting of the zirconium copper body and the welding of fittings on the manifold jacket (Item 4) for the second unit.

The status and any appropriate comments regarding fabrication of the individual components follows.

SPUN SKIRT

Spun Skirt

Figure III-19

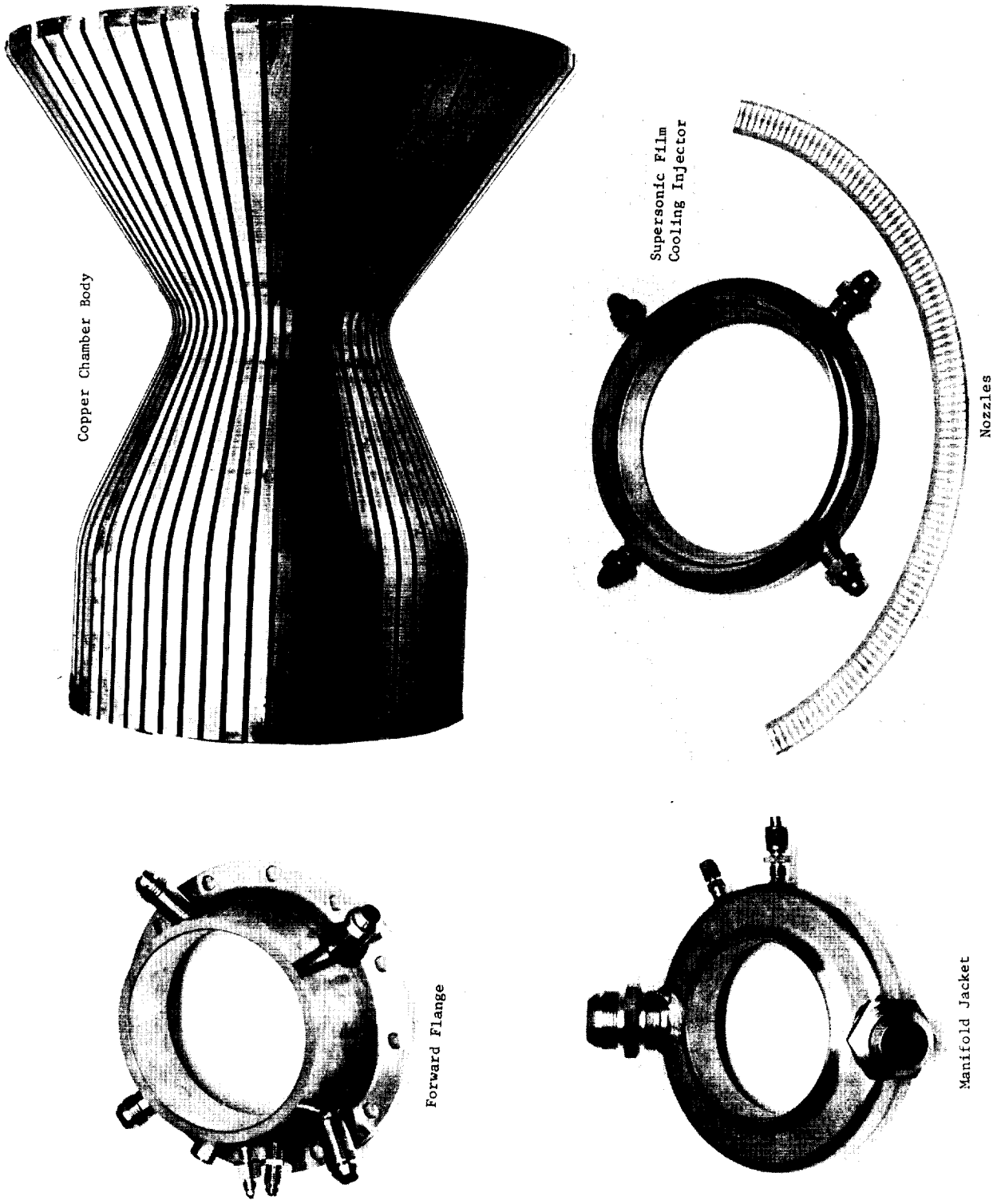

Regeneratively Cooled Chamber Components

Figure III-20

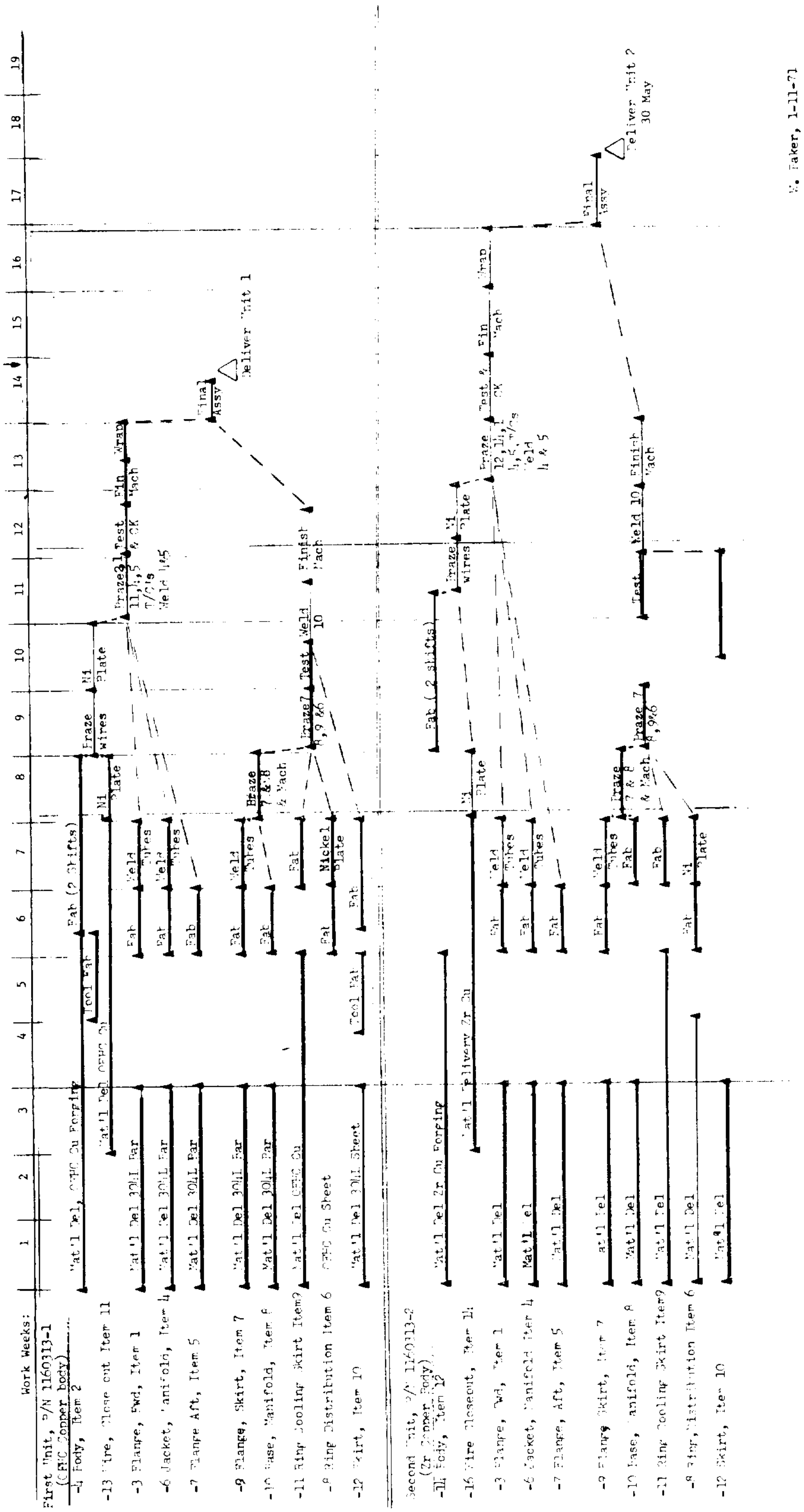

Regeneratively Cooled Chamber Fabrication Schedule

Figure III-21

III, A, Program Progress (By Task) (cont.)

(1) Copper Chamber Body

(a) First Unit (Item 2)

The OFHC copper body for the first unit has been slotted and machined up to the point where the copper wire closeouts are to be brazed in. The part is shown after slotting in Figure III-20. Brazing of the wires was to be accomplished by 14 April. Some difficulty was encountered in selecting the correct cutters to be used in cutting the deep and sharply contoured slots, resulting in some cutter breakage.

(b) Second Unit (Item 12)

The zirconium copper body for the second unit has been rough machined preparatory to slotting. Slotting of this unit is scheduled to start on 14 April.

(2) Supersonic Film Coolant Injector (Items 6, 7, 8 and 9)

The downstream supersonic injectors for both units have been fabricated. Figure III-22 shows these components prior to assembly. These units represented a design and fabrication "first". Item 6 was fabricated first. It consists of 100 small (0.058 in. throat), two-dimensional nozzles photoetched into a 0.015-in.-thick copper sheet. The sheet was so etched and formed as to represent a conical ring when completed. The nozzle strips were then plated on all surfaces with an Aerojet-formulated nickel alloy, so as to serve as the braze carrier in the next operation. The stainless manifold base (Item 8) and the flange (Item 7) were then welded together and machined and the copper cooling ring (Item 9) rough machined. Care was used to machine the mating conical surfaces of all parts with the same machine setup to ensure identical cone angles. The respective parts were then positioned, weighted,

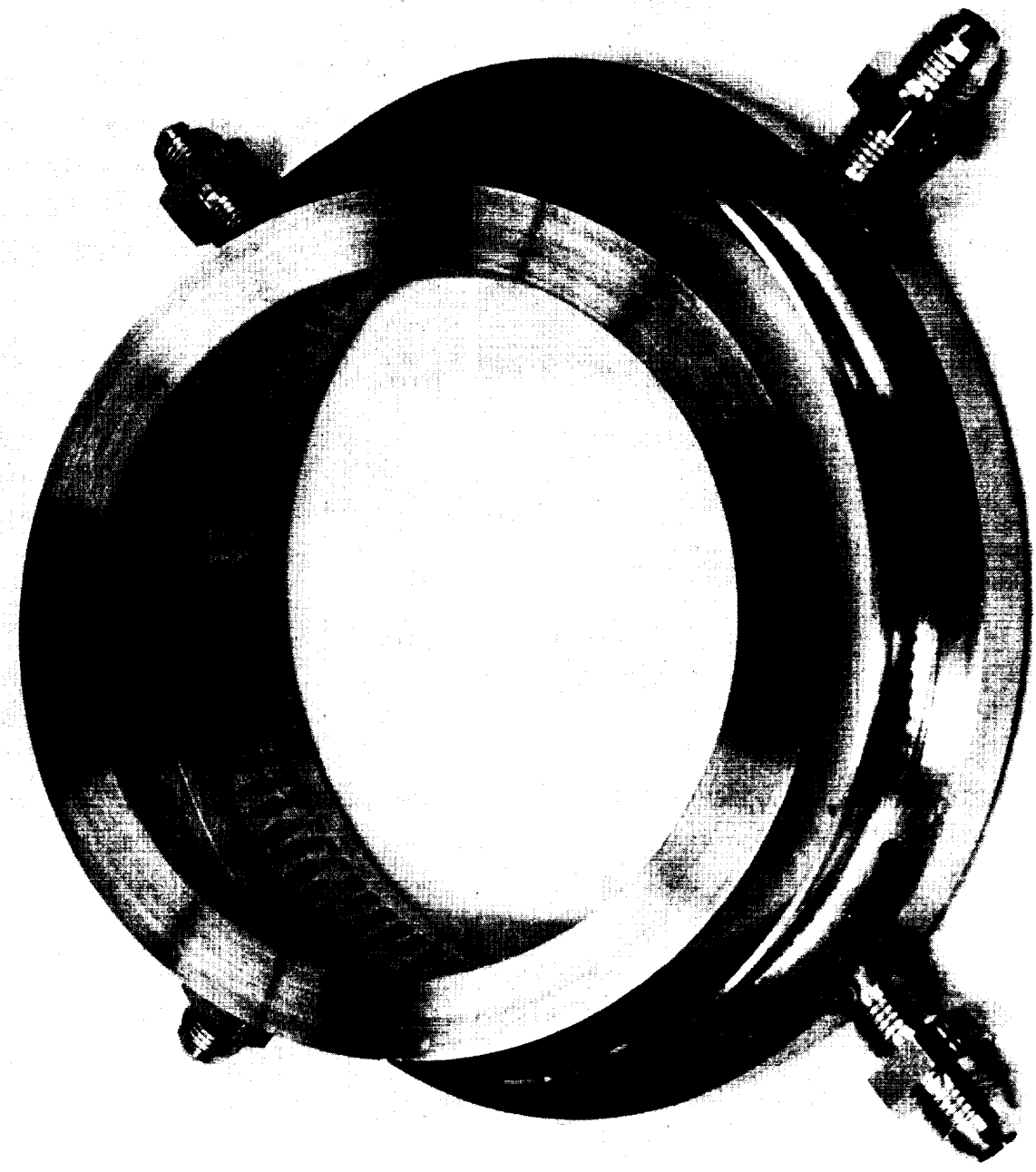

Supersonic Film Coolant Injection Ring and Photoetched Nozzles

Figure III-22

III, A, Program Progress (By Task) (cont.)

and vacuum brazed. The finished components were shown in Figure III-21. The flow rate vs pressure drop characteristics determined by GN_2 flow at selected sonic nozzle pressure ratios were within a few percent of the theoretical values, and the static pressure variation around the manifold was less than 3.0%.

(3) Forward Flange (Item 1)(Figure III-20)

The forward mounting flanges for both units have been rough machined, the fittings welded on, and the components stress relieved.

(4) Manifold Jacket (Item 4)(Figure III-20)

As previously stated, one of the two manifold jackets has been rough machined, fittings welded on, and the part stress relieved. The other part is presently being welded.

(5) Skirt (Item 10)(Figure III-19)

The stainless steel skirts for both units have been spun, stress relieved, and machined prior to welding onto the stub of the coolant ring flange. The regeneratively cooled chamber and film-cooled chamber use the same skirt design.

(6) Assembly

Final assembly involves coolant channel closeout with rectangular wires which are brazed into the copper body. Flanges which mate with the body are then machined for proper fitup and brazed to the body in a second operation. Gas wall thermocouples will also be installed in the second brazing operation. The finished machined part will then be coated with 0.050 in. of electroformed nickel in order to supply the required hoop load restraint. Final assembly consists of bolting the skirt and injector to the completed thrust chamber.

III, A, Program Progress (By Task) (cont.)

5. Task V - Igniter Analysis and Design

No activity.

6. Task VI - Igniter Checkout Tests

The two igniter concepts being evaluated on this program are the spark igniter and catalytic ignition system. Testing of these components was described in Quarterly Report No. 2. The spark ignition system has been selected over the catalytic system because of slightly faster response, greater reliability, the ability to safely cold flow the igniter without having an automatic ignition, and the demonstrated capability of maintaining rapid and repeatable restarts with very cold propellants over a wide range of mixture ratios. Cold propellant tests covered igniter chamber mixture ratios ranging from 30 to 120 with fuel down to 175°R and oxygen at 250°R. Ignition was successfully accomplished within about 0.010 sec under all test conditions. Figure III-23 summarizes the characterization of the igniter being employed in these test activities. A complete presentation of the igniter and ignition characteristics is being published as the final report to Contract NAS 3-14348.

7. Task VII - Valve Preparation and Checkout

A complete description of the valves was presented in Quarterly Report No. 2. Figure III-24 summarized the valve dynamic characteristics which were demonstrated in pulsing tests. Valve pressure drop is approximately 10 psi.

Performance of APS Thrust Chamber Valves
During 2500-Pulse Series 2K7-115

The performance of the valves was evaluated in two categories: motion repeatability and leakage. Leakage of both poppet and stem seals was checked periodically during the series of 2500 engine pulses.

TESTING ACCOMPLISHED

- 258 TOTAL TESTS INCLUDING:
  - 150 sec for durability demonstration
  - 78 tests at low temperature
  - 1000 pulses as igniter-only
  - 2500 pulses as igniter-complete thruster

CONDITIONS DEMONSTRATED

- 0.025-0.100 IN SPARK GAP RANGE
- 1-30 MILLIJOULES AT APPROXIMATELY 20,000 VOLTS
- 100-500 PSIA P_c RANGE
- 1 ATM TO 10^{-4} MM Hg P_a RANGE
- 30-120 CORE MR RANGE
- TEMPERATURE RANGE
  - Fuel: Ambient to 175°R
  - Oxidizer: Ambient to 250°R
  - Igniter: Ambient to 175°R

PROGRAM RESULTS

- 0.01 SEC IGNITION DELAY (LAGGING FLOW TO 90% P_c)
- NO LIMITING CONDITIONS ENCOUNTERED

Spark Igniter Test Parameters and Operating Characteristics

Figure III-23

	OXIDIZER VALVE		FUEL VALVE	
	OPEN	CLOSE	OPEN	CLOSE
1. TRAVEL TIME, SEC (150 PSIA HELIUM PRESSURE, P_C = 300 PSIA)	0.0087	0.010	0.010	0.0074
2. ELECTRICAL SIGNAL TO FULL TRAVEL, SEC	0.042	0.043	0.045	0.039

Valve Dynamic Characteristics

III, A, Program Progress (By Task) (cont.)

Prior to initiating the pulse series, both oxidizer and fuel valves indicated a very slight stem seal leak; no poppet leakage was detected. Stem seal leaks were tested for with a standard leak check fluid. Poppet leakage was tested for with a standard bubble indicator. Leak check pressure on both valves was 100 psi. The bubble indicator was left attached to each valve for 5 min. Pressurant was the effluent, i.e., GH_2, fuel valve; GO_2, oxidizer valve.

Valve motion during the pulse series was measured by linear potentiometers attached to the valve stem. Output signals from the potentiometers were recorded on an oscillograph. Valve data was collected at the 100th, 500th, 900th, 1200th, 1400th, and 2500th pulse. The following data resulted:

Pulse No.	Valve	External Leakage	Internal Leakage
100	Oxidizer	None	None
100	Fuel	None	None
500	Oxidizer	Stem - Moderate	None
500	Fuel	Stem - Slight	None
900	Oxidizer	Stem - Moderate	None
900	Fuel	Stem - Slight	None
1200	Oxidizer	None	None
1200	Fuel	Stem - Slight	None
1400	Oxidizer	Stem and Nut - Moderate	None
1400	Fuel	Stem and Nut - Slight	None
2500	Oxidizer	Stem and Nut - Heavy	None
2500	Fuel	Stem and Nut - Heavy	None

After each leak check, the packing nut on the oxidizer valve was tightened with the exception of Pulse No. 100 at which time no leakage was noted. Tightening of the packing nut reduced each measured leak to a negligible value. During the course of 2500 pulses, the oxidizer valve pack nut was advanced approximately 1/8 turn. The packing nut on the fuel valve was not tightened as its position was inaccessible.

III, A, Program Progress (By Task) (cont.)

Fuel valve motion appeared to be regular, approximately 10 ms opening and closing. Oxidizer valve motion appeared somewhat irregular, shifting on closing from approximately 10 ms to 20 ms after some 200 pulses.

8. Task VIII - Injector Checkout Tests

a. Summary of Test Activities

High P_c APS injector checkout testing was completed during the month of February on the Physics Lab Bay 7 test stand. A total of 90 tests have been completed to date, 15 more than in the original test plan. Of these tests, 81 were heat transfer and performance tests, four were streak chamber tests which were too short in duration (0.5 sec) to obtain accurate performance, four were combustion stability tests, and one was a short pulsing test series. Eighteen of these tests, including one streak chamber and the four stability tests, were conducted with cold propellant. Testing with heated propellants, originally planned for this task, has been rescheduled to be investigated in Task IX. Testing during the closing days of January and the month of February is summarized as follows:

Tests 159 to 161 were conducted on a 15 L* copper heat sink chamber with an I-triplet injector at MR = 4, 5 and 6 without film cooling. These tests provided repeat data points of earlier tests at MR = 4 and 5 and new data at a MR of 6. Test durations were 2 sec. The MR = 4 ERE was within 0.5% of earlier data, while the MR = 5 ERE of 97.1 was approximately 1% lower than recorded in earlier tests.

Tests 162 through 166 were conducted using the same injector in the adiabatic wall chamber at 20 L*, a 2.5-in.-long film cooling ring, and 30% film cooling. Test durations ranged from 2 to 10 sec with a nominal core MR from 4.5 to 5.0 and chamber pressures of 300 and 500 psia. These tests provided performance data with film cooling and demonstrated that the adiabatic wall temperature is not a significant function of chamber pressure.

III, A, Program Progress (By Task) (cont.)

Test 167 was a repeat of earlier tests at MR = 3.0 and 300 psia P_c for performance verification. Results were consistent within about 1.0%. Test 167 was the first test in which significant overpressure (200 psi) was noted in the oxidizer manifold.

Test 168 was a repeat of Test 167 to observe the ignition process. This ignition phenomenon was repeatable. The igniter was disassembled, inspected, and found in proper order. A possible cause for this overpressure is the longer than optimum fuel lead on these tests. Optimum sequencing is simultaneous flow, while actual data show a 0.009-sec fuel lead which, in conjunction with the low MR (3.0), can result in a combustible mixture in the oxidizer manifold.

Tests 169 through 171 were conducted in the thermally reinstrumented 15 L* copper heat sink chamber with a 1-in.-long film cooling ring having a reduced step height. Testing of 2-sec duration was conducted with cold oxidizer at a core MR of 5 and 30% and 20% film cooling at 300 and 500 psia chamber pressure.

Tests 172 through 175 investigated cold oxidizer in a 20 L* copper heat sink chamber with a 2.5-in.-long film cooling ring (30% film cooling) at chamber pressures of 100, 300 and 500 psia.

Tests 176 and 177 tested cold fuel and oxidizer and higher film coolant injection velocities.

Tests 178 through 185 employed the coaxial element injector with an aluminum face plate. This configuration provided swirlers on the oxidizer inlets and a tip recess of 0.080 in. All tests were conducted in the newly instrumented copper heat sink chamber for 2.0-sec duration, except Test 181 which was a 0.5-sec streak chamber test. Tests 178 through 183

III, A, Program Progress (By Task) (cont.)

were conducted with cold oxidizer and ambient fuel. In Tests 184 and 185, both propellants were cold. Test variables in this series were: L*, percent film cooling, mixture ratio, and chamber pressure. The performance of this configuration was generally lower than all others tested; however, the aluminum face plate gas-side surface thermocouples demonstrated the material feasibility since steady-state face temperatures were 230°F greater than the fuel temperature. With cold fuel, the injector face operates at a temperature less than 100°F

Tests 186 and 189 were combustion stability tests conducted in a 15 L* copper chamber with SN 2 I-impinging coaxial injector using cold propellants. The results of these tests are discussed in a separate section.

Test 190 involved a brief series of pulse tests to provide system response data for Task X testing.

b. Injector Performance Summary

The energy release efficiency of the four injector configurations tested to date, including the reduction in efficiency due to the use of up to 30% fuel film cooling, is summarized in Figures III-25 and III-26. Table III-2 provides a tabulation of the test conditions, test hardware, and measured performance for the test data points employed in preparing these figures. The upper part of Figure III-25 provides a data plot of injector efficiency for each design over a range of thrust chamber mixture ratios for various film cooling percentages. The loss in performance due to the diversion of a fixed percentage of the fuel to separate film cooling rings at the injector periphery is treated as a mixture ratio distribution loss which is additive to energy release loss of the core. The lower part of this figure is a cross plot of the data in the respective upper figures at a thrust chamber mixture ratio of 4.0. The upper dashed line at 98% ERE is the maximum

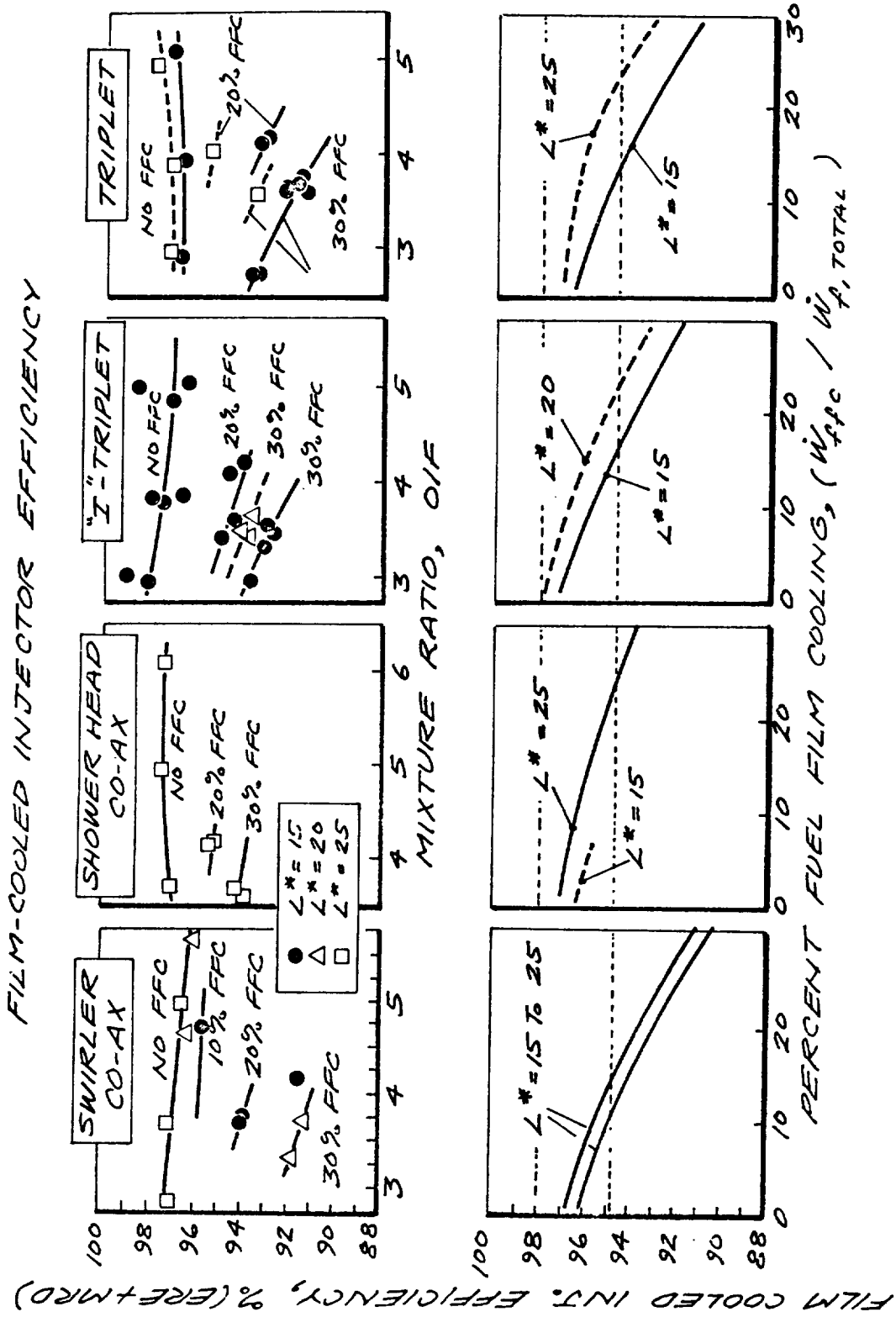

Film-Cooled Injector Efficiency

Figure III-25

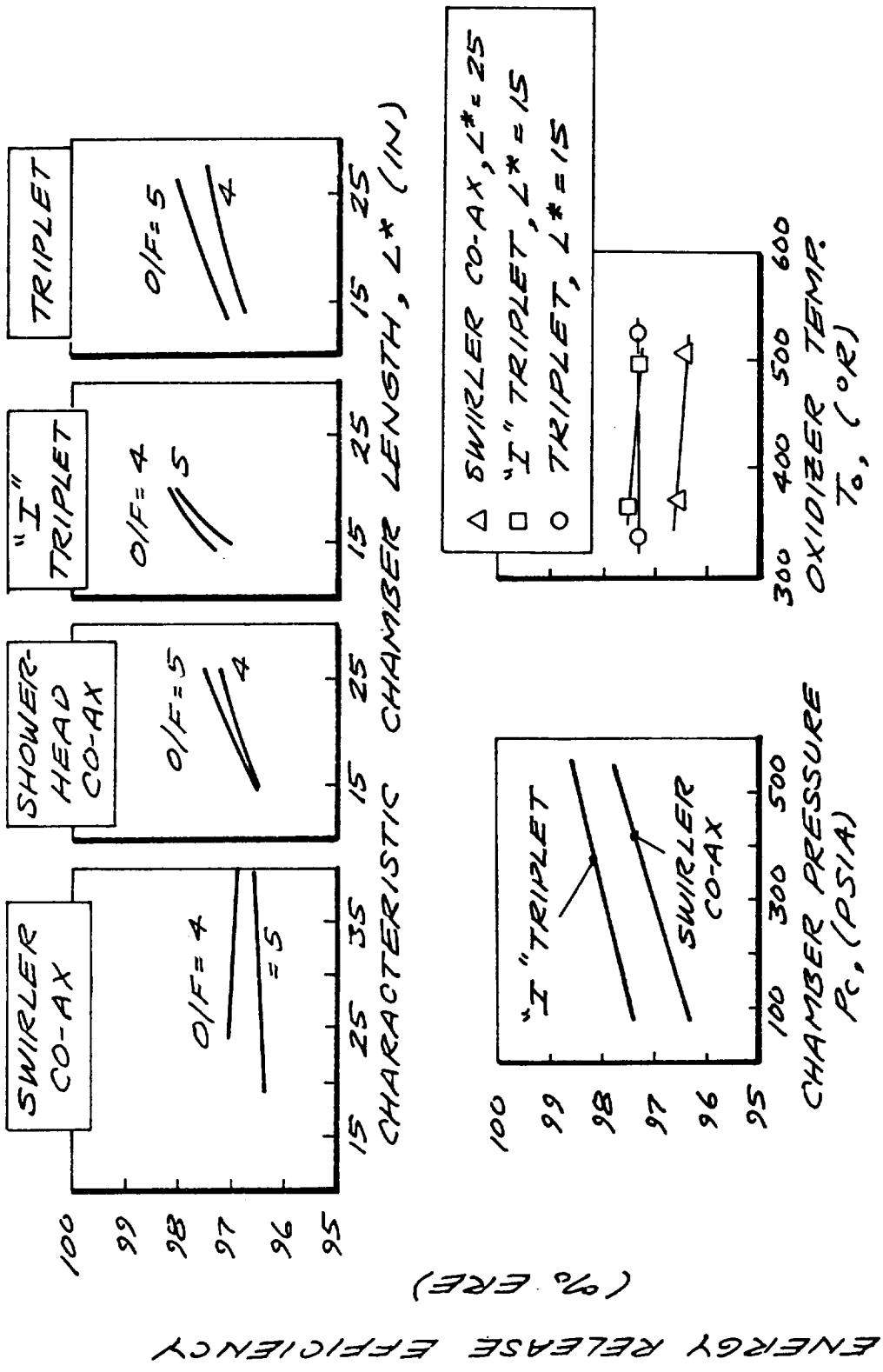

Injector ERE (No Film Cooling)

Figure III-26

TABLE III-2

SEA LEVEL PERFORMANCE SUMMARY

Test Series	2K-6												2K-9				
Run No.	101	102	103	104	105	106	108	109	110	111	112	113	102	103	106	107	108
Injector Type	Triplet SN 2								Triplet SN 1				Triplet SN 3				Triplet SN 1
Igniter (lbf, Type)[1]	25-S																
L* (Chamber Type)[2], in.	15 (Cu)				25 (Cu)				15 (Cu)							25 (Cu)	15 (Cu)
ϵ	2.91				2.99				2.93				2.87			3.20	2.87
Test Duration, sec	0.5			1.0					0.5	1.5	2.0		1.0				
Data Summary, sec	1.02-1.12	1.02-1.12	1.02-1.12	1.57-1.67	1.57-1.67	1.57-1.67	1.57-1.67	1.57-1.67	1.02-1.12	2.0-2.1	2.6-2.7	2.6-2.7	1.36-1.46	1.26-1.46	1.26-1.46	1.26-1.46	1.26-1.46
P_c, psia	288	294	290	291	292	291	297	289	295	294	297	293	297	306	299	298	310
$\dot{w}_o$, lbm/sec	2.629	2.464	2.835	2.664	2.678	2.623	2.465	2.809	2.618	2.649	2.433	2.848	2.663	2.506	2.960	2.911	2.720
$\dot{w}_f$, lbm/sec	0.651	0.807	0.575	0.661	0.666	0.666	0.819	0.568	0.657	0.660	0.823	0.572	0.683	0.841	0.577	0.577	0.712
$\dot{w}_{fI}$, lbm/sec	0.015	0.015	0.015	0.015	0.015	0.015	0.015	0.015	0.015	0.015	0.015	0.015	0.010	0.010	0.013	0.013	0.013
$(O/F)_{eng}=(O/F)_{core}$	3.95	3.00	4.80	3.94	3.94	3.85	2.95	4.81	3.90	3.93	2.90	4.86	3.84	2.94	5.02	4.94	3.75
$\dot{w}_T$, lbm/sec	3.295	3.286	3.425	3.339	3.359	3.305	3.299	3.392	3.289	3.324	3.271	3.435	3.356	3.357	3.550	3.500	3.445
F_{SL}, lbf	1104.7	1131.2	1118.6	1122.3	1129.7	1116.5	1137.6	1112.3	1105.3	1118.0	1129.1	1114.9	1107.8	1137.8	1153.7	1148.6	1156.7
$P_a A_e$, lbf	112.4	112.4	112.4	122.4	125.0	125.0	125.0	125.0	122.2	122.2	122.1	122.1	120.5	119.9	119.2	133.3	119.3
F_{vac}, lbf	1227.1	1253.6	1241.0	1244.7	1254.7	1241.5	1262.6	1237.3	1227.5	1240.2	1251.2	1237.0	1228.3	1257.7	1272.9	1281.9	1276.0
$I_{sp,vac}$, sec	372.4	381.5	362.3	372.8	373.6	375.7	382.7	364.8	373.2	373.1	382.5	360.1	366.0	374.6	358.5	366.2	370.4
$I_{sp,theo}$, sec	396.5	401.7	387.5	396.1	397.2	398.0	402.5	388.6	397.3	396.7	401.9	387.2	395.0	399.3	383.3	389.9	395.4
% I_{sp}	93.9	95.0	93.5	94.1	94.1	94.4	95.1	93.9	93.9	94.1	95.2	93.0	92.7	93.8	93.5	93.9	93.7
$\frac{P_c g A_T}{\dot{w}_T}$, fps	8140	8331	7882	8118	8036	8118	8299	7860	8302	8189	8414	7892	8146	8393	7754	7863	8292
c^*_{theo}, fps	8252	8412	8025	8245	8239	8260	8402	8016	8267	8251	8414	8010	8241	8378	7945	7968	8257
% c*	98.6	99.0	98.2	98.5	97.5	98.3	98.8	98.1	100.4	99.3	100.0	98.5	98.9	100.2	97.6	98.7	100.4
ΔCDL, sec	4.9	5.1	4.6	4.9	4.8	4.8	5.1	4.6	4.9	4.9	5.1	4.6	4.8	5.1	4.6	4.5	4.9
ΔBLL, sec	6.5	6.0	6.5	6.3	6.8	6.7	6.2	7.0	6.3	6.1	5.4	6.2	6.2	5.8	6.3	7.4	6.3
ΔVL, sec	2.0	1.1	2.1	1.9	1.9	1.9	1.1	2.1	1.9	1.9	1.0	2.0	1.8	1.0	1.9	2.1	1.5
ΔI_g FL, sec	1.3	0.7	1.9	1.2	1.2	1.2	0.7	2.0	1.2	1.2	0.7	2.0	0.8	0.5	1.8	1.8	0.9
ΔFFCL, sec	0.0																
ΔERL, sec	9.5	7.2	10.1	8.9	8.8	7.6	6.7	8.2	9.8	9.5	7.2	12.3	15.3	12.4	10.2	7.9	11.4
% (ERE + MRD)	97.3	98.0	96.9	97.4	97.5	97.8	98.1	97.4	97.2	97.3	98.0	96.3	95.9	96.8	96.9	97.5	96.9
% ERE	97.6	98.2	97.4	97.7	97.8	98.1	98.3	97.9	97.5	97.6	98.2	96.8	96.1	96.9	97.3	98.0	97.1
T_{ov}, °R	579	575	572	569	557	562	565	566	575	570	564	563	512	508	525	527	509
T_{fv}, °R	575	571	565	560	547	551	551	554	577	564	560	562	522	521	527	530	517

NOTES:
(1) 25 or 50 denotes nominal igniter thrust (lbf)
S: Spark igniter
P: Plasma igniter
C: Catalytic igniter

(2) Cu: Denotes copper heat sink chamber
FFC: Denotes adiabatic film cooled chamber
Abl: Denotes ablative streak chamber

TABLE III-2 (cont.)

Test Series	2K-7		2K-8														
Run No.	102	103	102	103	104	105	107	108	109	110	111	112	113	114	115	116	117
Injector Type	"U" Triplet						Swirler Coax										
Igniter (lbf, Type)	25-S																
L^* (Chamber Type), in.	15 (Cu)						25 (Cu)									40 (Cu)	40 (Cu)
ϵ	2.89	2.89	2.92				2.88			2.90	2.90	2.91					
Test Duration, sec	1.0			0.5			1.0				2.0	2.0	0.5			1.0	1.0
Data Summary, sec	1.46-1.66	1.46-1.66	1.46-1.66	0.98-1.18	0.98-1.18	0.98-1.18	1.5-1.7	1.5-1.7	1.5-1.7	1.5-1.7	2.4-2.6	2.4-2.6	1.0-1.2	1.0-1.2	1.0-1.2	1.5-1.7	1.5-1.7
P_c, psia	313	309	308	467	460	489	303	308	316	99	102	99	480	468	469	311	318
$\dot{w}_o$, lbm/sec	2.581	3.002	2.698	4.102	4.348	3.920	2.687	2.532	3.079	0.930	0.868	0.993	4.205	3.816	4.410	2.750	3.076
$\dot{w}_f$, lbm/sec	0.845	0.587	0.689	1.051	0.868	1.340	0.716	0.877	0.607	0.228	0.293	0.198	1.133	1.252	0.934	0.742	0.619
$\dot{w}_{fI}$, lbm/sec	0.013	0.013	0.013	0.020	0.020	0.020	0.013	0.013	0.013	0.004	0.004	0.004	0.020	0.020	0.020	0.013	0.013
$(O/F)_{eng}=(O/F)_{core}$	3.01	5.01	3.85	3.83	4.90	2.88	3.68	2.84	4.97	4.01	2.92	4.92	3.65	3.00	4.63	3.64	4.86
$\dot{w}_T$, lbm/sec	3.439	3.602	3.400	5.173	5.236	5.280	3.416	3.422	3.699	1.162	1.165	1.195	5.358	5.088	5.364	3.505	3.708
F_{SL}, lbf	1197.5	1191.3	1151.5	1837.0	1797.6	1918.1	1135.8	1154.3	1195.2	291.9	306.4	299.5	1872.2	1795.3	1834.7	1161.4	1198.0
$F_a A_e$, lbf	120.3	120.3	120.4	120.7	120.6	120.6	121.2	121.2	121.2	120.7	120.7	120.5	120.4	120.4	120.4	120.4	120.4
F_{vac}, lbf	1317.8	1311.6	1271.9	1957.7	1918.2	2038.7	1257.0	1275.5	1316.4	412.6	427.1	420.0	1992.6	1915.7	1955.1	1281.8	1318.4
$I_{sp,vac}$, sec	383.2	364.1	374.1	378.5	366.4	386.1	368.0	372.8	355.9	355.1	366.5	351.5	371.9	376.5	364.5	365.7	355.6
$I_{sp,theo}$, sec	399.6	383.8	395.7	396.4	386.5	400.6	397.1	400.7	385.2	392.4	399.4	381.8	397.1	399.7	389.2	396.7	385.6
% I_{sp}	95.9	94.9	94.5	95.5	94.8	96.4	92.7	93.0	92.4	90.5	91.8	92.1	93.7	94.2	93.7	92.2	92.2
$\frac{P_c g A_T}{\dot{w}_T}$, fps	8287	7818	8172	8188	7954	8400	8201	8334	7896	7819	8087	7665	8291	8516	8100	8212	7925
c* theo, fps	8365	7950	8241	8259	8003	8391	8272	8289	7961	8154	8369	7886	8287	8370	8071	8277	7984
% c*	99.1	98.3	99.2	99.1	99.4	100.1	99.1	99.3	99.2	95.9	96.6	97.2	100.0	101.7	100.4	99.2	99.3
ΔCDL, sec	5.1	4.6	4.9	5.0	4.6	5.2	4.9	5.1	4.5	4.7	4.9	4.5	4.9	5.1	4.7	4.8	4.5
ΔBLL, sec	5.7	6.3	6.2	5.7	5.9	5.3	10.0	9.4	7.7	12.7	12.0	9.8	9.3	9.1	8.4	11.3	9.0
ΔKL, sec	1.0	1.7	1.6	1.1	1.3	0.6	1.6	0.8	1.6	5.0	2.5	5.5	1.0	0.7	1.1	1.6	1.8
ΔI_g FL, sec	0.6	1.8	1.0	1.0	1.8	0.6	0.9	0.6	1.7	1.0	0.6	1.7	0.8	0.6	1.5	0.9	1.6
ΔFCL, sec	0.0																
ΔERL, sec	3.9	5.3	7.9	5.1	6.5	2.9	11.7	12.0	13.7	13.9	12.9	8.8	9.2	7.7	9.0	12.5	13.2
% (ERE + MRD)	98.9	98.2	97.8	98.4	97.9	99.1	96.8	96.9	96.0	96.2	96.6	97.3	97.5	97.9	97.3	96.6	96.2
% ERE	99.0	98.6	98.0	98.7	98.3	99.3	97.1	97.0	96.5	96.5	96.8	97.7	97.7	98.1	97.7	96.8	96.6
T_{ov}, °R	517	516	517	523	526	523	506	508	506	510	510	508	508	510	510	506	503
T_{fv}, °R	525	524	519	526	525	528	520	521	519	515	516	515	517	514	513	N.I.	515

TABLE III-2 (cont.)

Test Series	2K-8																
Run No.	118	120	121	122	123	124	125	126	128	129	131	132	133	134	135	136	137
Injector Type	Swirler Coax	SN 3													Showerhead Coax		
Igniter (lbf, Type)	25-S	25-C		25-S											25-C		
L* (Chamber Type), in.	15 (Alb)	25 (Cu)		15 (Cu)					15 (FFC)			25 (Cu)		15 (Abl)	25 (Cu)		
% FFC	0	0	0	30	20	30	30	20	30	30	30	30	20	0			
FFC - Plane, in.	N/A			0	0	2.5								N/A			
ϵ	3.05	2.90	2.90	3.00					3.07			2.93	2.93	3.10	2.93		
Test Duration, sec	0.5	1.0									5.0	1.0	1.0	0.5	1.0	1.0	0.7
Data Summary, sec	1.0-1.2	1.5-1.7	1.5-1.7	1.1-1.3	1.1-1.3	1.1-1.3	1.1-1.3	1.1-1.3	1.0-1.2	1.2-1.4	5.0-5.2	1.3-1.5	1.3-1.5	0.97-1.17	1.4-1.6	1.4-1.6	1.1-1.3
P_c, psia	318	302	310	345	333	337*	335	328	318*	316*	320*	337*	330*	310	313	319	316
$(O/F)_{eng}$	4.81	3.89	2.98	3.62	4.10	3.59	3.76	4.18	3.67	3.64	2.73	3.58	4.00	5.10	3.71	4.95	6.05
$\dot{w}_o$, lbm/sec	3.026	2.715	2.558	3.091	3.073	3.072	3.097	3.089	3.111	3 061	2.803	3.044	3.023	3.073	2.733	3.045	3.240
$\dot{w}_f$, lbm/sec	0.617	0.683	0.842	0.592	0.593	0.592	0.569	0.584	0.586	0.581	0.711	0.587	0.597	0.590	0.720	0.599	0.519
$\dot{w}_{ffc}$, lbm/sec	0	0	0	0.249	0.143	0.252	0.242	0.142	0.249	0.247	0.302	0.250	0.145	0	0	0	0
$\dot{w}_{fi}$, lbm/sec	0.013	0.016	0.016	0.013	0.013	0.013	0.013	0.013	0.013	0.013	0.013	0.013	0.013	0.013	0.016	0.016	0.016
$\dot{w}_T$, lbm/sec	3.656	3.414	3.416	3.945	3.822	3.928	3.920	3.828	3.959	3.902	3.829	3.893	3.778	3.676	3.469	3.659	3.775
$(O/F)_{core}$	4.81	3.89	2.98	5.11	5.07	5.08	5.33	5.18	5.20	5.15	3.87	5.07	4.96	5.10	3.71	4.95	6.05
F_{SL}, lbf	1217.4	1137.8	1163.1	1290.1	1245.2	1281.0	1271.3	1246.1	1287.0	1275.5	1286.4	1294.4	1262.4	1205.1	1160.8	1191.8	1184.5
$P_a A_e$, lbf	129.4	120.0	120.0	123.4	123.4	123.6	123.6	123.6	132.2	130.9	130.7	122.2	122.2	131.6	121.9	122.0	122.0
F_{vac}, lbf	1346.8	1257.8	1283.1	1413.5	1368.6	1404.6	1394.9	1369.7	1419.2	1406.4	1417.1	1416.6	1384.6	1336.7	1282.7	1313.8	1306.5
$I_{sp,vac}$, sec	368.4	368.4	375.6	358.3	358.1	357.6	355.9	357.8	358.4	360.4	370.1	363.9	366.5	3[illegible]	369.8	359.0	3[illegible]
$I_{sp,theo}$, sec	388.8	394.9	399.3	398.4	395.1	398.6	397.6	394.4	399.2	399.4	402.8	397.4	394.6	386.0	396.4	384.8	370.9
% I_{sp}	94.8	93.3	94.1	90.0	90.6	89.7	89.5	90.7	89.8	90.2	91.9	91.6	92.9	94.2	93.3	93.3	93.3
$\frac{P_c g A_T}{\dot{w}_T}$, fps	8172	8137	8348	7868	7847	7732	7691	7724	7549	7619	7866	7897	7971	7839	8220	7936	7636
c* theo, fps	8001	8226	8367	8282	8184	8288	8257	8167	8272	8279	8392	8286	8204	7914	8258	7954	7632
% c*	102.1	98.9	99.8	95.0	95.9	93.3	93.1	94.6	91.3	92.0	93.7	95.3	97.2	99.1	99.5	99.8	100.0
Δ_{CDL}, sec	4.6	4.9	5.1	4.7	4.6	4.7	4.6	4.6	4.6	4.7	4.9	4.8	4.8	4.5	4.9	4.5	4.3
Δ_{BLL}, sec	4.1	6.9	6.3	3.7	4.8	2.5	2.4	3.2	2.0	2.0	1.9	3.0	4.2	3.5	7.4	7.6	6.1
Δ_{FL}, sec	1.9	1.7	1.0	1.3	1.6	1.4	1.5	1.7	1.6	1.5	0.7	1.4	1.6	1.9	1.6	1.8	1.6
$\Delta_{I_g FL}$, sec	1.6	1.2	0.7	0.8	1.0	0.8	0.8	1.1	0.8	0.8	0.5	0.8	1.0	1.8	1.1	2.1	3.0
Δ_{FFCL}, sec	0.0			19.0	13.5	19.9	21.6	14.5	20.6	19.5	10.7	18.3	10.7	0.0			
Δ_{FRL}, sec	8.2	11.7	10.5	10.5	11.4	13.4	10.8	11.6	11.2	10.6	14.0	6.3	5.9	10.7	11.6	9.7	9.8
% (ERE + MRD)	97.5	96.7	97.2	92.4	93.4	91.5	91.6	93.1	91.8	92.3	93.8	93.6	95.6	96.8	96.8	96.9	96.6
% ERE	97.9	97.0	97.4	97.4	97.1	96.7	97.3	97.1	97.2	97.3	96.5	98.4	98.5	97.2	97.1	97.5	97.4
T_{ox}, °R	511	501	501	497	498	500	502	503	504	505	499	503	502	503	498	[illegible]	501
T_{f_o}, °R	512	511	512	507	507	509	510	510	511	512	514	511	511	508	508	[illegible]	506

Based on F_{oJI}

TABLE III-2 (cont.)

Test Series	2K-8																
Run No.	138	139	140	141	142	143	145	146	148	149	150	151	152	153	154	157	158
Injector Type	Showerhead Coax						SN 4		SN 3-D		"I" Triplet						
Igniter (lbf, Type)	25-S						50-S		50-P		25-P						
L* (Chamber Type), in.	25 (Cu)				15 (Cu)					15(FFC)	15 (Cu)					15(FFC)	15(Abl)
% FFC	30	20	30	20	0					30	0					30	0
FFC - Plane, in.	0	0	2.5	2.5	N/A					2.5	N/A					2.5	N/A
ϵ	2.93				2.92	2.92	2.94	2.94	2.96	3.00	2.97					3.00	3.10
Test Duration, sec	1.0															5.0	0.5
Data Summary, sec	1.35-1.55	1.35-1.55	1.35-1.55	1.35-1.55	1.35-1.55	1.35-1.55	1.35-1.55	1.35-1.55	1.1-1.5	1.3-1.5	1.35-1.55	1.35-1.55	1.35-1.55	1.35-1.55	1.35-1.55	5.5-5.7	0.92-1.02
P_c, psia	346*	338*	344*	337*	311	311	300	293	314	315*	309	317	104	106	101	321*	312
$(O/F)_{eng}$	3.67	4.14	3.59	4.17	3.88	6.21	4.30	5.37	3.93	2.75	3.87	5.05	3.90	5.07	6.05	3.47	4.93
$\dot{w}_o$, lbm/sec	3.062	3.067	3.036	3.058	2.736	3.235	2.712	2.897	2.791	2.747	2.729	3.049	0.932	1.033	1.054	3.049	2.934
$\dot{w}_f$, lbm/sec	0.577	0.585	0.584	0.580	0.692	0.508	0.608	0.517	0.687	0.685	0.694	0.592	0.228	0.193	0.163	0.608	0.584
$\dot{w}_{ffc}$, lbm/sec	0.246	0.142	0.248	0.141	0.0					0.292	0.0					0.259	0.0
$\dot{w}_{fi}$, lbm/sec	0.013	0.013	0.013	0.013	0.013	0.013	0.022	0.022	0.023	0.023	0.011	0.011	0.011	0.011	0.011	0.011	0.011
$\dot{w}_T$, lbm/sec	3.898	3.807	3.881	3.792	3.441	3.756	3.343	3.436	3.501	3.746	3.434	3.652	1.171	1.236	1.228	3.926	3.529
$(O/F)_{core}$	5.19	5.13	5.08	5.16	3.88	6.21	4.30	5.37	3.93	3.88	3.87	5.05	3.90	5.07	6.05	4.93	4.93
F_{SL}, lbf	1291.8	1259.1	1289.2	1256.9	1145.2	1158.0	1110.9	1083.4	1168.6	1251.0	1148.2	1183.9	306.9	312.9	294.3	1291.9	1194.7
$P_a A_e$, lbf	120.0	120.0	119.8	119.8	118.9	118.9	120.3	120.3	121.6	128.3	120.8	120.7	120.7			129.4	132.2
F_{vac}, lbf9	1411.8	1379.1	1409.0	1376.7	1264.1	1276.9	1231.2	1203.7	1290.2	1379.3	1269.0	1304.6	427.6	433.6	415.0	1421.3	1326.9
$I_{sp,vac}$, sec	362.3	362.3	363.0	363.0	367.4	340.0	368.3	350.3	368.6	368.2	369.5	357.3	365.2	350.7	338.0	362.0	376.0
$I_{sp,theo}$, sec	396.8	393.4	397.1	393.2	395.2	368.6	388.0	376.6	395.8	401.7	396.2	384.5	394.5	380.9	367.3	399.3	388.6
% I_{sp}	91.3	92.1	91.4	92.3	93.0	92.2	94.9	93.0	93.1	91.7	93.3	92.9	92.6	92.1	92.0	90.7	96.7
$\frac{P_c g A_T}{\dot{w}_T}$, fps	8044	8047	8043	8062	8138	7471	8069	7666	8061	7908	8034	7734	7965	7651	7349	7879	8239
c* theo, fps	8268	8169	8282	8165	8223	7584	8047	7770	8224	8389	8230	7931	8182	7845	7538	8307	7974
% c*	97.3	98.5	97.1	98.7	99.0	98.5	100.3	98.7	98.0	94.3	97.6	97.5	97.4	97.5	97.5	94.9	103.2
ΔCDL, sec	4.8	4.7	4.8	4.7	4.8	4.2	4.8	4.4	4.8	4.9	4.8	4.5	4.8	4.4	4.2	4.7	4.6
ΔBLL, sec	5.4	6.5	3.6	4.8	6.8	5.2	6.5	6.1	6.3	1.9	6.1	6.1	7.9	7.8	6.7	2.0	3.4
ΔKL, sec	1.4	1.6	1.3	1.6	1.7	1.7	1.9	2.0	1.6	0.7	1.6	1.6	4.8	5.4	5.4	1.3	1.8
$\Delta$$I_g$ PL, sec	0.8	1.1	0.8	1.1	1.0	2.6	2.2	3.7	1.8	2.8	0.9	1.5	2.7	4.5	6.5	0.6	1.5
ΔFFCL, sec	12.1	7.4	13.5	8.1	0.0					10.4	0.0					17.8	0.0
ΔIRL, sec	10.0	9.9	10.0	9.9	13.6	14.9	4.3	10.1	12.8	12.9	13.3	13.5	9.1	8.1	6.5	10.9	1.3
% (ERE + MRD)	94.2	95.3	93.9	95.1	96.3	95.3	98.3	96.3	96.3	92.5	96.4	96.1	97.0	96.7	96.5	92.7	99.3
% ERE	97.5	97.5	97.5	97.5	96.6	96.0	98.9	97.3	96.8	96.8	96.6	96.5	97.7	97.9	98.2	97.3	99.7
T_{ov}, °R	496	497	498	499	498	498	329	334	505	510	507	509	511	511	509	512	523
T_{fv}, °R	505	506	507	507	507	507	344	344	512	514	513	513	515	515	514	514	528

*Based on P_{oJ1}

TABLE III-2 (cont.)

Test Series	2K-8 →																
Run No.	159	160	161	163	166	167	169	170	171	172	173	174	175	176	177	178	179
Injector Type	"I" Triplet →																
Igniter (lbf, Type)	25-S →															Recessed	Swirl Coax
L* (Chamber Type), in.	15 (Cu) →			20(FPC) →		15 (Cu) →				20 (Cu) →				15 (Cu) →			
% FPC	0 →			30	30	0	30	20	30 →					20	20	30	20
FPC - Plane, in.	N/A →			2.5	2.5	N/A	1.0 →			2.5 →				1.0	1.0	0	0
ϵ	2.95 →			3.03	3.03	2.96	2.92	2.92	2.94 →					2.93 →			
Test Duration, sec	2.0 →			10.0	1.0	2.0 →											
Data Summary, sec	2.3-2.5	2.3-2.5	2.3-2.5	10.3-10.5	1.2-1.4	2.5-2.7	2.2-2.4	2.2-2.4	2.2-2.4	2.2-2.4	2.2-2.4	2.2-2.4	2.2-2.4	2.2-2.4	2.2-2.4	2.2-2.4	2.2-2.4
P_c, psia	310	314	313	331*	473*	318	298	295	467	488	301	297	99	288	284	310	298
$(O/F)_{eng}$	3.82	4.87	5.89	3.45	3.52	2.96	2.97	3.42	3.34	3.63	3.34	3.55	3.47	3.59	4.22	4.16	3.68
$\dot{w}_o$, lbm/sec	2.719	2.984	3.178	3.152	4.516	2.566	2.612	2.668	4.255	4.554	2.767	2.786	0.938	2.675	2.771	3.040	2.761
$\dot{w}_f$, lbm/sec	0.701	0.602	0.528	0.633	0.888	0.855	0.610	0.619	0.882	0.867	0.574	0.544	0.187	0.595	0.521	0.506	0.595
$\dot{w}_{ffc}$, lbm/sec	0.0 →			0.268	0.377	0.0	0.259	0.150	0.376	0.368	0.243	0.230	0.080	0.140	0.124	0.214	0.143
$\dot{w}_{fI}$, lbm/sec	0.011	0.011	0.011	0.011	0.019	0.011	0.011	0.011	0.018	0.018	0.011	0.011	0.004	0.011	0.011	0.012	0.011
$\dot{w}_T$, lbm/sec	3.451	3.597	3.717	4.064	5.800	3.432	3.492	3.448	5.531	5.807	3.595	3.571	1.209	3.421	3.427	3.772	3.510
$(O/F)_{core}$	3.82	4.87	5.89	4.89	4.98	2.96	4.21	4.24	4.72	5.14	4.73	5.02	4.91	4.42	5.21	5.88	4.55
F_{SL}, lbf	1158.7	1176.8	1171.5	1360.2	2007.0	1186.4	1150.3	1143.7	1880.1	1985.0	1177.3	1162.8	310.9	1103.9	1084.8	1189.3	1139.3
$P_a A_e$, lbf	121.3	121.3	121.3	130.4	130.4	121.4	124.8	124.8	125.1	125.1	125.0 →			124.0	124.0	125.5	125.5
F_{vac}, lbf	1280.0	1298.1	1292.8	1490.6	2137.4	1307.8	1275.1	1268.5	2005.2	2110.1	1302.3	1287.8	435.9	1227.9	1218.8	1314.8	1264.8
$I_{sp,vac}$, sec	373.0	360.9	347.8	366.7	368.5	381.0	365.2	367.9	362.5	363.4	362.3	360.7	360.5	358.9	355.6	348.6	360.3
$I_{sp,theo}$, sec	396.0	386.1	373.3	399.7	399.3	400.4	399.2	397.5	398.0	396.9	398.2	397.2	396.7	390.5	388.7	392.2	395.3
% I_{sp}	94.2	93.5	93.2	91.8	92.3	95.1	91.5	92.6	91.1	91.6	91.0	90.8	90.9	91.9	91.5	88.9	91.1
$\frac{P_c g A_T}{\dot{w}_T}$, fps	8105	7830	7543	7654	7650	8288	7985	7998	7906	7870	7856	7802	7673	7885	7755	7689	7925
c* theo, fps	8236	7978	7680	8307	8300	8369	8355	8299	8309	8271	8311	8279	8266	8139	8059	8139	8237
% c*	98.4	98.2	98.2	92.1	92.2	99.0	95.6	96.4	95.1	95.2	94.5	94.2	92.8	96.9	96.2	94.5	96.2
ΔCDL, sec	4.9	4.6	4.3	4.8	4.8	5.1	4.9	4.9	4.8 →					4.7	4.6 →		
ΔBLL, sec	5.8	6.1	5.4	2.1	2.0	5.5	3.2	4.2	2.9	2.5 →			3.1	3.6	3.5	3.7	4.8
ΔKL, sec	1.7	1.8	1.7	1.3	1.0	1.0	1.1	1.5	0.9	1.0	1.4	1.6	4.2	1.7	2.0	1.8	1.7
Δl_g FL, sec	0.9	1.4	2.0	0.6	0.7	0.5	0.5	0.7	0.7	0.7	0.6	0.7	0.7	0.8	1.1	1.0	0.8
ΔFFCL, sec	0.0	0.0	0.0	17.9	17.6	0.0	13.0	9.6	17.6	17.9	16.8	18.8	21.3	10.1	13.5	23.7	10.9
ΔERL, sec	9.7	11.3	12.2	6.3	4.7	7.4	11.3	8.7	8.6	6.6	9.8	8.1	2.1	10.7	8.4	8.8	12.2
% (ERE + MRO)	97.3	96.7	96.2	93.8	94.2	98.0	93.8	95.0	93.3	93.7	93.2	93.1	93.9	94.5	94.1	91.4	93.9
% ERE	97.5	97.1	96.7	98.4	98.8	98.2	97.2	97.8	97.8	98.3	97.5	98.0	99.5	97.3	97.8	97.7	96.9
T_{ov}, °R	492	499	507	500	491	499	356	371	341	326	358	365	359	347	303	316	352
T_{fv}, °R	505	506	508	513	506	513	519	519	513	522	523	522	523	289	353	491	494

*Based on P_{oJI}

TABLE III-2 (cont.)

Test Series	2K-8						
Run No.	180	181	182	183	184	185	186
Injector Type	Recessed	Swirl Coax					I-Triplet
Igniter (lbf, Type)	25-S						
L* (Chamber Type), in.	15 (Cu)	15(Abl)	20 (Cu)				15 (Cu)
% FFC	20	10	0	0	30	30	20
FFC - Plane, in.	0	0	N/A	N/A	2.5	2.5	0
ϵ	2.93	3.09	2.93				
Test Duration, sec	2.0	0.5	2.0				1.0
Data Summary, sec	2.2-2.4	0.8-1.0	2.2-2.4	2.2-2.4	1.4-1.5	2.2-2.4	1.2-1.4
P_c, psia	449	333	284	278	307	300	314
$(O/F)_{eng}$	3.75	4.72	4.65	5.65	3.31	3.71	4.09
$\dot{w}_o$, lbm/sec	4.169	3.212	2.789	2.926	2.821	2.860	3.018
$\dot{w}_f$, lbm/sec	0.880	0.606	0.589	0.506	0.593	0.534	0.587
$\dot{w}_{ffc}$, lbm/sec	0.214	0.064	0	0	0.249	0.226	0.140
$\dot{w}_{fI}$, lbm/sec	0.018	0.011					
$\dot{w}_T$, lbm/sec	5.281	3.893	3.389	3.443	3.674	3.631	3.756
$(O/F)_{core}$	4.64	5.20	4.65	5.65	4.67	5.24	5.05
F_{SL}, lbf	1781.8	1281.6	1089.5	1069.8	1170.4	1145.7	1222.1
$P_a A_e$, lbf	125.5	131.7	125.3				125.2
F_{vac}, lbf	1907.3	1413.3	1214.8	1195.1	1295.7	1271.0	1347.3
$I_{sp,vac}$, sec	361.2	363.0	358.5	347.1	352.6	350.1	358.7
$I_{sp,theo}$, sec	395.6	390.1	387.6	375.0	393.8	393.5	390.7
% I_{sp}	91.3	93.1	92.5	92.6	89.5	89.0	91.8
$\frac{P_c g A_T}{W_T}$, fps	7948	7958	7837	7551	7807	7723	7837
c^*_{theo}, fps	8239	8011	8022	7726	8205	8189	8107
% c*	96.5	99.3	97.7	97.7	95.1	94.3	96.7
ΔCDL, sec	4.5	4.5	4.5	4.5	4.7	4.6	4.7
ΔBLL, sec	4.4	3.6	8.0	6.5	2.7	2.7	4.8
ΔKL, sec	1.1	1.8	2.0	2.0	1.4	1.7	1.7
ΔI_g FL, sec	0.9	1.3	1.4	2.1	0.6	0.8	0.9
ΔFFCL, sec	10.1	7.1	0	0	16.2	19.9	12.9
ΔERL, sec	13.4	8.8	13.2	12.8	15.6	13.7	7.0
% (ERE + MRD)	93.8	95.6	96.2	96.0	91.8	91.3	94.7
% ERE	96.6	97.7	96.6	96.6	96.0	96.5	98.2
T_{ov}, °R	370	342	369	370	371	389	379
T_{fv}, °R	492	503	508	506	341	399	376

*Based on $P_{o,I}$

III, A, Program Progress (By Task) (cont.)

reproducible performance for the most efficient injector configuration tested (the I-triplet at 20 L*). The relative ranking of the remaining injector configurations indicates the triplet and showerhead coaxial to be close seconds and the swirler coaxial to be lowest ranking.

The second dashed line at 94.8% ERE indicates the lowest injector energy release plus mixture ratio distribution efficiency which can be employed in conjunction with the selected 40:1 Rao nozzle contour and still maintain the performance goal of 435 sec. The intersection of this line with the experimental performance line for each injector at the respective L* values determines the maximum amount of fuel which can be employed as fuel film coolant for extending chamber life at a nominal thrust chamber mixture ratio of 4.0. Longer L* values allow additional film cooling to be employed. The swirler coaxial design allows the least amount of film cooling (approximately 12%), while the maximum amounts range between 22 and 25% for the other injectors, depending on L*.

Figure III-26 shows: (1) the influence of characteristic chamber length (L*) for each design at mixture ratios of 4 and 5, (2) the effect of chamber pressure at mixture ratio of 4.0, and (3) the influence of oxidizer temperature on the 0% film cooling energy release efficiency. Energy release efficiency is noted to increase with chamber pressure and remain unaffected by oxidizer inlet temperature.

c. Injector Performance Evaluation

This section is subdivided into four headings: Section (1) presents the sea level (ε = 3) uncooled injector performance summary. Section (2) compares the hot fire mixing data with the empirical cold flow mixing results. Data supporting the validity of the film-cooled performance evaluation model as applicable to sea level testing is presented in Section (3). The last

III, A, Program Progress (By Task) (cont.)

section extrapolates the sea level test results to ε = 40 flight vacuum performance. The analytical performance model which was used to evaluate APS test data is described in the last quarterly report and was therefore omitted from this document.

(1) Uncooled Injector Energy Release Efficiency

I-Triplet Injectors

Three I-triplet injector assemblies were tested. The thrust based ERE results are tabulated in Table III-2 and shown graphically in Figure III-25. The first unit fired (SN 5) gave very high performance (98.0 to 99.3% ERE) at mixture ratios between 3 to 5 at both P_c = 300 and 500 psia. The second unit (SN 2A) was converted from a triplet pattern by bonding on a new set of face plates, while the third assembly was SN 5 with a second set of identical face plates designated 5A. Experimental energy release efficiency of the three assemblies were reproducible within a 1% band with the exception of one data point at mixture ratio of 5.0. The first unit tested provided the upper limit, while the second provided the lower. The deviation of the first two about the nominal, or third assembly data, provided a variance of $\pm$0.5%, which is about equal to the level of experimental accuracy. SN 5A I-triplet operated at intermediate ERE's between 97 and 98% at 15 L* and is considered representative of "I" injector performance. Backed out ERE's from three film-cooled tests at 20 L* indicate as much as 1% higher ERE than for 15 L*. This represents a higher gain with L* than for any other injector.

Triplet Injectors

Two assemblies of the triplet pattern were tested (SN 3 and 4). A variation of the triplet pattern (SN 3D) was obtained by crimping the fuel element to bias the fuel impingement momentum inboard toward the chamber axis to improve chamber compatibility.

III, A, Program Progress (By Task) (cont.)

The normal triplet injectors deliver from 0 to 1% lower ERE than the "I" configuration, depending upon the mixture ratio and L*. Although the triplet injectors at best can only approach the "I" performance, they have the advantage of operating at lower injector face temperatures due to the fuel-rich periphery around each element. If injector face life cycle is a primary consideration, it may be preferable to sacrifice a few seconds in performance to obtain the lower face temperature by using SN 3D or SN 4 injector. Chamber compatibility and heat flux appear comparable for both normal and I-triplet injector patterns. Testing of the crimped injector to determine its success in improving chamber compatibility was very limited, although wall temperatures appeared to be more uniform in the few tests conducted. However, to take full advantage of this modification, it must be tested in a lower contraction ratio chamber with conical walls parallel to the resultant momentum of the injected stream.

Swirler Coaxial Injector

The swirler coaxial element injector was tested with both a shallow and a deep recess. Both configurations had identical (96.6 to 97.0%) ERE, indicating that the recess had no influence on performance. Furthermore, increasing L* from 20 to 40 in. merely resulted in lower engine performance due to an increase in chamber (boundary layer) heat loss with no discernible improvement in ERE. Besides being the lowest performer of any injector tested, the swirler coaxial also had the highest chamber heat flux. Because of these undesirable injector characteristics, the concept has been dropped from further evaluation.

Showerhead Coaxial Injector

At 15 L*, the showerhead coaxial operates at 0.5% lower ERE than the swirler coaxial. However, it delivers approximately 0.5% higher ERE than the swirler at 25 in. L*. Chamber heat flux on the showerhead

III, A, Program Progress (By Task) (cont.)

is intermediate between the swirler and the triplets. The showerhead coaxial continues to produce high heat fluxes in the nozzle convergent section upstream of the throat. This is attributed to the oxidizer-rich core beneath each element. The cooling performance loss is significantly lower per percent fuel film coolant on the showerhead design than for the triplets. This indicates the oxidizer-rich core from each element is reacting with the fuel coolant in the nozzle convergent zone. Although this may appear to be an advantage from the performance standpoint, the advantage is lost because the coolant reaction results in a slower rate of heat flux reduction per percent coolant.

(2) Comparison of Cold Flow Data with Hot Test Results

When it is assumed that the injection mixture ratio distribution due to injector manifolding is reasonably uniform (as demonstrated in manifold cold flow tests), loss can be attributed to local mixture ratio striations within a single injection element. The mixing efficiency of an element is characterized by the parameter E_m, which is a mass weighted measure of the average local mixture ratio deviation from the overall injection mixture ratio. This was discussed in the first quarterly report under cold flow testing, which documented the empirical cold flow injection element test programs which were conducted to optimize the triplet and coaxial injection element designs. The triplet and I-triplet element designs were characterized reasonably well by the cold flow tests. The hot fire test results qualitatively substantiated the cold flow mass and mixture ratio profiles. This was especially true in its predicted enhancement of injector face and chamber wall compatibility. In absolute terms, however, the hot fire mixing efficiencies were considerably lower than those expected on the basis of cold flow testing. Cold flow testing indicated it was possible to achieve reasonably uniform mixture ratio distributions on the order of 1 in. from the injector face. Hot fire data, on the other hand, still indicate significant local mixture ratio gradients still exist

III, A, Program Progress (By Task) (cont.)

5 to 8 in. from the injector at the nozzle throat plane, as indicated from ERE data if it is assumed that the injection mixture ratio distribution due to injector manifolding was uniform.

An analytical energy release model was formulated by dividing the injector into two stream tubes. Stream tube 1 was assumed to be lower than the nominal overall mixture ratio by the factor E_m. Stream tube 2 was assumed to be higher by the reciprocal of E_m. Energy release efficiencies were then predicted for both sea level (ε = 3) and vacuum (ε = 40) nozzle exit area ratios for overall engine mixture ratios ranging from 3 to 6. The results are shown in Figure III-27. By comparing the ERE's tabulated in Table III-2 with the model depicted in Figure III-27, the hot fire mixing efficiency (E_m) is seen to vary from approximately 0.58 to 0.72 instead of the 0.90 to 0.99 values anticipated from cold flow E_m data.

This apparently poor correlation between cold flow and hot fire mixing results is thought to be caused by the energy released by the combustion products which are not present during cold flow. Thus, in cold flow, chemically inert gases are hydraulically mixed as a function of injection element hydraulics. During hot firing, however, the combustion which occurs on the interface between the fuel and oxidizer streams presents a high energy gradient against which both the oxidizer and fuel must migrate against before they are allowed to mix with the other. This condition is analogous to the "blow apart" phenomenon of hypergolic liquid propellant streams which causes spray separation.

(3) Cooled Injector Performance

The film coolant performance loss model was analytically described in Quarterly Report No. 2. Briefly, the requirement for fuel film coolant penalizes the injector performance by the following physical mechanisms:

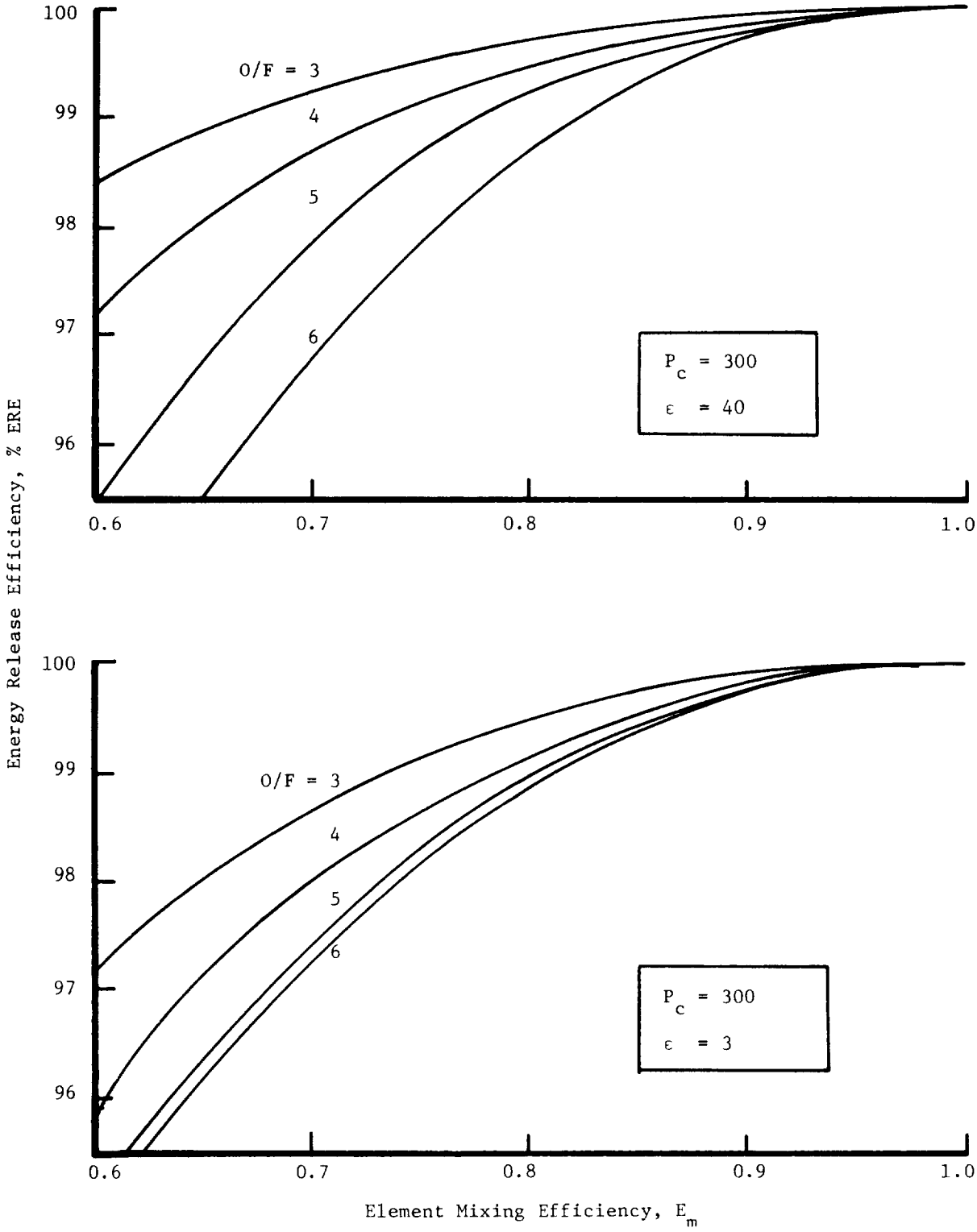

Effect of Element Mixing Efficiency on ERE

Figure III-27

III, A, Program Progress (By Task) (cont.)

(a) At a given overall engine mixture ratio, provision for chamber film coolant raises the core mixture ratio which lowers the theoretical I_{sp} of the core.

(b) Enthalpy is extracted from the core combustion gases to raise the temperature of the coolant which further reduces the core performance.

(c) Higher core mixture ratio increases the nozzle kinetic loss due to greater thermal dissociation of the combustion gas products.

(d) A higher core mixture ratio alters the element mixing efficiency (E_m).

In the above coolant performance loss model, it is assumed that there is no chemical interaction between the core and film coolant combustion gases. The validity of this assumption depends upon the injector and operating mixture ratio as described in the following subsections.

Impinging Coaxial (Triplet) Injectors

Cooled injector performance efficiencies for the SN 3 and 4 triplets and the I-triplet injectors are shown in Figure III-25. The ERE for these injectors, which were backed out from film-cooled performance data, agree identically with uncooled ERE data below 4.0 core mixture ratio, supporting the validity of the no interaction assumption. At 5.0 core mixture ratio, the cooled performance efficiency is 0.5 to 1.0% higher than the sum of the uncooled ERE and the analytical no interaction film cooling performance decrement. This indicates a weak interaction at high core mixture ratios in which the fuel coolant chemically reacts with some portion of the core, improving performance. It is reasonable to expect the interaction to occur at high core mixture ratio since thermal dissociation and oxidizer-free radical concentrations increase as the stoichiometric mixture ratio is approached. The combined analytical/experimental cooled injector efficiency is shown vs % fuel film coolant at nominal engine mixture ratio for the various injectors on the bottom half of Figure III-25.

III, A, Program Progress (By Task) (cont.)

Showerhead Coaxial Injector

The film-cooled showerhead coaxial injector demonstrated 1.5 to 2.0% interaction gain between the fuel coolant and the core gases. This was two to three times the interaction of the triplet and I-triplet injectors.

Swirler Coaxial Injector

The film-cooled swirler coaxial performance data indicates nil coolant interaction like the triplet injectors. Besides having a lower uncooled injector ERE, no ERE improvement with longer chamber length, and highest chamber heat flux, the lack of coolant interaction performance gain makes the swirler coaxial injector the least attractive injector to develop from both injector performance and chamber compatibility standpoints.

(4) Performance Extrapolation to $\varepsilon = 40$

The low ($\varepsilon = 3$) area ratio sea level performance data were extrapolated to $\varepsilon = 40$ vacuum design conditions for the 20 L* film-cooled chamber at 4.0 overall engine mixture ratio. Ambient inlet temperature propellants were assumed for 300 psia nominal chamber pressure. Both uncooled and 20% fuel film coolant cases were calculated for the SN 3 and 4 normal triplet, the I-triplet, and the showerhead coaxial injector designs.

Extrapolated Injector Efficiency

The low area ratio ERE data were used to back out a hot fire mixing efficiency which was then used to extrapolate a high area ratio ERE. Higher nozzle exit area ratios cause the peak I_{sp} to occur at higher mixture ratio. Below a core mixture ratio of 5.3, the $\varepsilon = 40$ ERE exceeds the

III, A, Program Progress (By Task) (cont.)

ε = 3 ERE for a given E_m. Above 5.3, the high area ratio ERE is lower. This is shown in Figure III-28. Therefore, the greater the amount of fuel film coolant required, the lower will be the ERE as a result of the higher core mixture ratio as will be discussed further in the next section.

Figure III-29 provides a tabulation of the hot fire E_m for both the uncooled and 20% film cooled core mixture ratio for the three injectors. However, the energy release loss is only specified at the uncooled core mixture ratio. The interaction loss (or gain) is attributed solely to the fuel film cooling performance loss. Although part of the fuel film cooling performance loss due to performance interactions actually manifests itself in the energy release loss or the nozzle kinetic losses, it is attributed to the cooling loss for clarity of discussion on the basis that, if the coolant requirement were eliminated, the performance loss interactions on ERE and nozzle kinetics would also be eliminated.

To extend the APS igniter life cycle, once thruster ignition is accomplished, the oxidizer to the igniter is terminated but the fuel to the igniter is left on at full flow to keep the igniter cooled. For the 25 lbf thrust spark igniter assumed for this extrapolation, this amounts to 2% of the total fuel flow rate to the thruster. The performance loss associated with the igniter fuel coolant flow rate is a 1.0-sec I_{sp} penalty on the overall thruster performance. If the igniter can be cooled with less fuel flow rate, this sacrifice in performance can be salvaged.

Another 1.0-sec performance loss results due to argon (and trace N_2) contamination within the specification oxygen propellant. The substitution of chemically inert argon and nitrogen in place of oxygen produces an enthalpy loss of the above magnitude.

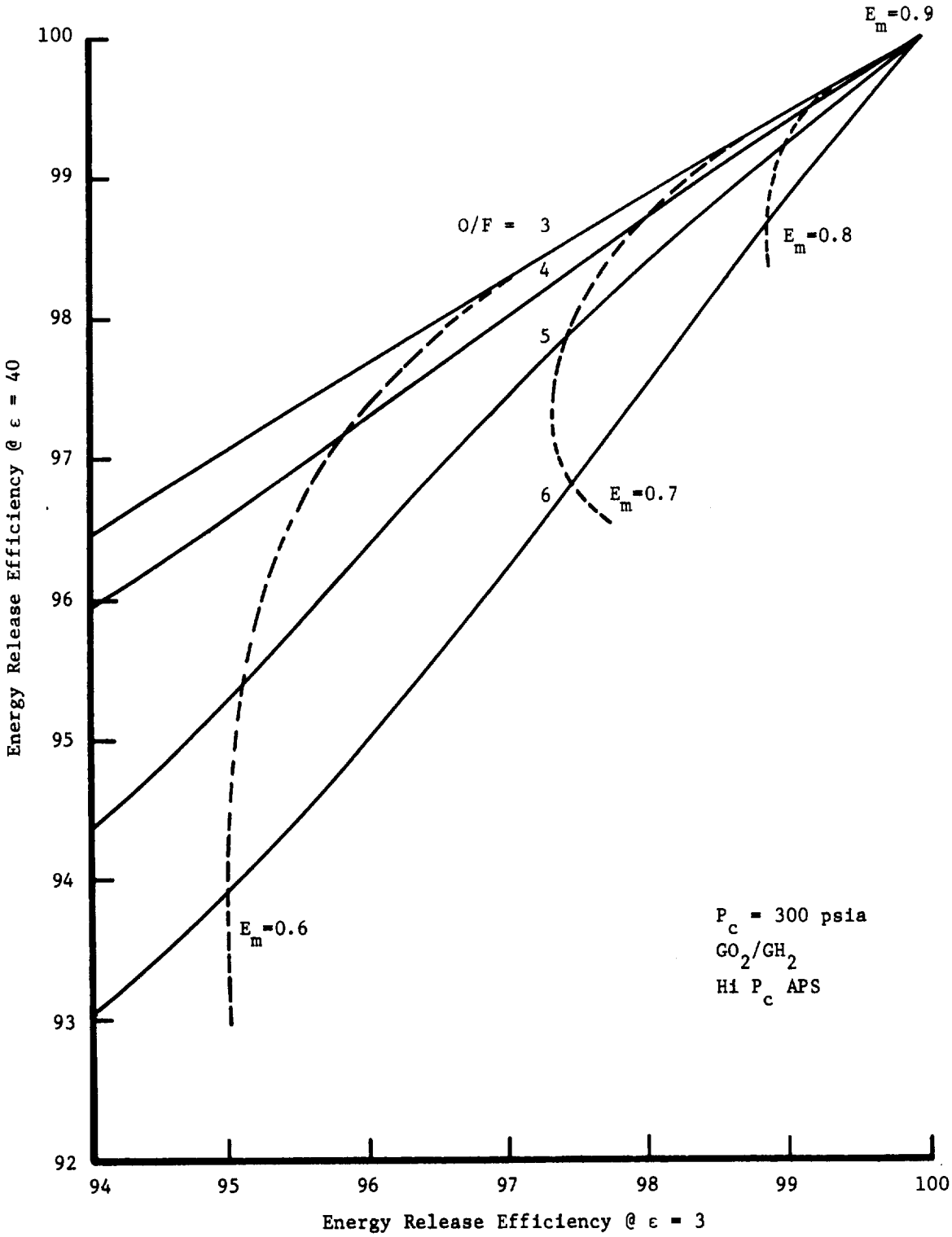

Effect of Nozzle Exit Area Ratio on ERE

Figure III-28

P_c = 300 psia
O/F = 4.0
ε = 40 Rao
L* = 20
$T_o = T_f$ = 540°R

$I_{sp(vac,theo)}$	474.3
Argon contaminant loss	1.0
Nozzle kinetic loss	4.2
Igniter fuel cooling loss	1.0
Boundary layer loss	6.0
Mixture ratio maldistribution loss	0.0

Injector type	I-Triplet		Triplet		Showerhead Coaxial	
Percent fuel film coolant, % FFC	0	20	0	20	0	20
Mixing efficiency, E_m	0.69	0.71	0.64	0.70	0.63	0.68
Energy release loss, ΔERL, sec	7.7	7.7	11.7	11.7	12.6	12.6
Fuel film cooling loss, ΔFFCL, sec	0	14.3	0	11.2	0	12.1
Curvature-divergence loss, ΔCDL, sec	3.6	3.4	3.5	3.4	3.5	3.4
Predicted performance						
$I_{sp(vac,pred)}$, sec	450.8	436.7	446.9	435.8	446.0	434.0

Figure III-29

Extrapolated Flight Performance

III, A, Program Progress (By Task) (cont.)

Extrapolated Nozzle Efficiency

The curvature divergence efficiency of the 40:1 Rao contour is 99.2%. This results in a performance loss between 3.4 to 3.6 sec in I_{sp}, depending upon the delivered performance.

The theoretical nozzle kinetic loss at 4.0 overall engine mixture ratio with completely mixed and combusted propellants is 4.2 sec in the above nozzle. The additional kinetic loss due to mixture ratio maldistribution within the core was assigned to the energy release loss. This was done because, if there were a perfect (100% E_m) injector, there would be no additional kinetic losses. Similarly, the kinetic/fuel film cooling interaction loss was attributed only to the cooling loss since it could be eliminated by eliminating the film cooling requirement.

The nozzle boundary layer loss was calculated to be 6.0 sec and constant for all operating conditions pending further definition of the chamber design and insulating method.

Predicted Performance Extrapolation

It is predicted from the above extrapolations that the uncooled $\varepsilon = 40$ performance with ambient temperature propellants is approximately 450 sec with the I-triplet at 4.0 injector mixture ratio in a 20 L* chamber. Approximately 20% fuel film coolant flow rate is allowable to satisfy the 435 sec I_{sp} goal of the contract. With a less efficient injector or shorter chamber L*, less fuel coolant flow rate will be allowable.

III, A, Program Progress (By Task) (cont.)

d. Stability Testing

Stability Tests 2K8-187, -188, and -189 were conducted in a 15 L* copper heat sink chamber instrumented with two flush-mounted Photocon 307 transducers located 120 degrees apart and 1-in. downstream of the injector as shown schematically in Figure III-30. All tests were conducted with SN 2 ("I" pattern) impinging coaxial element injector using cold propellants. The test conditions are summarized in Table III-3. The combustion dynamic stability was evaluated by perturbing the chamber pressure with a thermally detonated 2-grain Teflon-encased RDX charge. The results of one of these stability tests is displayed in Figures III-30 and III-31. Prior to bomb detonation, peak-to-peak pressure amplitude oscillations are approximately 5% of chamber pressure, otherwise stated as 300 psia $\pm$ 7.5 psi. The bomb detonation resulted in a nominal 200% overpressure as recorded by the Photocon pressure transducers. From Figure III-30, in which each major time division represents 0.001 sec, it can be seen that the pressure oscillations decay to within a few percent of the pre-excited state in 0.006 sec. Figure III-31 shows the results of a spectral density analysis of the chamber pressure oscillations at all frequencies. Also shown are the predicted frequencies at which some resonance could be expected.

9. Task IX - Cooled Chamber Testing

As a result of the stop work order on Low P_c chamber testing and redirection of the program to provide an expanded High P_c test program with cold propellants, it is now planned to conduct all High P_c testing in altitude cell J-3 rather than J-4. Test Stand J-3, currently being employed in Low P_c testing, now contains propellant flow control valves, tube type heat exchanger for propellant condition, and the potential for more cost effective altitude testing.

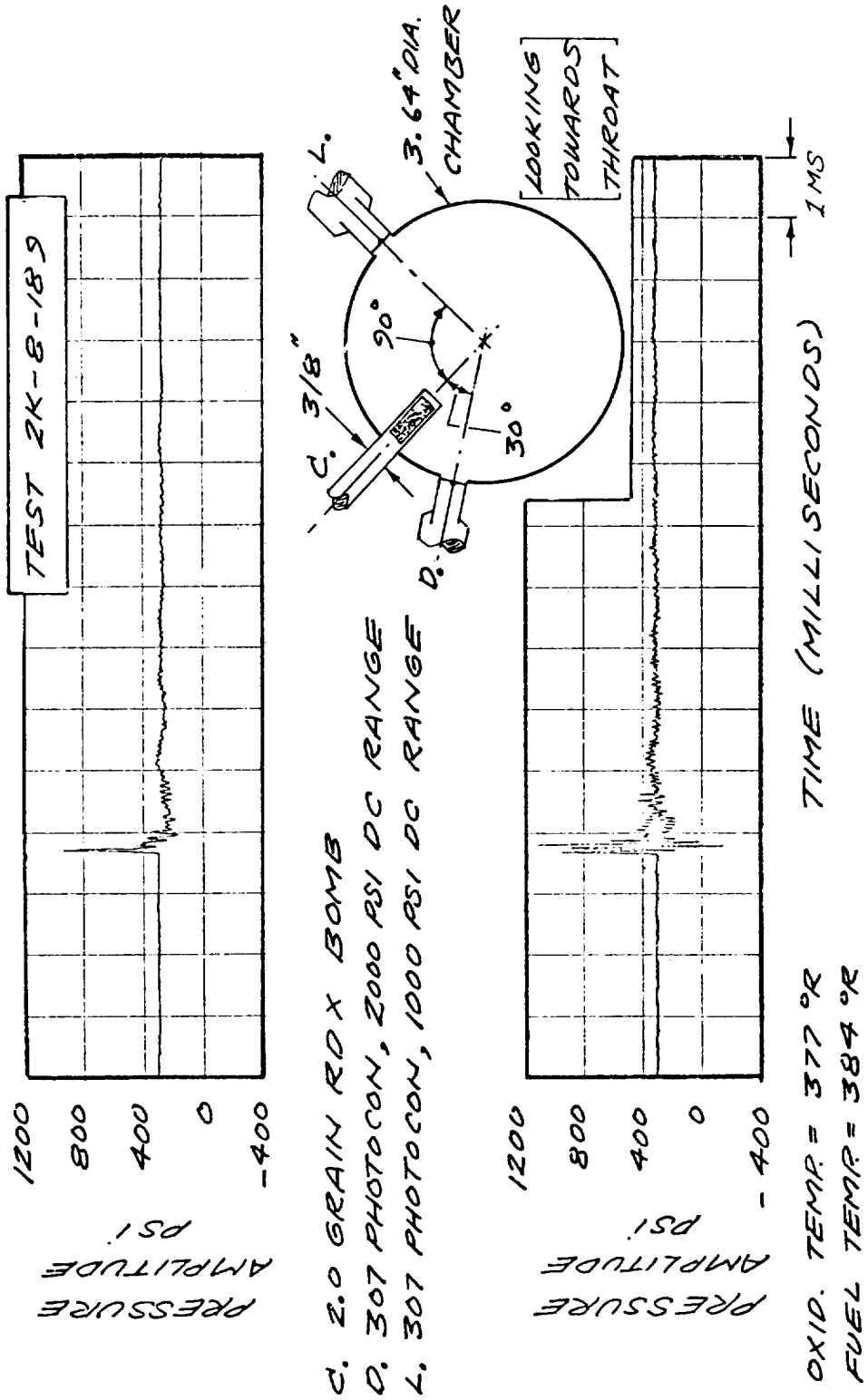

Combustion Stability Bomb Test Results

Figure III-30

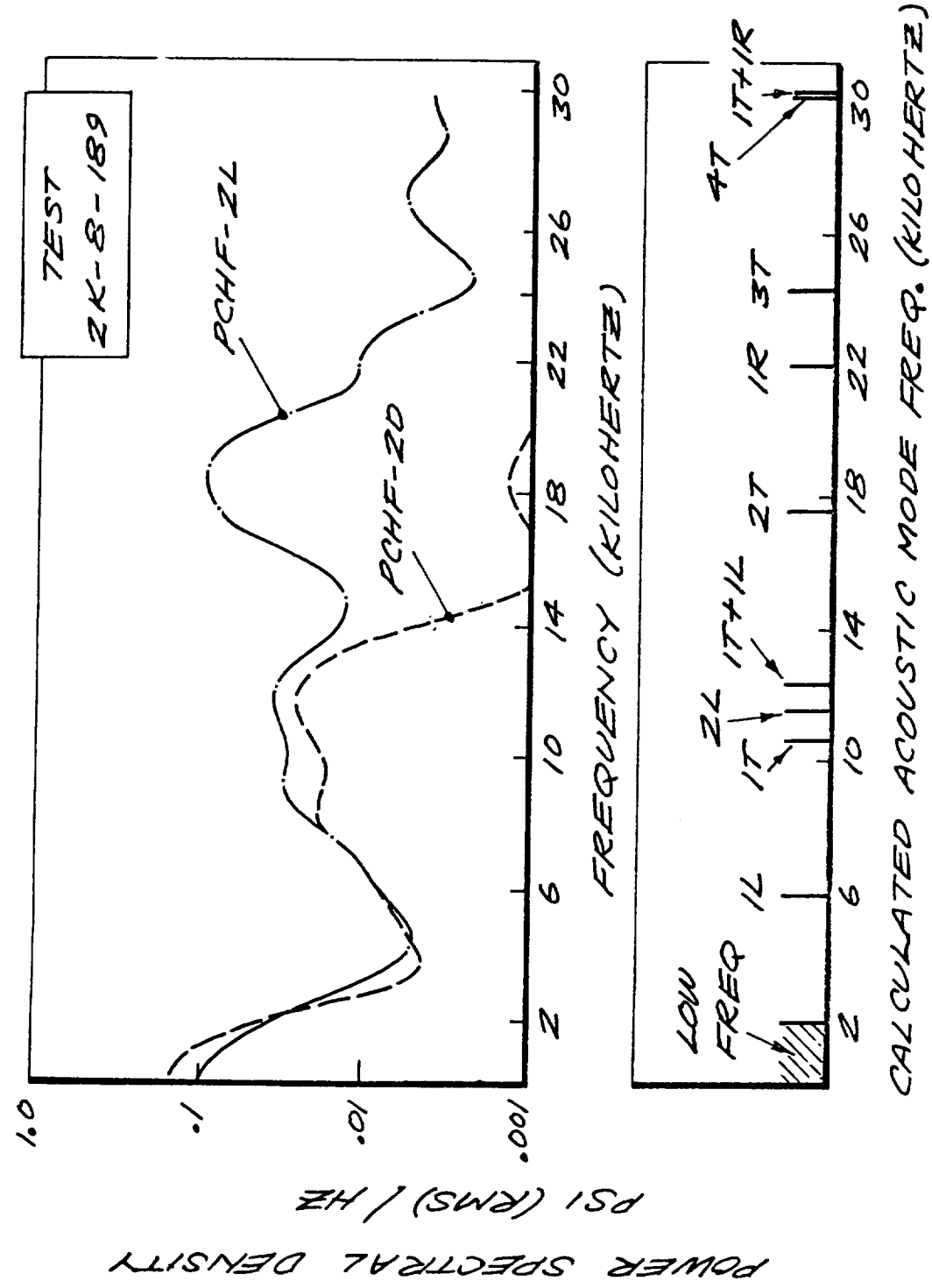

Spectral Analysis of Bomb Test Data

Figure III-31

Table III-3

SUMMARY OF STABILITY TESTING

Test No.	Propellant Temp, °R		P_c 2K*	P_c 1K
	Oxidizer	Fuel		
2K-8-187	408	400	680/680	580/670
2K-8-188	360	390	230/370	510/240
2K-8-189	377	384	720/720	650/810

*Initial ΔP/maximum ΔP, psia

III, A, Program Progress (By Task) (cont.)

A preliminary plan for testing the 40:1 area ratio cooled thrust chambers in Test Stand J-3 was prepared for presentation at a 2 March program review with the NASA program manager. This test plan was based on transient thermal analyses conducted during the last report period to determine the fire durations required to approach thermal steady state of the film-cooled nozzle at 40:1 area ratio (the slowest responding location). This analysis provided the following estimated times:

% of Steady-State Temperature	Seconds
95	70
98	140

Because of the long skirt warmup times, the recommended test plan includes evaluating several film cooling flow rates and thrust chamber mixture ratios, during a long single burn, to incorporate improvements suggested by the NASA project manager. The preliminary test plan was revised. The final test planning document was essentially complete at the close of the report period. This document, which will be submitted for NASA approval prior to testing, defines test objectives, instrumentation, thrust and flow measurement techniques, and data accuracy. Figures III-32 and III-33 provide flow and instrumentation schematics for the two designs to be tested.

Task IX testing is now scheduled to begin in mid-April.

10. Task X - Pulse Testing

Durability of the new Brute III DC power supply (which provides a single power source for the two igniter valves, two thrust chamber valves and a film cooling valve and the spark igniter and thrust chamber valves discussed*

*Quarterly Report No. 2

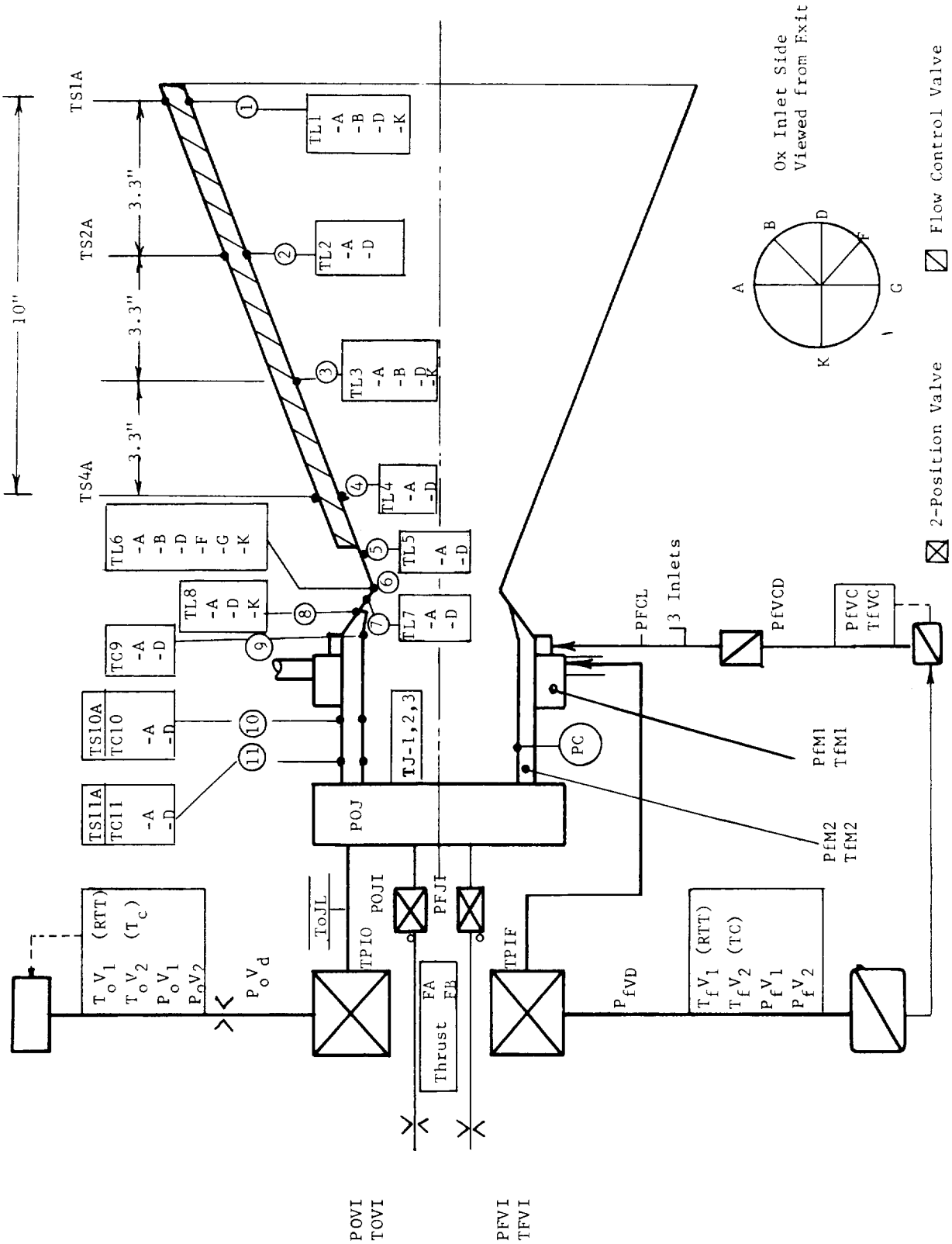

Film-Cooled Chamber Instrumentation - PN 1160334

Figure III-32

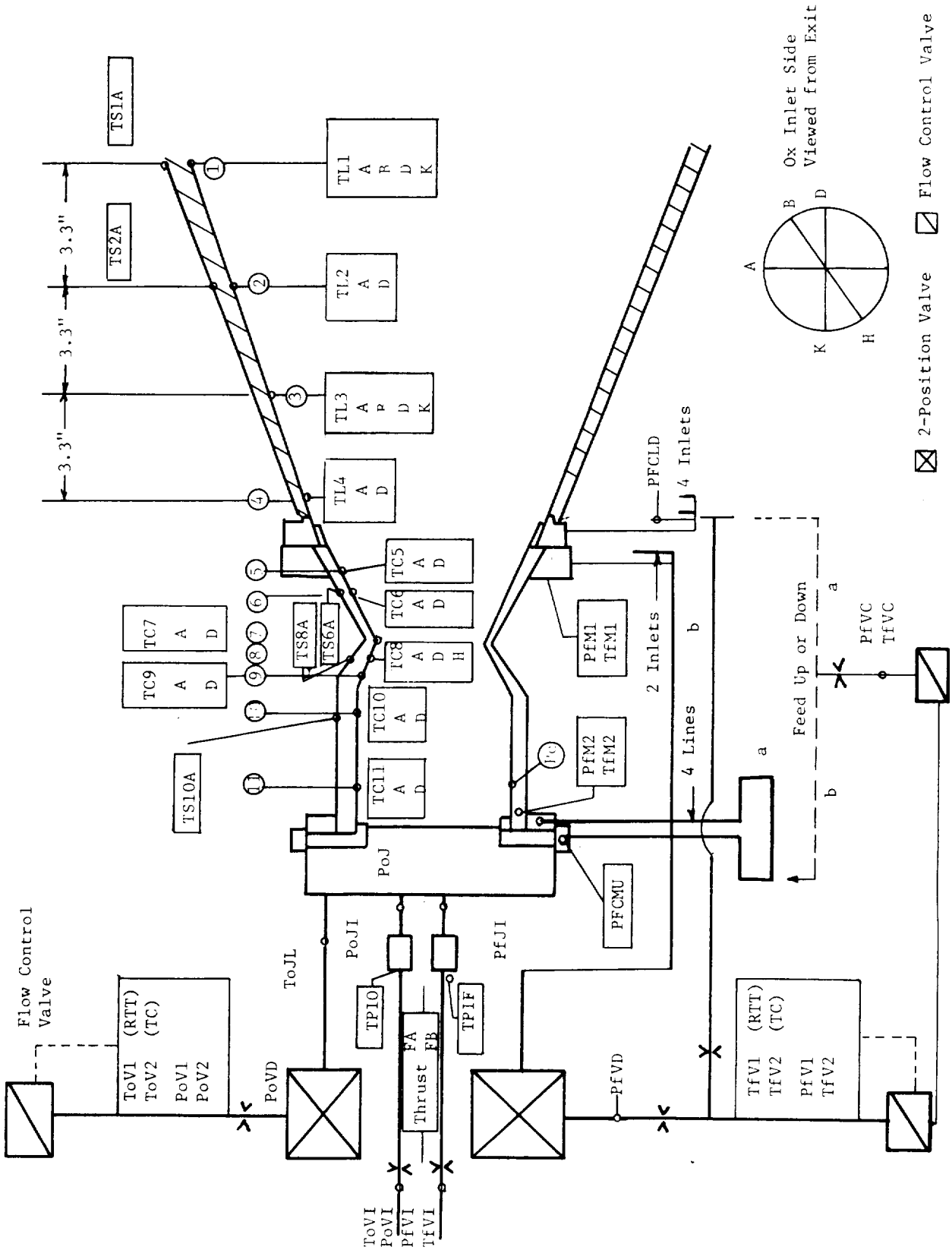

Regeneratively Cooled Chamber Instrumentation - PN 1160313

Figure III-33

III, A, Program Progress (By Task) (cont.)

in Tasks VI and VII) has been successfully demonstrated in a series of 2500 thruster hot pulses. The test duty cycle consisted of 0.050-sec on times and 0.150-sec off times in a film-cooled 3:1 expansion ratio chamber. The system functioned flawlessly except for minor propellant leakage through the valve stems. These same components will be employed in the Task X altitude pulse tests with a 40:1 cooled thruster.

A flow system schematic and test plan for obtaining bit impulse and bit specific impulse with 40:1 cooled chambers was formulated and presented at the 2 March program review with the NASA program manager. Accurate measurement of the propellant temperatures and flow rates in pulsing is anticipated to be the most difficult aspect of this task. The planned flow configuration incorporates a critical flow venturi discharging into a fixed volume storage tank and a high response anometer at the thrust chamber valve inlet.

B. CURRENT PROBLEMS

No significant technical problems have been encountered during this report period.

C. WORK TO BE PERFORMED IN THE NEXT REPORT PERIOD

Task I - Injector Analysis and Design - No activity.

Task II - Injector Fabrication

Modify selected injectors for use in cooled chamber testing.

Task III - Cooled Chamber Analysis and Design

Continue to evaluate results of Task VIII heat transfer tests and determine impact on selected designs.

III, C, Work to be Performed in the Next Report Period (cont.)

Task IV - Cooled Chamber Fabrication

Continue fabrication of four cooled thrust chambers--two units of each concept. First units should be available for instrumentation and testing during the next report period.

Tasks V through VII - No activity.

Task VIII - Injector Checkout Tests

Complete documentation of test activities in this task.

Task IX - Cooled Chamber Tests

Finalize cooled chamber test plan for the J-3 altitude test facilities and propellant requirements for longer duration tests. Prepare J-3 test facility for a mid-April start date for testing. System checkout tests and first chamber tests should be initiated during this period. Checkout new propellant heat exchangers to determine minimum temperature vs flow rate.

Task X - Pulse Tests - No activity.

IV. LOW PRESSURE TECHNOLOGY PROGRAM

A. PROGRAM PROGRESS (TASKS XI THROUGH XX)

On 11 February 1971 a contract stop work order was received from the NASA/LeRC contracting officer, directing that all work relative to the following areas be stopped:

- Analysis, design, fabrication and testing of the low pressure vaned injector.
- Valve preparation for low P_c.
- Low pressure cooled thrust chamber analysis, design, fabrication and testing.
- Low pressure pulse testing.

A reduced scope coaxial element injector test program was prepared for and approved by the NASA/LeRC program manager. Four additional test series were conducted concluding this task with a total of 34 tests: 10 tests for ignition, facility verification and control sequecing and 24 tests for performance and thermal data.

1. Task XI - Injector Analysis and Design

The coaxial injector design was completed during the previous report period. The vaned injector design was completed and approved for fabrication. Figure IV-1 shows the hydrogen orifice size and location selection based on the Task XVIII cold flow test results.

Hot fire tests of the cold flow hardware were conducted to atmosphere to determine the vane heating characteristics. The results indicated that flow from the hydrogen injection orifices was causing a nonuniform flow of oxygen in the area of transition from a double row to a single row of hydrogen orifices. Undesirable O/F ratios resulted in high temperatures in

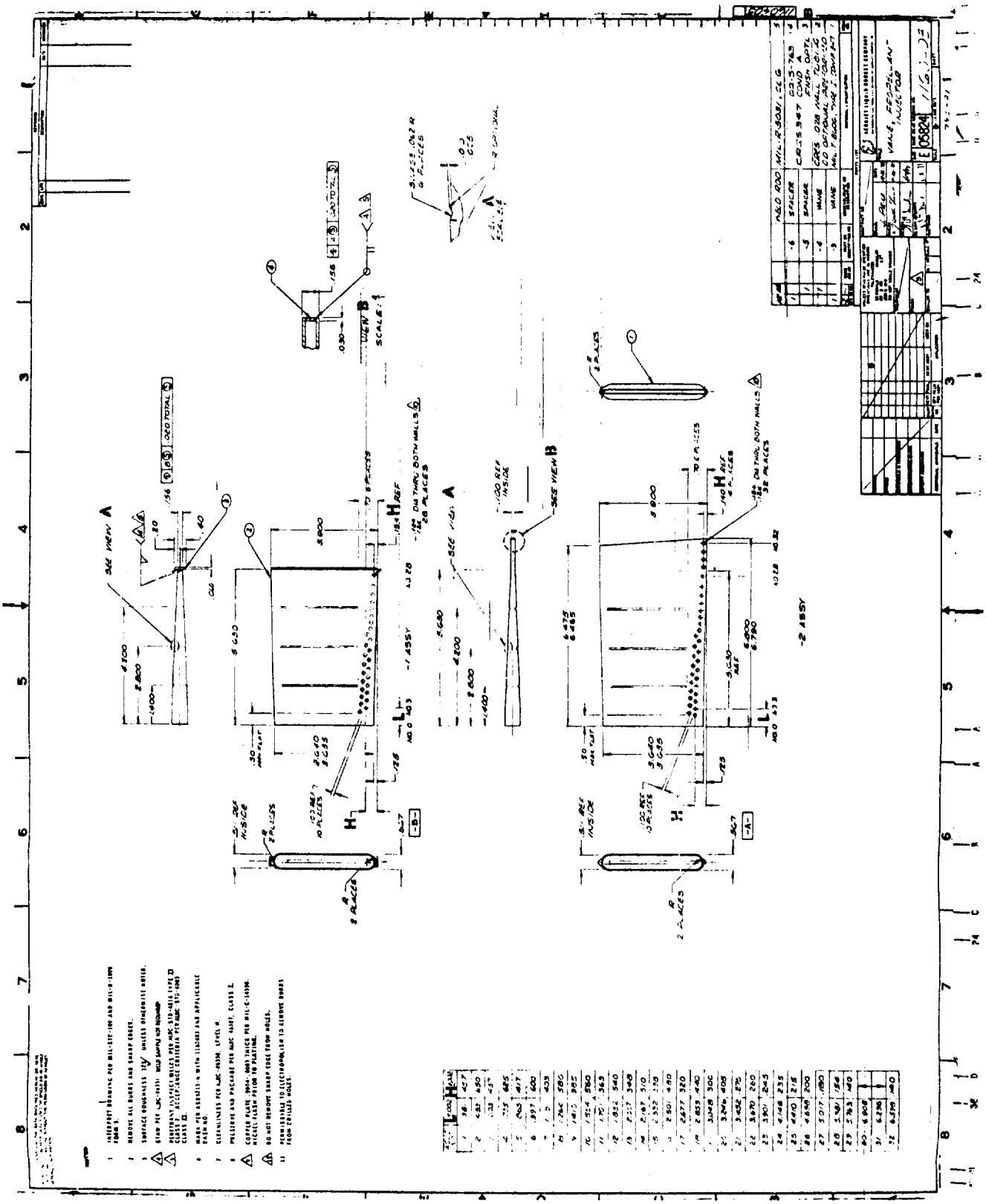

Low Pressure Injector Vane

Figure IV-1

IV, A, Program Progress (Tasks XI Through XX) (cont.)

the vane. A modified vane set was prepared but not tested at the time this activity was stopped.

2. Task XII - Injector Fabrication

Fabrication of two coaxial injector element assemblies was completed in the previous report period. Fabrication of a vaned injector element assembly and components for a second unit was initiated. Fabrication of the vaned injector was stopped during this reporting period.

3. Task XIII - Thrust Chamber Analysis and Design

a. Design and Structural Analysis

Design and structural analysis of the film cooled and reverse dump cooled chambers were described in the first quarterly report. Subsequently, the reverse dump cooled chamber to nozzle skirt attachment flanges were modified to key one to the other to restrain the thermal expansion of the uncooled nozzle extension flange. This change ensures more uniform loading of the retaining band clamp. The thermal conditions used in this analysis were conservative (no heat transfer between flanges or to the band clam;); however, the modification was easily incorporated alleviating the possible occurrence of this condition.

b. Hydraulic Analysis

A flow distribution analysis of the reverse dump cooled chamber design was conducted. Nominal chamber design conditions used in this analysis were as follows:

IV, A, Program Progress (Tasks XI Through XX) (cont.)

Chamber Coolant Medium:	Gaseous Hydrogen
Coolant Inlet Temperature:	540°R
Coolant Outlet Temperature:	615°R
Coolant Inlet Pressure:	19 psia
Chamber Pressure:	15 psia
Coolant Flowrate:	0.137 lbm/sec (12%)

The calculated pressure losses for the coolant are shown in Table IV-1.

TABLE IV-1

REVERSE DUMP COOLED CHAMBER PRESSURE LOSS DISTRIBUTION

Chamber Inlet	0.1 psia
Inlet Manifold	0.2
Inlet Metering Orifice	0.3
Chamber Friction & Turning Turbulence	1.0 (approximate)
Exit Metering Orifice & Forward Flange Plenum	0.8
Total Circuit	3.3 psia

The design philosophy for this chamber was to introduce the fuel coolant at a low velocity to minimize dynamic head losses to the distribution circuit. A moderate pressure loss was introduced at the inlet metering orifice to obtain positive flow control to achieve a uniform circumferential coolant distribution in the chamber coolant passages. The chamber coolant passage pressure drop was assumed to be uniform as a result of the uniform circumferential flow distribution. A higher pressure drop was taken at the exit metering orifice at the forward flange to maintain a uniform

IV, A, Program Progress (Tasks XI Through XX) (cont.)

coolant distribution. Finally, the maximum pressure loss was taken at the film coolant injection gap to obtain a uniform chamber internal (hot gas side) film coolant distribution.

The criterion for hydraulic design was to progressively increase the gas velocity. Other ALRC gas/gas injector and chamber distribution manifolds have employed this technique with success. The circumferential flow distribution uniformity will be verified by cold flow testing as part of the fabrication sequence. Modifications to inlet and outlet metering orifices will be made to fine tune the coolant flow distribution.

This analysis was conducted for equal chamber wall and film coolant sleeve temperatures. If the coolant sleeve is heated relative to the chamber wall, the thermal expansion will reduce the injection gap thereby increasing the injection velocity and the injection pressure drop. The film coolant sleeve design will be selected on the basis of Task XVIII test results. Thrust chamber coolant flow will be balanced for steady state coolant sleeve temperatures. Initial operation, with a cold film coolant sleeve, will result in an overflow of fuel coolant; approximately 10% for a 250°F design temperature gradient.

4. Task XIV - Thrust Chamber Fabrication

Cooled chamber designs have been submitted for cost estimates for review to improve fabricability. Fabrication of thermal instrumentation and application of the ablative material for streak chamber testing was completed during this period. Activities related to the fabrication of cooled chambers were stopped.

IV, A, Program Progress (Tasks XI Through XX) (cont.)

5. Task XV - Catalytic Igniter Analysis and Design

This task has been completed.

6. Task XVI - Catalytic Igniter Fabrication and Test

Subsequent to completion of fabrication, the low P_c catalytic igniter was prepared for testing. Preparations consisted of assembly of the components, installation of the flow "split" balance orifices, and packing of the catalyst bed. The igniter test position in Bay 1 of the Physics Laboratory was modified to accept the catalytic unit. The modifications required consisted of the rerouting of propellant lines, repositioning of the igniter valves, and installation of instrumentation and the associated electrical cabling. Before testing was begun, each propellant circuit was cold flowed for calibration. A propellant simulant was used for the flow calibrations (i.e., nitrogen simulating the oxygen and helium simulating the hydrogen), so combustible mixtures of gases would not accumulate in the vacuum system. When enough flow data were available from the calibration tests and each circuit was considered balanced, testing was initiated.

The test program consisted of seven test series, including two series where the effects of cold hardware and cold propellants were investigated. During testing, a total of 222 tests were performed. The major objectives of the test program were to understand the operation of the igniter, conduct enough tests at ambient conditions to provide baseline data, and proceed directly to testing with cold propellants.

Figure IV-2 is a schematic of the test setup showing the igniter and the four propellant flow circuits and the propellant feed systems located in Bay 1 of the Physics Laboratory. The fuel feed system consists of

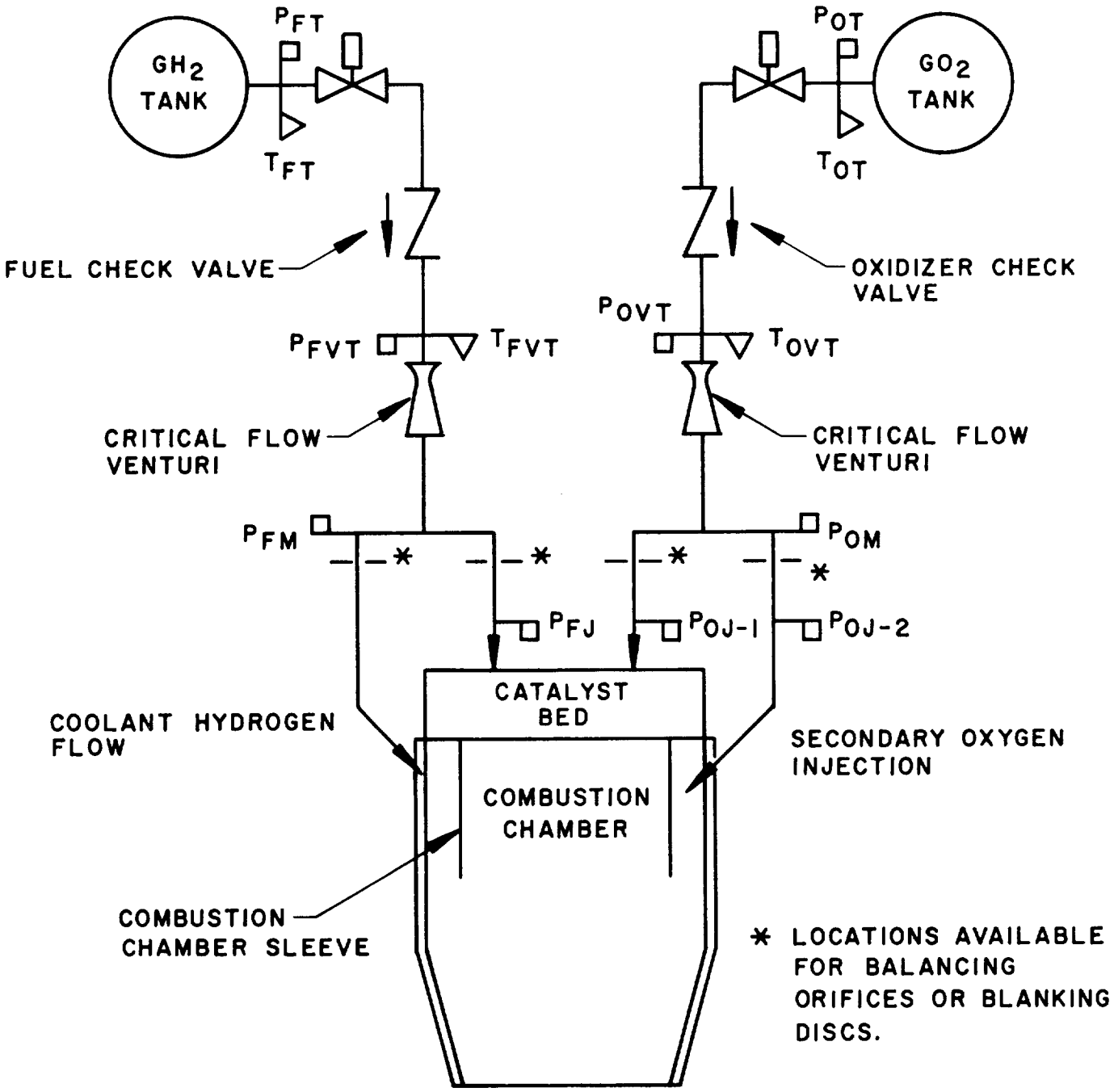

Low Pressure Catalytic Igniter Test Schematic

Figure IV-2

the gaseous hydrogen storage sphere, the fuel control valve, a check valve to prevent back-flow of oxygen into the fuel system, a flow control venturi, and the pressure and temperature instrumentation needed to control tests and provide the data required. The oxygen feed system is a duplicate of the fuel system and consists of matching components and instrumentation to provide similar measurements. The igniter schematic depicts the four propellant circuits, the relative locations of the catalyst bed, combustion chamber, combustion chamber sleeve, and the hydrogen coolant jacket. Also shown are the locations where the propellant balancing orifices were installed to obtain the desired propellant "splits". Note: Undrilled orifice plates can, be and were, installed in these locations to flow each circuit independently.

Because of the number of tests conducted and the quantity of data measured, the following discussion of the testing and the results have been divided into seven test sections. A description of the tests and the test results are contained in the following paragraphs. Analysis of these data will be included in the final report.

Test Series 1 - Initial Tests

The initial investigations with the Low P_c catalytic igniter consisted of five tests conducted to characterize operation. The data resulting from these tests is presented in Table IV-2. An examination of the oscillograph traces indicated that the oxidizer manifold pressure (PoJ-2), i.e., meaning oxidizer flow split, remained approximately the same during the first four tests (13.0 psia). The upstream bed thermocouple (nearest to the injector face) did not respond during the first two tests, reached 181°F at the end of Test 103, and 431°F at the end of Test 104; the test durations are shown in Table IV-2. These results indicate a very low level of propellant reaction within the bed and no involvement of the secondary oxygen in the combustion process.

TABLE IV-2

DATA OBTAINED DURING TEST SERIES 1 AND 2

Test Number IG-2C-	$\dot{w}_{O_2}$-T, lbm/sec	$\dot{w}_{H_2}$-T, lbm/sec	MR, Overall	$\dot{w}_{O_2}$-Bed, lbm/sec	$\dot{w}_{H_2}$-Bed, lbm/sec	MR, Bed	P_c, psia	Duration, sec	Delay,* sec
				Test Series 1					
101	0.063	0.013	4.85	0.002	0.002	1.0	--	0.2	--
102	0.063	0.013	4.85	0.002	0.002	1.0	--	0.2	--
103	0.063	0.013	4.85	0.002	0.002	1.0	--	1.0	--
104	0.063	0.013	4.85	0.002	0.002	1.0	--	5.0	--
105	0.084	0.017	4.94	0.003	0.003	1.0	--	2.0	0.855
				Test Series 2					
106	0.084	0.017	4.94	0.003	0.003	1.0	--	2.0	--
107	0.084	0.017	4.94	0.003	0.003	1.0	--	2.0	--
108	0.125	0.013	9.62	0.004	0.002	2.0	--	2.0	1.64
109	0.156	0.013	12.00	0.005	0.002	2.5	--	2.0	0.09

*NOTE: The ignition delay is defined as the time from first action in the oxidizer manifold (i.e., the lagging propellant) to first indication of involvement of the secondary oxygen in a combustion process.

IV, A, Program Progress (Tasks XI Through XX) (cont.)

Test 105 behaved quite differently. For the first 760 msec, the traces indicate a very low level of bed activity with PoJ-2 running at 16.3 psia. The upstream bed thermocouple responded very early in the test at an indicated temperature of 307°F at 760 msec. At that point, the photocell indicated ignition and PoJ-2 rose to 18.0 psia. PoJ-2 gradually declined to 17.1 psia at the end of the test but the bed thermocouple indicated a gradual temperature rise to 481°F at the end of 2.0 sec. The bed responded to the increased propellant flow rate and reached a higher temperature in 2.0 sec (481°F) than it did in the 5.0 sec of the previous test (431°F). Once again, a low level of propellant reaction in the bed is indicated. The photocell indicates that the secondary oxygen became involved at 760 msec into the test.

Posttest inspection of the igniter revealed neither damage to any component nor evidence of heating within the igniter. In preparation for the next series of tests, the catalyst was replaced with fresh material as a precautionary measure, four holes were drilled in the inner sleeve to introduce oxygen into the combustion process earlier, and a thermocouple was installed in the combustion chamber and a second was positioned on the igniter nozzle as additional witness instrumentation.

Test Series 2 - Evaluation of Drilled Sleeve

This series consisted of 4 tests and was conducted primarily to evaluate the introduction of secondary oxygen into a combustion process earlier in the chamber. The data from these tests is also presented in Table IV-2. Testing commenced with the flow rates and mixture ratios the same as those which resulted in ignition during Test Series 1, Test 105. As the data show, ignition was not achieved, so the test was repeated. Again, there was no secondary reaction. The third test (Test 108) was conducted with the mixture ratio doubled and the oxygen content increased in an attempt to improve

responsiveness. Ignition was achieved, but response was sluggish. The overall MR was then increased to 12 and more oxygen enrichment was provided, but the high flow rates required to achieve secondary ignition reflected improper operation of the igniter, so testing was stopped.

Posttest inspection of the igniter revealed neither damage nor unwanted heating of interior components. Because the holes drilled in the chamber sleeve did not appear to enhance operation, they were welded closed.

Test Series 3

This series consisted of 11 tests conducted with progressively increasing propellant weight flows and mixture ratios. The resulting data are shown in Table IV-3. The trend of data from these tests seems to indicate that either higher than design values of propellant flow rate or mixture ratio are required for proper operation of the igniter. The catalyst bed temperatures, which were reached near the end of the test periods, were lower than expected indicating that the catalyst bed mixture ratio was lower than designed.

Posttest inspection of the igniter revealed some damage to the igniter injector face plate. The damage was limited to the final distribution plate which was removed prior to the next test series. With this plate removed, the propellants will be injected into the bed more coarsely than originally designed. Also with this plate removed, the hydraulic calibration and propellant "splits" between the bed and secondary circuits are no longer valid. To further evaluate this condition, the next series of tests was conducted to examine operation of the catalyst bed alone.

Test Series 4 - Evaluation of the Catalyst Bed Alone

This series consisted of 26 tests (i.e., Tests 121 through 146) and was conducted with propellant flow to the catalyst bed alone. A set

TABLE IV-3

DATA OBTAINED DURING TEST SERIES 3

Test Number 1G-2G-	$\dot{w}_{O_2}$-T, lbm/sec	$\dot{w}_{H_2}$-T, lbm/sec	MR, Overall	$\dot{w}_{O_2}$-Bed, lbm/sec	$\dot{w}_{H_2}$-Bed, lbm/sec	MR, Bed	P_c,*** psia	Duration, sec	Delay,* sec
110	0.063	0.013	4.85	0.002	0.002	1.0	--	0.3	--
111	0.063	0.013	4.85	0.002	0.002	1.0	--	0.3	--
112	0.063	0.013	4.85	0.002	0.002	1.0	--	2.0	--
113	0.093	0.019	4.89	0.003	0.003	1.0	--	2.0	--
114	0.093	0.019	4.89	0.003	0.003	1.0	7.5	2.0	0.74
115	0.093	0.019	4.89	0.003	0.003	1.0	7.7	2.0	0.25
116	0.093	0.019	4.89	0.003	0.003	1.0	7.9	2.0	0.68
117	0.093	0.013	7.15	0.003	0.002	1.5	8.4	2.0	0.59
118	0.110	0.013	8.46	0.004	0.002	2.0	9.2	2.0	0.12
119	0.110	0.016	6.88	0.004	0.002	2.0	10.3	2.0	0.39
120	0.110	0.016	6.88	0.004	0.002	2.0	10.8	2.0	0.03**

*NOTE: The ignition delay is defined as the time from first action in the oxidizer manifold, i.e., the lagging propellant, to first indication of involvement of the secondary oxygen in a combustion process.

** Hot-bed restart.

*** Inferred from PoJ2.

IV, A, Program Progress (Tasks XI Through XX) (cont.)

of small critical-flow venturis were installed in the propellant feed circuits to meter fuel and oxidizer to the bed only. The secondary circuits were "blanked off" for these tests. The data resulting from these tests are presented in Table IV-4.

A posttest disassembly of the igniter revealed evidence of heating on the combustion chamber sleeve, but otherwise the igniter components were undamaged. In preparation for the next test series, the bed was repacked with fresh catalyst and the proper orifice was installed to achieve the correct "split" between the catalyst bed and secondary circuit. The secondary hydrogen circuit, i.e., coolant, was left closed to permit precise control of fuel flow to the bed. A thermal analysis indicated that there was sufficient margin of safety to test the igniter, without cooling, for short durations. The igniter was reassembled and mounted in place in preparation for the next test series.

Test Series 5 - Evaluation of Secondary Oxygen Injection

Twenty-one tests were conducted during this series for evaluation of secondary oxygen injection. The data are presented in Table IV-5. Testing was started with both propellant flow rates set at the design values. The first tests resulted in a low level of bed activity, i.e., the bed thermocouples measured temperatures not greater than 600°R (Tests 147 through 151). The flow rate of oxidizer was increased and bed activity improved as the bed temperatures reached approximately 1000°F during the next four tests (Tests 152 through 155). As testing progressed, the oxidizer flow rate and bed mixture ratio were steadily increased until secondary reactions were obtained (Tests 160 through 167). Catalyst bed temperatures were in the range of 1200 to 1800°F during these tests.

After successfully achieving repeatable secondary reactions, the igniter and facility were prepared for cold tests, including replacement of the catalyst bed.

TABLE IV-4

DATA OBTAINED DURING TEST SERIES 4

EVALUATION OF THE CATALYST BED ALONE

Test Number IG-2C-	$\dot{w}_{O_2}$-B, lbm/sec	$\dot{w}_{H_2}$-B, lbm/sec	MR, Bed	Duration, sec	Test Results
121	0.0013	0.0013	1.00	0.15	No reaction in catalyst bed (1)
122	0.0013	↕	1.00	0.15	No reaction in catalyst bed (1)
123	0.0014	↕	1.08	0.25	Reaction obtained
124	0.0011	↕	0.85	0.25	No reaction (2)
125	0.0011	↕	0.85	0.25	No reaction (2)
126	0.0013	↕	1.00	0.25	Reaction obtained
127	0.0013	↕	1.00	0.50	Reaction obtained (3)
128	0.0012	↓	0.92	↕	↕
129	↕	0.0013	0.92	↕	↕
130	↕	0.0012	1.00	↕	↕
131	↕	0.0013	0.92	↕	↕
132	↕	↕	↕	↕	↕
133	↕	↕	↕	↕	↕
134	↕	↕	↕	↕	↕
135	↕	↕	↕	↕	↕
136	↕	↕	↕	↕	↕
137	↕	↕	↕	↕	↕
138	↕	↕	↕	↕	↕
139	↕	↕	↕	↕	↕
140	↕	↕	↕	↕	↕
141	↕	↕	↕	↕	↕
142	↓	↕	↓	↓	↕
143	0.0012	↕	0.92	0.50	↕
144	0.0013	↕	1.00	1.50 (4)	↕
145	0.0013	↕	1.00	1.50 (4)	↕
146	0.0013	0.0013	1.00	1.50 (4)	Reaction Obtained (3)

(1) Bed reactions were not obtained because a later data review revealed that the oxidizer valve did not open.

(2) Reactions were not obtained within the test duration at low mixture ratio, i.e., less than 1.0.

(3) Bed temperatures, during the repeat tests, and the 1.50 sec tests did not rise higher than 1800°F.

(4) The longer durations resulted in the same bed temperatures, so thermal equilibrium had been reached.

TABLE IV-5

DATA OBTAINED DURING TEST SERIES 5

EVALUATION OF SECONDARY OXYGEN INJECTION

Test Number 1G-2C-	$\dot{w}_{O_2}$-T, lbm/sec	$\dot{w}_{O_2}$-sec, lbm/sec(2)	$\dot{w}_{O_2}$-Bed, lbm/sec(2)	$\dot{w}_{H_2}$-Bed, lbm/sec(3)	MR, Bed	Duration, sec	P_c psia	Delay, sec(4)
147	0.063	0.061	0.0020	0.0022	0.91	0.80	Bed Reaction Only	
148	0.063	0.061	0.0020		0.91	0.80	Bed Reaction Only	
149	0.070	0.068	0.0022		1.00	0.80	Bed Reaction Only	
150	0.070	0.068	0.0022		1.00	0.80	Bed Reaction Only	
151	0.070	0.068	0.0022		1.00	0.80	Bed Reaction Only	
152	0.080	0.078	0.0026		1.18	0.90		
153	0.080	0.078	0.0026		1.18			
154	0.080	0.078	0.0026		1.18			
155	0.080	0.078	0.0026		1.18			
156	0.100	0.097	0.0032		1.45			
157	0.100	0.097	0.0032		1.45			
158	0.100	0.097	0.0032		1.45	0.90		
159	0.080	0.078	0.0026		1.18	1.00	Bed Reaction Only	
160	0.080	0.078	0.0026		1.18		15.1	
161	0.100	0.097	0.0032		1.45		Bed Reaction Only	
162	0.115	0.111	0.0037		1.68		17.4	0.095
163	0.117	0.113	0.0038		1.73		17.8	0.090
164	0.112	0.108	0.0036	0.0022	1.64		17.4	0.075
165	0.102	0.099	0.0033	0.0020	1.65		15.6	0.075
166	0.102	0.099	0.0033	0.0020	1.65		15.5	0.075
167	0.102	0.099	0.0033	0.0020	1.65	1.00	15.6	0.065 (5)

(1) Total oxidizer flow, $\dot{w}_{O_2}$-T, was measured

(2) Bed and secondary oxidizer flows were calculated based upon cold flows and previous tests.

(3) Fuel flow to the bed, $\dot{w}_{H_2}$-Bed, was measured.

(4) Bed reactions were monitored and verified by thermocouples buried in the bed. The secondary reaction was monitored and verified by a photocell and by thermocouples.

(5) The fast response was obtained with a fast restart of the hot bed.

IV, A, Program Progress (Tasks XI Through XX) (cont.)

Test Series 6 - Initial Low Temperature Tests

The purpose of these tests was to evaluate the effect of bed temperature on the igniter start transient. Eighteen tests were conducted in this series and the resulting data are presented in Table IV-6. These tests were conducted with the coolant hydrogen circuit "blanked" off and the oxygen flow split automatically to the primary and secondary circuits. The plan was to test the igniter at ambient conditions first to provide assurance that it was working properly and to provide baseline data at ambient conditions for comparison with the results to be obtained from a cold bed.

The first test resulted in a malfunction because the oxidizer valve did not open; however, the flow of hydrogen alone served to activate the bed because the next test was successful and the response was rapid, i.e., 135 msec to secondary reaction (Test 169). The next two tests resulted in bed reactions only; so for the next test (Test 172), the oxidizer flow rate was increased resulting in secondary reaction. Three more tests were conducted at slightly reduced oxygen flow to ensure that the catalyst was operating properly. When the igniter appeared to be responding well (Test 175), the oxidizer flow rate was adjusted to the value desired for the cold tests and three tests were conducted for baseline data (Tests 176, 177 and 178).

The outside of the igniter was soaked in LN_2 in preparation for the first cold test. The attempt resulted in a very low level bed reaction with no secondary reaction occurring within the 1.0-sec test duration. Another test was tried immediately, which resulted in another low level bed reaction only but accompanied with increased temperature activity within the bed. Note the pretest bed temperature had risen by 55°R above that for the previous test. A third test (Test 181) resulted in a high level bed reaction accompanied by a secondary reaction which was delayed by 560 msec. The next tests were not conducted until the catalyst bed temperature had returned to the desired chilled

TAELE IV-6

DATA OBTAINED DURING TEST SERIES 6, INITIAL COLD TESTS

Test Number 1G-2C-	$\dot{w}_{O_2}$-T, lbm/sec(1)	$\dot{w}_{O_2}$-Bed, lbm/sec(1)	$\dot{w}_{H_2}$-Bed, lbm/sec(2)	MR, Bed	P_c, psia	Duration, sec	Delay sec	T_{Bed}, °R(3)	Propellant Conditions
168	0.102	0.0031	0.0019	1.63	Oxidizer valve did not open				
169	0.102	0.0031	0.0019	1.63	15.0	1.0	0.135	Amb	Amb
170	0.102	0.0031	0.0019	1.63	9.0	1.0	Bed Reaction Only		
171	0.102	0.0031	0.0019	1.63	9.0	1.0	Bed Reaction Only		
172	0.112	0.0036	0.0019	1.89	16.0	1.0	0.275	Amb	Amb
173	0.107	0.0034	0.0019	1.79	15.9	1.0	0.55	↓	↓
174	0.107	0.0034	0.0019	1.79	15.9	1.0	0.185		
175	0.107	0.0034	0.0019	1.79	15.9	1.0	0.165		
176	0.102	0.0031	0.0019	1.63	15.0	1.0	0.140		
177	0.102	0.0031	0.0019	1.63	15.2	1.0	0.230		
178	0.102	0.0031	0.0019	1.63	15.1	1.0	0.220	Amb	Amb
179	0.102	0.0031	0.0019	1.63	8.2(5)	1.0	-	310	Amb
180	↓	↓	↓	↓	8.2(6)	↓	-	365	↓
181					14.9		0.560	395	
182					15.1		0.540	390	
183					15.0		0.190	410	
184(4)					15.4		0.410	426	
185	0.102	0.0031	0.0019	1.63	15.0	1.0	0.210	443	Amb

(1) Total oxygen flowrate, $\dot{w}_{O_2}$-T, was measured, and the oxygen flow to the bed, $\dot{w}_{O_2}$-Bed, was calculated based upon previous calibrations.

(2) Hydrogen flow to the bed, $\dot{w}_{H_2}$-Bed, was measured.

(3) Bed temperature measurements were obtained just prior to each test from thermocouples located in the catalyst bed.

(4) The fuel valve opened erratically causing slow igniter response.

(5) Bed reaction only, but hardly any temperature rise.

(6) Bed reaction only, detectable temperature rise.

IV, A, Program Progress (Tasks XI Through XX) (cont.)

condition. The long ignition delay of Test 184 (i.e., 410 msec), in comparison with the results from companion tests, was caused by an erratic fuel valve which did not open fully during the test. Because the data appeared to give the results desired, no further tests were conducted in this series.

Upon disassembly of the igniter, some damage to the catalyst bed was observed. The downstream portion of the bed, near the aft trap, contained slag and there was a hole through the bed, approximately 1/4 in. dia, on the side closest to the inlet to the oxidizer manifold. There was also evidence of heating of the inner sleeve, but no damage.

The damage to the bed was caused by an oxygen maldistribution due to the reduced pressure drop which resulted when the injector face plate was removed. To improve distribution, a plate was placed between the injection orifices and the catalyst bed to break up the oxidizer-rich streams from the modified injector, and a pressure drop plate was installed over the oxygen orifice inlets.

The results of these tests indicate that bed activity is sensitive to temperature. The bed had been run several times before the cold tests were begun and appeared to be operating reproducibly. Also, enough test time had been accumulated to eliminate the possibility that contaminants in the bed had confused the results obtained with the chilled bed.

The results so far obtained with the Low P_c catalytic igniter-only seem to strongly indicate that the condition of the catalyst bed may have caused a major portion of the low level bed reactions. All test series have resulted in no secondary oxygen ignitions during the initial tests. To evaluate the effect of catalyst preconditioning, the repacked catalyst bed remained in a vacuum oven at 200°F for approximately 30 hours and was returned to atmospheric pressure under a blanket of hydrogen gas before the next test series.

IV, A, Program Progress (Tasks XI Through XX) (cont.)

Test Series 7 - Tests with Cold Propellants

The initial tests of this series were conducted at ambient conditions to evaluate the effects of the pretest catalyst decontamination and activation with hydrogen. The resulting data are presented in Table IV-7. As the data show, bed response was slow during the first test, better during the second, and responded well during each following test. Only slight improvement in initial test catalyst response resulted from the special precautions.

These initial tests at ambient conditions were also accompanied by sporadic secondary reactions, even though the test conditions remain unchanged for blocks of tests and the bed response was adequate in each test to cause an ignition. The results seem to indicate that the igniter is sensitive to secondary mixing and, in this design, it is marginal.

The next 11 tests (Tests 203 through 213) were conducted with chilled propellants and the igniter bed at ambient temperature. The tests were conducted at intervals of propellant chilling to evaluate the effect on igniter response of cold propellants entering the ambient temperature catalyst bed. Each test resulted in good bed response, i.e., bed temperature increasing to approximately 1800°F directly after entrance of the propellants into the bed. Four tests resulted in no secondary reactions possibly due to the method of secondary oxygen injection with this design. The results of these tests indicate that good bed reaction can be achieved even through the incoming propellant temperatures are below 300°R. The propellant flow rates were maintained from test to test by correcting venturi inlet pressure for temperature.

The last tests were conducted with both the propellants and igniter chilled. The intent of these tests was to find a lower limit where bed reactions cease to be effective. The test technique used was to chill the

TABLE IV-7

DATA OBTAINED FROM TESTS WITH THE LOW P_c CATALYSTIC IGNITER DURING TESTS WITH COLD PROPELLANTS, TEST SERIES 7

Test Number IG-2C-	General Test Conditions	$\dot{w}_{O_2}$-T, lbm/sec (1)	$\dot{w}_{O_2}$-sec, lbm/sec (2)	$\dot{w}_{O_2}$-Bed, lbm/sec (2)	$\dot{w}_{H_2}$-Bed, lbm/sec (3)	MR, Bed	MR, Sec	T_{ign}, °R	T_{OT}, °R	T_{FT}, °R	P_c, psia	Dur. sec	Delay sec	Remarks
Tests at Ambient Conditions														
186	Prepurge Bed with GH_2	0.102	0.099	0.0031	0.0019	1.63	53.7	Amb	Amb	Amb	9.5	1.0	-	Low Level Bed Response
187	Repeat Test	0.102	0.099	0.0031	0.0019	1.63	53.7				9.5		-	Better Bed Response
188	Increase $\dot{w}_T$ and MR	0.114	0.110	0.0036	0.0021	1.71	54.4				16.1		0.175	Good Bed Response
189	Repeat Test					1.73					16.0		0.210	Good Bed Response
190	Repeat Test										16.1		0.165	Good Bed Response
191	Repeat Test										-		-	Bed Response Same as Prev. Test
192	Repeat Test										-		-	Bed Response Same as Prev. Test
193	20 msec Fuel Lead										15.9		0.170	Good Bed Response (4)
194	Repeat Test				0.0021	1.73	54.4				-		-	Good Bed Response (4)
195	Reduce Fuel Flowrate				0.0020	1.80	57.0				-		-	
196	Repeat Test										16.0		0.342	
197	Repeat Test										-		-	
198	Use GH_2 Prepurge										16.1		0.128	
199	Repeat Test										16.1		0.250	
200	Prepurge and Wait 30 sec										-		-	
201	Prepurge and Wait 1 min										16.0		0.370	
202	Repeat Test	0.114	0.110	0.0036	0.0020	1.80	57.0	Amb	Amb	Amb	16.0	1.0	0.340	Good Bed Response (4)

(1) Total oxidizer flow, $\dot{w}_{O_2}$-T, was measured.

(2) Primary and Secondary oxidizer flowrates, $\dot{w}_{O_2}$-Bed and $\dot{w}_{O_2}$-sec, were calculated.

(3) Total Fuel Flow, $\dot{w}_{H_2}$-Bed, was measured.

(4) Bed temperature rise started immediately upon arrival of propellants at bed.
During these tests they reached approximately 1900°F within 0.500 sec whether-or-not there was a secondary reaction.

TABLE IV-7 (cont.)

Test Number IG-2C-	General Test Conditions	$\dot{w}_{O_2}$-T, lbm/sec (1)	$\dot{w}_{O_2}$-sec, lbm/sec (2)	$\dot{w}_{O_2}$-Bed, lbm/sec (2)	$\dot{w}_{H_2}$-Bed, lbm/sec (3)	MR, Bed	MR, Sec.	T_{Bed}, °R	T_{oT}, °R	T_{FT}, °R	P_c, psia	Dur. sec	Delay sec	Remarks
Tests with Propellants-Only Chilled														
203	Initial Test, Cold Prop.	0.114	0.110	0.0036	0.0020	1.80	57.0	Amb	443	443	-	1.0	-	Good Bed Response (4)
204	Repeat Test	↑	↑	↑	↑	↑	↑	↑	429	429	-	↑	-	↑
205	↑	↑	↑	↑	↑	↑	↑	↑	429	429	-	↑	-	↑
206	↑	↑	↑	↑	↑	↑	↑	↑	425	425	16.0	↑	0.405	↑
207	↑	↑	↑	↑	↑	↑	↑	↑	428	419	15.0	↑	0.075	↑
208	↑	↑	↑	↑	↑	↑	↑	↑	400	388	16.0	↑	0.185	↑
209	↑	↑	↑	↑	↑	↑	↑	↑	336	361	12.0	↑	0.075	↑
210	↑	↑	↑	↑	↑	↑	↑	↑	340	343	17.0	↑	0.065	↑
211	↑	↑	↑	↑	↑	↑	↑	↑	281	280	14.0	↑	0.085	↑
212	↓	↓	↓	↓	↓	↓	↓	↓	282	278	-	↓	-	↓
213	Repeat Test	0.114	0.110	0.0036	0.0020	1.80	57.0	Amb	288	283	12.5	1.0	0.345	Good Bed Response (4)
Tests with Propellants and Igniter Chilled														
214	Initial Test, Cold System	0.114	0.110	0.0036	0.0020	1.80	57.0	290	288	285	13.0	1.0	0.380	Good Bed Response (4)
215	Repeat Test	↑	↑	↑	↑	↑	↑	300	288	285	13.0	↑	0.091	Good Bed Response (4)
216	↑	↑	↑	↑	↑	↑	↑	350	288	284	7.0	↑	-	Good Bed Response (4)
217	↑	↑	↑	↑	↑	↑	↑	400	288	283	↑	↑	-	Slightly Delayed Response
218	↑	↑	↑	↑	↑	↑	↑	↑	288	284	↑	↑	-	Poor Bed Response
219	↑	↑	↑	↑	↑	↑	↑	↑	288	285	↑	↑	-	↑
220	↑	↑	↑	↑	↑	↑	↑	↑	288	285	↑	↑	-	↑
221	↓	↓	↓	↓	↓	↓	↓	↓	290	285	↓	↓	-	↓
222	Repeat Test	0.114	0.110	0.0036	0.0020	1.80	57.0	400	291	286	7.0	1.0	-	Poor Bed Response

IV, A, Program Progress (Tasks XI Through XX) (cont.)

hardware to the lowest level attempting ignition as the temperature increased. This approach was used to preclude the need for cooling to remove the heat from reactions expected at higher temperatures. Bed response and secondary oxygen reaction was achieved with the first two tests; at the coldest bed temperatures. Good bed response but no secondary oxygen reaction occurred with a bed temperature of 350°R followed by poor bed response with increasing bed temperatures.

Preliminary Conclusions - Relatively fast response of a catalytic ignition system for low pressure oxygen hydrogen is possible. Reproducible operation of either the catalyst or the secondary oxygen reaction were not achieved.

At these operating conditions, and possibly with this design, catalyst bed condition appears to be critical as evidenced by the good temperature response achieved with cold bed and cold propellants followed by the unexpected degradation as the bed temperature was increased. It is suspected that water vapor from the initial tests was adversly affecting the cold catalyst. This condition may have been aggravated by the short test durations (selected to limit the introduction of combustibles into the closed vacuum system) and the somewhat limited bed heating during a successful test.

7. Task XVII - Propellant Valves Preparation

Completion of this task has been awaiting the installation of heat exchangers for hot and cold propellant tests. This activity has been stopped and no further effort is anticipated.

The modified Titan valves have functioned well through the 17 igniter tests and the 34 engine tests. Pressure decay leak tests conducted during engine hardware changes indicated no valve leakage.

IV, A, Program Progress (Tasks XI Through XX) (cont.)

8. Task XVIII - Injector Testing

a. Status

The contract stop work order stops all effort related to the vaned injector testing. The scope of the coaxial injector testing was reduced to conclude with four test series for performance and thermal data. These tests have been conducted and no additional hot fire tests are scheduled. This task is being concluded by the reduction, analysis, and documentation of the test results. Thermal data analysis has been completed and is reported. Performance data analysis, which will incorporate the thermal data as a heat loss, will be included in the next report.

b. Flow Distribution Tests

Flow tests were conducted to determine the distribution characteristics of the 200-element coaxial injector assembly when installed in the ALRC-owned hydrogen and oxygen manifolds. Gaseous nitrogen was flowed through the oxygen side and then the hydrogen side of the injector at a flow rate selected to simulate the Mach numbers at rated oxygen and hydrogen flow.

The objective of these tests was to identify adverse inlet, manifold or element assembly induced flow conditions and, further, to determine the mixture ratio of each element in the outer ring of the injector for comparison with the results of the scheduled compatibility tests. The flow from selected elements was measured by a gas flow meter connected to pick-up probes which collected the flow from individual elements. The probes were designed to collect the flow with minimum pressure loss (probe pressures were monitored) and without allowing recirculation into the opposite propellant manifold.

IV, A, Program Progress (Tasks XI Through XX) (cont.)

The technique used for the oxygen element provided good test results because the good sealing and alignment of the sampling probe to the oxygen tube. The hydrogen sampling probe was not as easily aligned and sealed because of element geometry differences. Also, icing on the injector face interfered with proper interfacing of the probe providing somewhat erratic hydrogen flow data.

Seventy-nine elements were sampled; each of the outer ring elements and every fifth inner ring element were selected to define overall manifold distribution characteristics and expected chamber wall mixture ratio. The outer ring of 47 elements showed an oxygen flow deviation of $\pm$ 3.7% with no bias due to the inlet location. Fuel flow distribution for these same elements was within $\pm$ 10.5%, again with no adverse inlet effects. The mixture ratio profiles expected for each ring of elements are shown in Figure IV-3.

c. Hot Fire Test Summary

The thirty-four tests were conducted during this period. Ten tests were to check out igniter and engine hardware and to adjust the safety interlocks which were used to preclude introduction of excessive quantities of hydrogen into the close altitude facility. The operating conditions of the 24 engine tests are summarized in Table IV-8.

The initial sequence of Tests 1680-D02-0A-001 through -022 were conducted in the J-3 altitude simulation facility using the J-3 steam ejector system. For the final test series (-023 through -034) the higher capacity J-4 steam ejector system was used to minimize cell pressure build up thereby increasing the allowable test duration.

Tests were conducted using the SN 001 coaxial element injector. Chamber L*'s of 16 and 26 in. were evaluated. Three film coolant

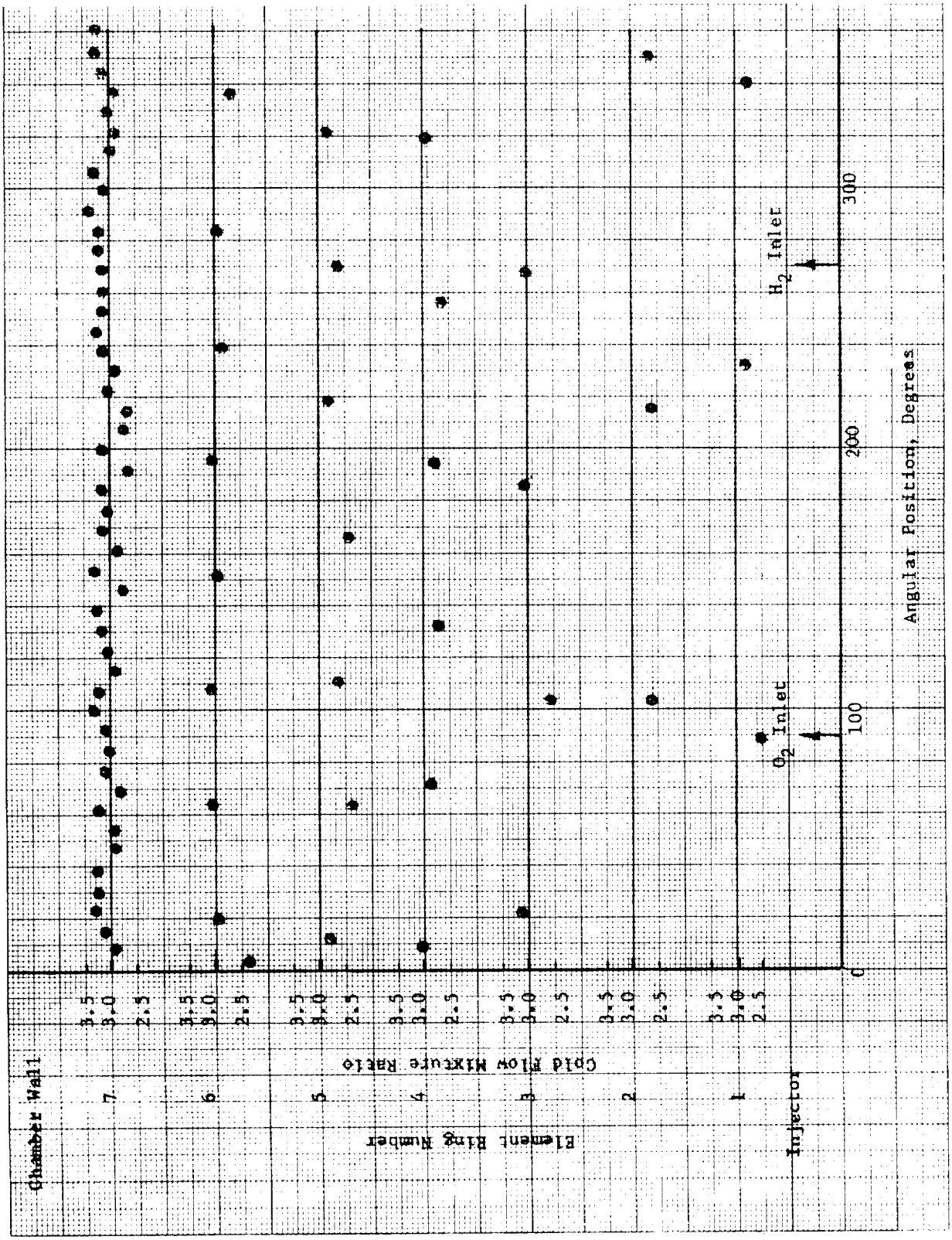

Low Pressure Coaxial Injector Flow Distribution

Figure IV-3

TABLE IV-8

LOW P_c O_2/H_2 APS ENGINE TEST SUMMARY

Test 1680-D02-OA	Dur, sec	Data Time, sec	Injector	Chamber	L*/L', in.	P_c, psia	$MR_{O/A}$	MR_J	% FFC	P_A, psia	$\dot{w}_{oJ}$, lb/sec	$\dot{w}_{fJ}$, lb/sec	$\dot{w}_{fc}$, lb/sec	$\dot{w}_T$,* lb/sec	% $\dot{w}_I$	I_{spv}, lbf-sec/lbm	F_{vac}, lbf	c*, ft/sec
-001	0.3	N/A	200 Ele Coax SN 001	Film Cooled SN 1 20% 2.78" Ring	26/12	Sea Level Ignition Check												
-002	0.3	N/A				Altitude Ignition Check												
-003	1.04	0.5-1.0				15.1	2.55	3.69	30.0	0.137	2.90	0.79	0.34	4.04	0.27	376.0	1519.3	7929
-004	2.59	2.2-2.35				15.3	2.62	3.71	28.5	0.565	2.99	0.80	0.33	4.13	0.25	377.8	1559.5	7871
-005	--	--				Facility Safety Sequence Test												
-006	--	--				Facility Safety Sequence Test												
-007	--	--				Facility Safety Sequence Test												
-008	--	--				Facility Safety Sequence Test												
-009	--	--				Facility Safety Sequence Test												
-010	2.59	1.0-2.5				15.5	2.53	3.26	21.4	0.345	2.95	0.91	0.25	4.12	0.27	384.1	1581.5	7963
-011	--	--				Facility Safety Sequence Test												
-012	5.07	1.0-2.9				15.2	2.48	2.80	11.2	0.385	2.85	1.02	0.13	4.01	0.27	386.0	1539.1	8056
-013	5.08	1.0-2.9				14.4	2.28	2.99	22.7	0.386	2.65	0.89	0.26	3.81	0.28	381.6	1448.5	7991
-014	5.09	1.0-4.5				15.9	3.93	5.07	21.3	0.421	3.54	0.70	0.19	4.44	0.24	366.8	1624.8	7586
-015	5.09	1.0-1.8				15.2	1.97	2.48	19.9	0.523	2.64	1.06	0.26	3.98	0.27	374.8	1490.7	8093
-016	5.09	1.0-5.0		Uncooled SN 1		14.9	3.90	3.95	0	0.234	3.25	0.82	0	4.08	0.25	375.8	1534.2	7739
-017	5.08	1.0-3.3				20.1	2.57	2.59	0	0.517	3.76	1.45	0	5.22	0.20	384.3	2005.9	8139
-018	5.09	1.0-5.0				15.1	3.01	3.09	0	0.435	3.03	0.98	0	4.01	0.26	378.3	1518.0	7943
-019	5.09	1.0-3.4				14.8	2.00	2.02	0	0.488	2.59	1.29	0	3.89	0.27	378.1	1469.8	8052
-020	5.08	1.0-5.0				9.3	2.33	2.36	0	0.341	1.77	0.75	0	2.53	0.41	375.4	951.4	7739
-021	5.08	1.0-4.0				15.1	2.50	2.52	0	0.524	2.84	1.13	0	3.97	0.27	383.4	1523.0	8069
-022	5.09	1.0-5.0		Streak SN 2		15.7	3.16	3.20	0	0.413	3.05	0.95	0	4.02	0.29	378.2	1519.7	8246
-023				Film Cooled SN 1 10% 2.78" Ring		Sea Level Ignition Check												
-024	10.1	3.0-10.0				15.0	2.49	3.18	20.8	1.038	2.84	0.89	0.236	3.97	0.26	380.0	1510.0	7948
-025	10.1	3.0-10.0				14.8	2.47	2.80	10.1	1.110	2.75	0.98	0.122	3.86	0.28	400.5	1547.8	8069
-026	10.6	3.0-10.0				14.8	2.41	2.72	6.3	1.057	2.72	1.05	0.072	3.85	0.28	402.2	1546.5	8097
-027	10.1	3.0-10.0		20% 2.78" Ring		14.6	2.44	2.77	10.9	1.093	2.74	0.99	0.122	3.86	0.29	398.4	1537.9	7988
-028	10.1	3.0-10.0				16.1	2.47	3.16	21.0	1.167	2.78	0.88	0.236	3.90	0.26	429.3**	1675.2	8687
-029	10.1	3.0-10.0		20% 0.5" Ring		15.3	2.60	3.70	28.9	0.931	2.96	0.80	0.330	4.10	0.26	384.7	1578.0	7863
-030	10.1	3.0-10.0				15.3	2.52	2.86	20.9	1.045	2.86	0.89	0.237	3.99	0.25	400.4	1597.8	8064
-031	10.2	3.0-10.0				14.9	2.47	2.80	10.8	1.024	2.76	0.99	0.120	3.87	0.25	404.5	1567.5	8103
-032	10.1	3.0-10.0		10% 2.78" Ring	16/8	15.3	2.56	3.25	20.3	0.986	2.89	0.89	0.229	4.01	0.26	377.5	1513.6	8045
-033	10.1	3.0-10.0				14.6	2.44	2.76	10.7	1.076	2.74	0.99	0.120	3.86	0.26	394.1	1522.3	7950
-034	10.1	3.0-10.0				14.5	2.41	2.60	6.4	1.099	2.74	1.05	0.073	3.88	0.26	398.1	1546.1	7883

*Includes igniter flow.
**Questionable altitude performance; possible nozzle separation.

IV, A, Program Progress (Tasks XI Through XX) (cont.)

injection sleeves were tested to evaluate the effect of coolant injection velocity and injection location. A streak chamber was prepared and tested.

The first series of tests were conducted for a nominal duration of 5 sec using a 26 L* chamber and a 20% film coolant ring (designed for a coolant-to-gas velocity ratio of 1) 2.78 in. long. The matrix for these tests was planned to evaluate coolant quantity (30, 20, and 10%) at a fixed engine O/F of 2.5, followed by an evaluation of engine O/F (4 to 2) with the nominal 20% coolant flow.

For the second series of tests, the film coolant sleeve was removed and uncooled tests were conducted at three O/F ratios (2.0, 2.5, and 4) at the nominal 15 psia chamber pressure, followed by two tests at the chamber pressure extremes (10 and 20 psia) at a nominal 2.5 O/F ratio.

For the third series, the ablative lined chamber was installed and a 5-sec streak test was conducted without film cooling.

The fourth test series was conducted using the 2.78 in. long 10% nominal design flow coolant ring. Nominal coolant flows of 20, 10 and 5 percent of the fuel were selected for these tests. The injector flow balance was adjusted for each test to provide a nominal overall engine O/F ratio of 2.5. These tests were conducted for a duration of 10 sec to improve the quality of the thermal data.

The sixth series of tests continued the use of the 26 L* chamber but with a short 0.5 in. long film coolant sleeve designed for optimum injection velocity at 20% coolant flow. This short coolant sleeve introduced the hydrogen coolant 0.5 in. from the injector face plane. As with the preceding coolant tests, the overall engine O/F ratio was held at 2.5 during coolant flows of 10, 20, and 30% of the total fuel flow.

II, A, Program Progress (Tasks XI Through XX) (cont.)

The seventh, and final series of tests evaluated the effect of L* and coolant injection station on performance and coolant effectiveness. The chamber L* was reduced to 16 in. and the 2.78 in. long nominal 10% coolant sleeve was installed. This configuration then injected the coolant at the point where the chamber begins to converge toward the throat. As with the earlier tests using this coolant sleeve configuration, 20, 10, and 5 percent of the fuel was passed through the sleeve while the overall engine O/F was maintained at a nominal O/F ratio of 2.5. This concluded the revised injector test series.

d. Test Results

(1) Performance Data

The data from the engine tests conducted during this period are shown on Table IV-8. Analysis of these data to determine boundary losses and energy release efficiency have not been completed. Figure IV-4 shows the delivered vacuum specific impulse for the four hardware configurations tested. These configurations, summarized below, are shown schematically on Figure IV-5.

L*, in.	Coolant Sleeve Length, in.	Coolant Sleeve Design Flow Rate, % Fuel for $V_{coolant} = V_{comb.\ prod.}$
26	2.78	10
26	2.78	20
26	0.5	20
16	2.78	10

Two film coolant sleeves designed to flow 20% of the hydrogen as coolant (at $V_{coolant} = V_{combustion\ products}$) were tested in a

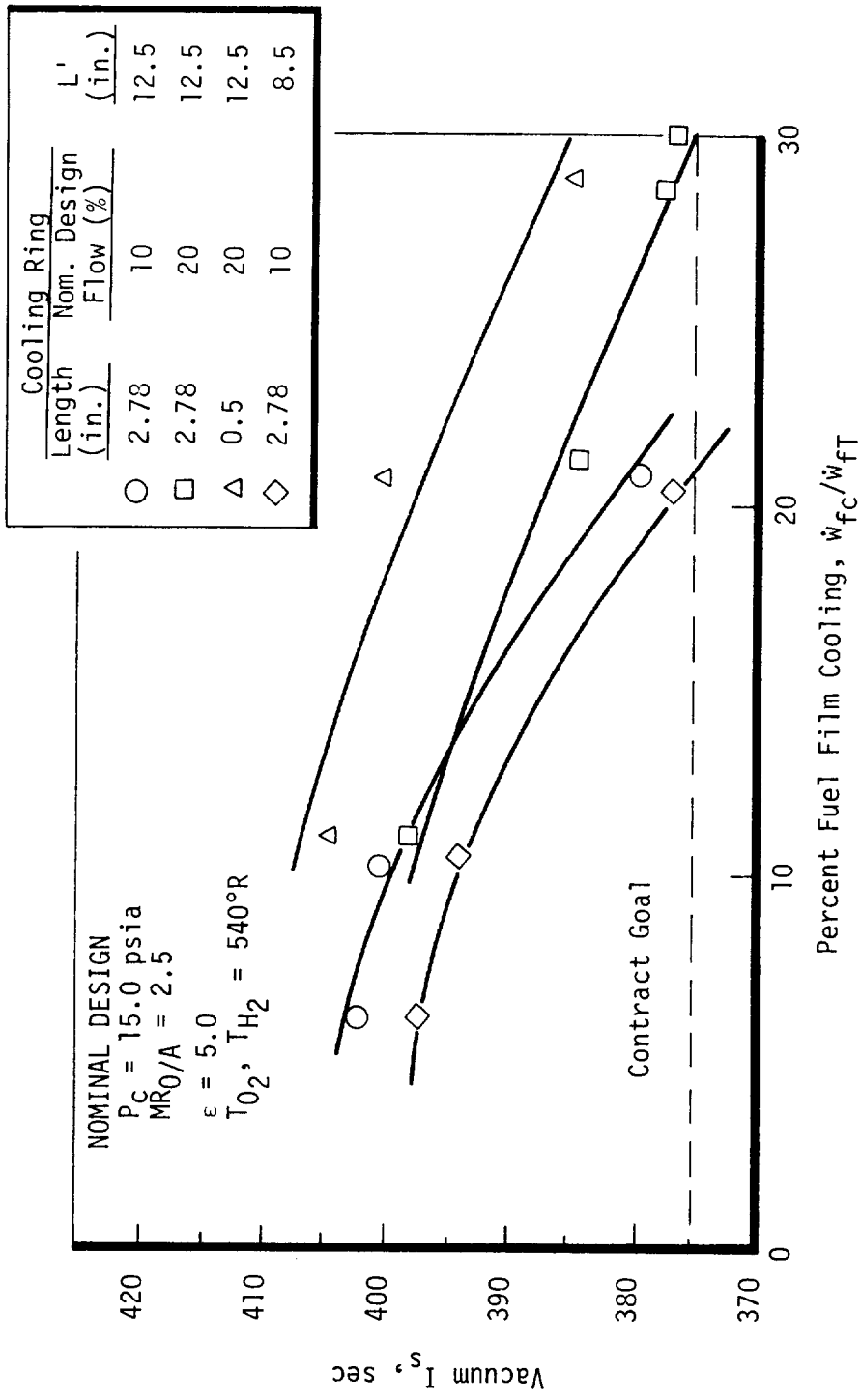

Low Pressure Delivered Performance

Figure IV-4

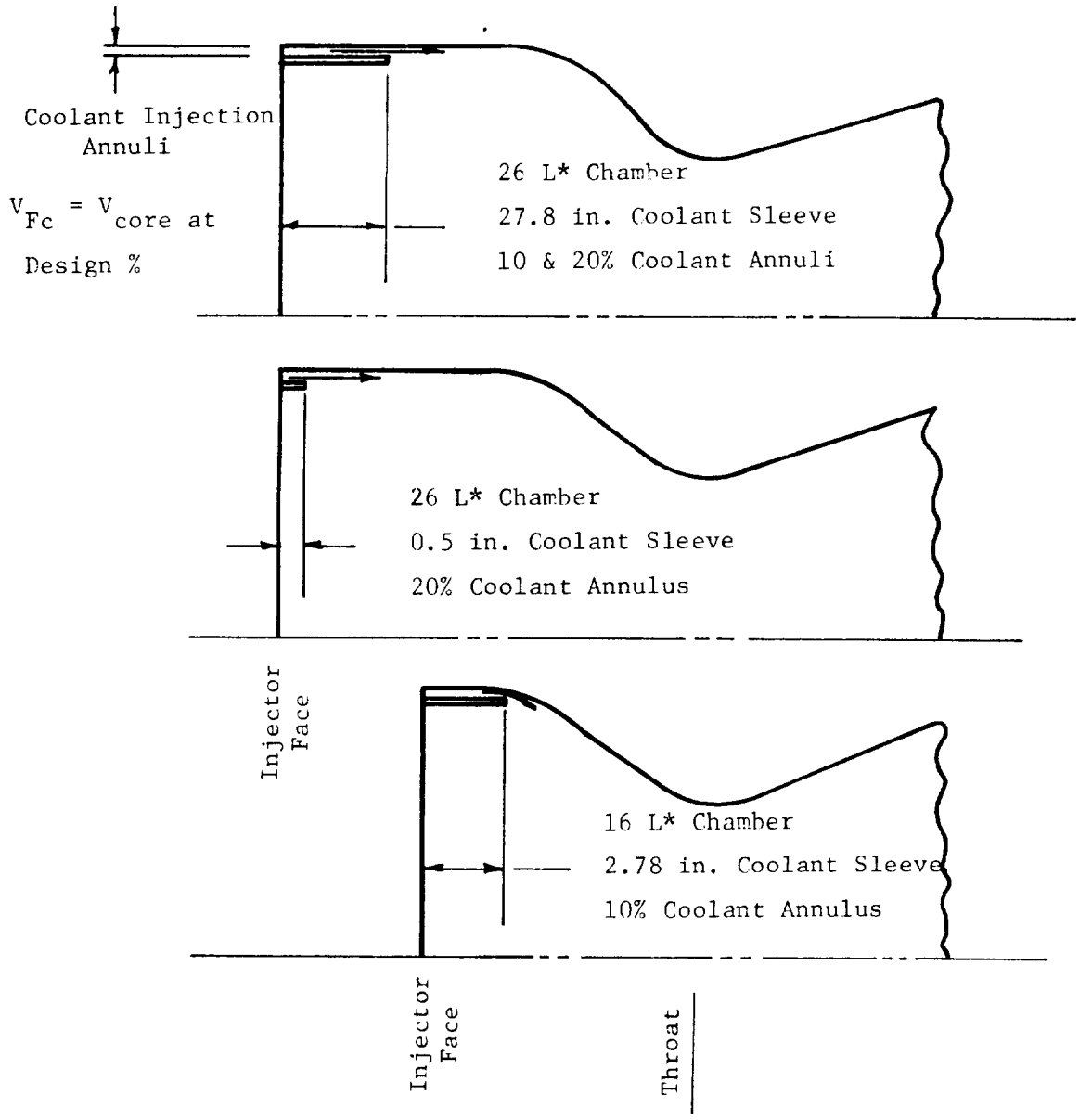

Low Pressure Test Hardware Configurations

Figure IV-5

IV, A, Program Progress (Tasks XI Through XX) (cont.)

26 L* chamber. One sleeve was 0.5 inches long and the other 2.78 inches long. The shorter coolant sleeve was the highest performing configuration tested in this test program and was nominally 7 seconds higher than was achieved with the long sleeve design over a range of coolant flow from 10% to 30% of the fuel. The higher performance achieved with the shorter coolant sleeve is probably due to the increased mixing and heating of the hydrogen coolant which degraded film cooling effectiveness.

A test series was conducted using the 26 L* chamber and a 2.78 inch long film coolant sleeve designed for the 10% fuel fraction. These tests are compared with the 2.78 inch long 20% coolant sleeve to show the effect of coolant injection velocity on delivered performance and heat transfer. At a nominal 10% coolant fraction little performance difference is seen between operation at design injection velocity or half design injection velocity. At a 20% coolant fraction, the sleeve designed for 20% coolant flow produced about 4 seconds higher performance than the smaller gap coolant sleeve flowing at two times the design velocity. The scheduled performance loss analysis will identify the effect of the boundary layer loss on these performance differences.

The 10% nominal coolant sleeve was also tested in a 16 L* chamber for comparison with the results obtained from the 26 L* chamber tests. The shorter chamber length reduced delivered performance by about 5 seconds when compared with the results from the same coolant ring in the longer chamber. Preliminary performance loss analysis indicates that the injector energy release efficiency (ERE) is near 97%. The delivered performance for all tests exceeds the contract goal of 375 seconds.

(2) Heat Transfer

Chamber wall temperature data from selected Low P_c

IV, A, Program Progress (Tasks XI Through XX) (cont.)

engine tests have been reduced. Data analysis is in process and will be completed in the next report period.

The heat transfer data are reduced by conducting a transient thermal analysis of the chamber wall using the time - wall temperature test data as the gas-side boundary condition. Inputting these data as a pseud-recovery temperature across a large film coefficient, h, forces the wall temperature, T_w, to closely follow the test data, T_{exp}, thus allowing determination of the heat flux at the surface of the chamber by the expression.

$$q/A_{wall} = h\ (T_{exp} - T_w)$$

Both the heat flux to the wall, as a function of wall temperature, and the adiabatic or recovery temperature are of interest. In order to obtain the recovery temperature directly from the tests, it would have been necessary to extend the test durations until steady-state temperatures were achieved. An alternative method is to extrapolate the heat flux-wall temperature curve obtained from this analysis to zero heat flux. At this condition, wall temperature is equal to recovery temperature. An example of the transient thermal analysis and an extrapolation to obtain recovery temperature are shown in Figure IV-6.

Data from twenty tests were reduced to evaluate the effects of film coolant quantity, mixture ratio, chamber pressure and four different combinations of chamber and coolant sleeve geometry on chamber heat transfer. Data applicable to film-cooled adiabatic wall chamber design are shown in Figure IV-7. This plot shows the adiabatic chamber wall temperature from near the injector out to the nozzle exit for two quantities of fuel film coolant. These data are consistent with those obtained with the high pressure engine, where the shortest chamber also resulted in the highest throat temperatures and the temperature dropped downstream of the throat.

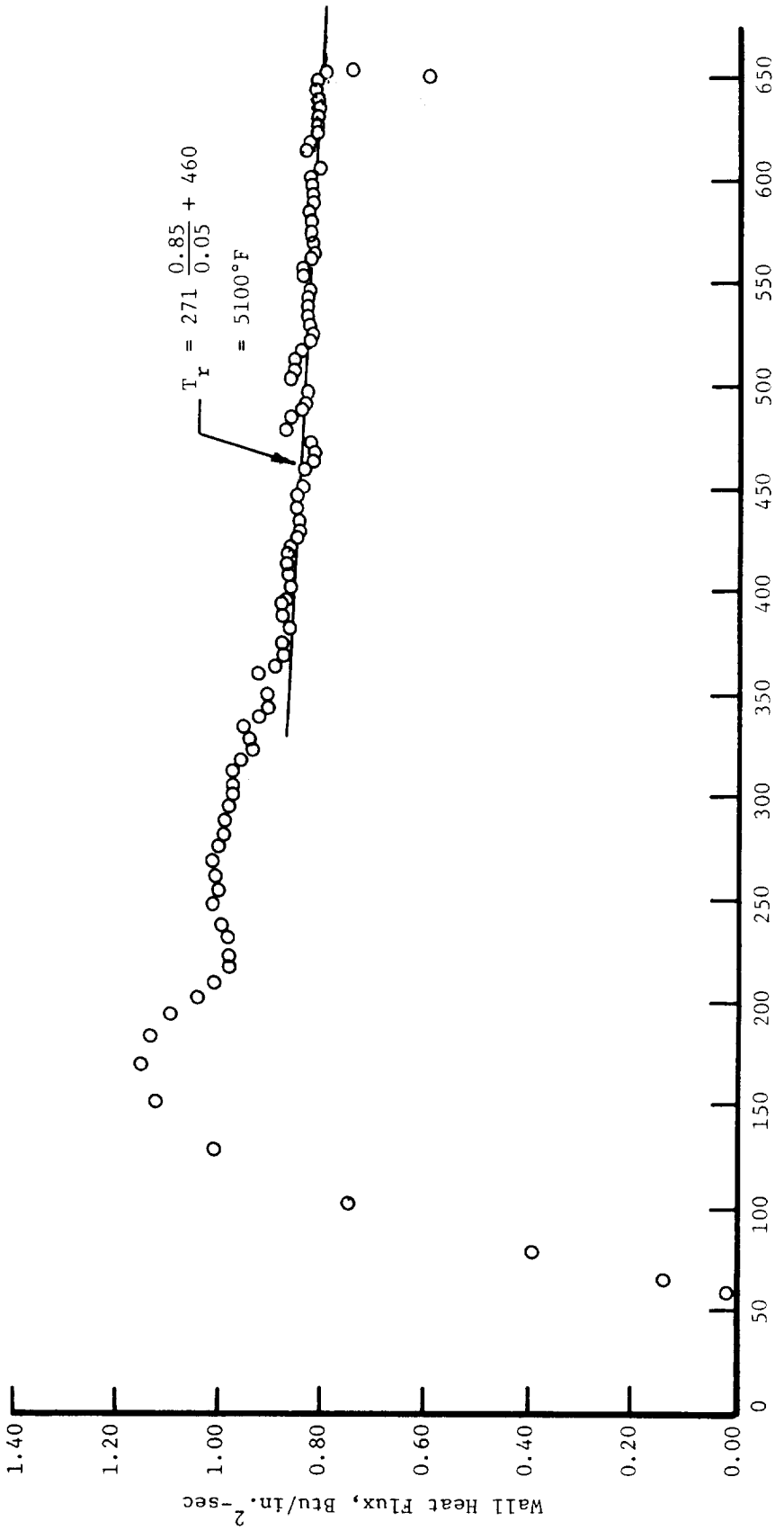

Low Pressure Thermal Data Reduction

Figure IV-6

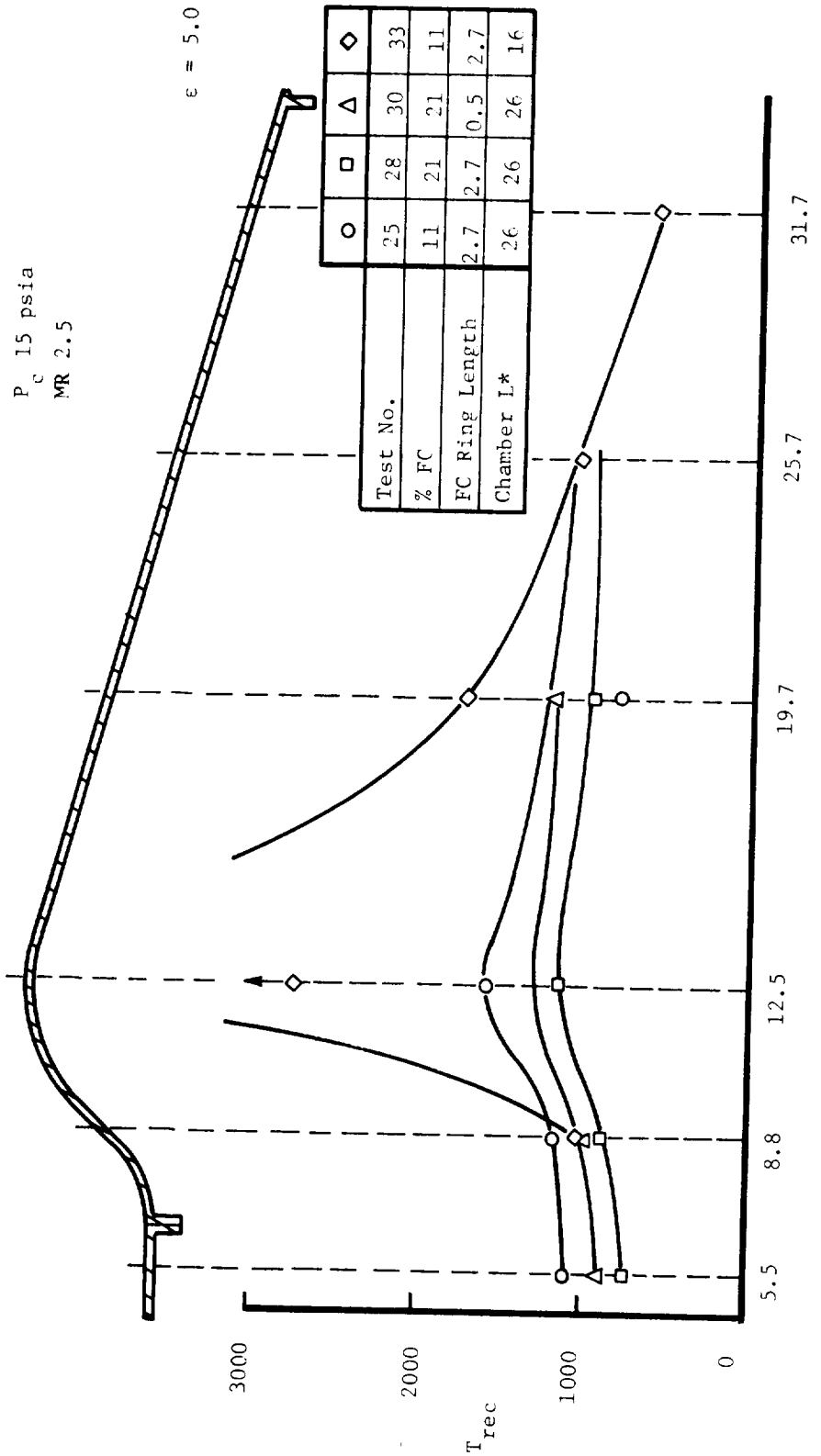

Low Pressure Chamber Heat Transfer

Figure IV-7

IV, A, Program Progress (Tasks XI Through XX) (cont.)

The preliminary conclusion reached is that it is possible to construct a film cooled chamber employing 10% of the fuel as coolant to operate with a peak chamber wall temperature of 1500°F. With 21% coolant the peak temperature can be reduced to 1200°F.

B. CURRENT PROBLEMS

No significant technical problems have been encountered.

C. WORK TO BE PERFORMED IN THE NEXT REPORT PERIOD

Effort during this period will be directed to completing test data analysis and preparation of a final report.

REFERENCES

1. R. L. Schact, R. J. Quentmeyer, W. L. Jones, "Experimental Investigation of Hot Gas-Side Heat Transfer Rates for a Hydrogen-Oxygen Rocket," NASA TN D-2832, Lewis Research Center, June 1965.

2. P. M. Moretti and W. M. Kays, "Heat Transfer to a Turbulent Boundary Layer with Varying Freestream Velocity and Varying Surface Temperature - An Experimental Study," Int J. Heat and Mass Transfer, Vol i, 1965, pp 1187-1202.

3. L. Schoenman, P. Block, "Laminar Boundary Layer Heat Transfer in Low-Thrust Rocket Nozzles," Journal of Spacecraft and Rockets, 5 (9), 1968, pp 1082-1089.

4. D. R. Boldman, H. E. Neumann, J. F. Schmidt, "Heat Transfer in 30° and 60° Half-Angle of Convergence Nozzles with Various Diameter Uncooled Pipe Inlet," NASA TN D-4177, Lewis Research Center, September 1967.

5. D. R. Boldman, J. F. Schmidt, and A. K. Gallagher, "Laminarization of a Turbulent Boundary Layer as Observed from Heat-Transfer and Boundary-Layer Measurements in Conical Nozzles," NASA TN D-4788, 1968.

6. L. H. Back, P. F. Massier, and R. F. Cuffel, "Flow Phenomena and Convective Heat Transfer in a Conical Supersonic Nozzle," J Spacecraft, Vol 4, No. 8, 1967, pp 1040-1047.

FORECAST AND CONSUMPTION OF GOVERNMENT-FURNISHED PROPELLANTS

Contract NAS 3-14354

Material	Monthly Usage	Cumulative	Next Month's Requirements	Next 3 Month Requirements
LO_2 (ton)	0	0	10	35
LH_2 (ton)	1930	3268	1300	9200
LN_2 (ton)	49	214	80	305
GHe (SCF), Bulk	0	99,100	0	25,000
GHe (SCF), Cylinders	0	0	2600	8500

NATIONAL AERONAUTICS AND SPACE ADMINISTRATION

Lewis Research Center

CONTRACT PROGRESS SCHEDULE

REPORT FOR MONTH ENDING: 30 March 1971

FORM APPROVED BUDGET BUREAU NO. 104-R0007

9. NASA Use Only

a. NASA CODE

b. PROJECT MGR.

c. EVALUATION DATE

d. EXCEPTION CATEGORY

e. | f. | g.

1. CONTRACT TITLE: Hydrogen-Oxygen APS Engines (High P_c)

2. CONTRACTOR (Name and address): Aerojet Liquid Rocket Co., P.O. Box 13222 Sacramento, California 95813

3. CONTRACT NO.: NAS 3-14354

4. APPROVED (Contractor's Project Manager): L. Thorman

PREPARATION DATE: 4-7-71

5. NASA APPROVED SCHEDULE DATE: 8-30-70

Task	6. REPORTING CATEGORY	7. 1970 J A S O N D / 1971 J F M A M J J	8. TECH. OBJECTIVE % COMP.
I	Injector Analysis and Design		100
II	Injector Fabrication		95
III	Thrust Chamber Analysis and Design		95
IV	Thrust Chamber Fabrication		60
V	Ignition System Analysis and Design		100
VI	Ignition System Fabrication and Checkout		100
VII	Bipropellant Valve Preparation		100
VIII	Injector Tests		100
IX	Thrust Chamber Cooling Tests		2
X	Pulsing Tests		1

NASA-C-63 (Rev. 1-68)

NASA APPROVED SCHEDULE

CONTRACTOR'S WORKING SCHEDULE

NATIONAL AERONAUTICS AND SPACE ADMINISTRATION

Lewis Research Center

CONTRACT PROGRESS SCHEDULE

REPORT FOR MONTH ENDING: 30 March 1971

FORM APPROVED BUDGET BUREAU NO: 104-R0007

9. NASA Use Only
a. NASA CODE
b. PROJECT MGR
c. EVALUATION DATE
d. EXCEPTION CATEGORY

1. CONTRACT TITLE: Hydrogen-Oxygen APS Engines (Low P_c)

2. CONTRACTOR (Name and address): Aerojet Liquid Rocket Company, P.O. Box 13222 Sacramento, California

3. CONTRACT NO.: NAS 3-14354 Amendment I

4. APPROVED (Contractor's Project Manager): A. A. Dare — PREPARATION DATE: 4-7-71

5. NASA APPROVED SCHEDULE DATE: 8-31-70

Task	6. REPORTING CATEGORY	8. TECH. OBJECTIVE % COMP.	e.	f.	g.
XI	Injector Analysis and Design	90			
XII	Injector Fabrication	90			
XIII	Thrust Chamber Analysis and Design	85			
XIV	Thrust Chamber Fabrication	40			
XV	Ignition System Analysis and Design	100			
XVI	Ignition System Fabrication and Checkout	75			
XVII	Bipropellant Valves Preparation	85			
XVIII	Injector Tests	50			
XIX	Thrust Chamber Cooling Tests	0			
XX	Pulsing Tests	0			

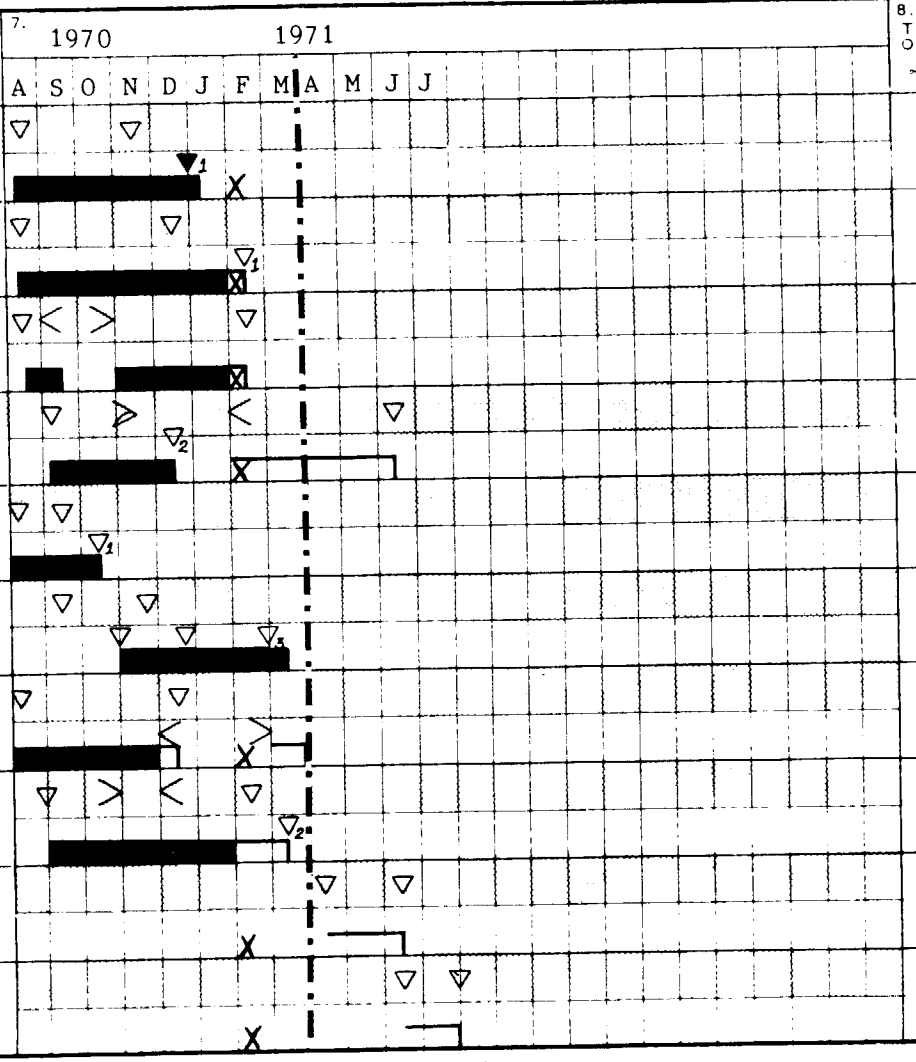

NASA-C-63 (Rev. 1-68)

NASA APPROVED SCHEDULE

CONTRACTOR'S WORKING SCHEDULE

X Indicates activities halted by stop work order dated 11 February 1971.

NATIONAL AERONAUTICS AND SPACE ADMINISTRATION

Lewis Research Center

CONTRACT PROGRESS SCHEDULE

REPORT FOR MONTH ENDING: 28 March 1971

FORM APPROVED BUDGET BUREAU NO: 104-R0007

9. NASA Use Only
a. NASA CODE
b. PROJECT MGR
c. EVALUATION DATE
d. EXCEPTION CATEGORY

1. CONTRACT TITLE: Hydrogen-Oxygen APS Engines

2. CONTRACTOR (Name and address): Aerojet Liquid Rocket Company, P.O. Box 13222 Sacramento, California 95813

3. CONTRACT NO.: NAS 3-14354

4. APPROVED (Contractor's Project Manager): R J Sobey

PREPARATION DATE: 4-10-71

5. NASA APPROVED SCHEDULE DATE: 8-31-70

Task: XXI

6. REPORTING CATEGORY	8. TECH. OBJECTIVE % COMP.	e.	f.	g.
Program Plan and Test Plans				
High P_c	50			
Low P_c	66			
Monthly Reports	63			
Quarterly Reports	75			
Final Report Draft	0			

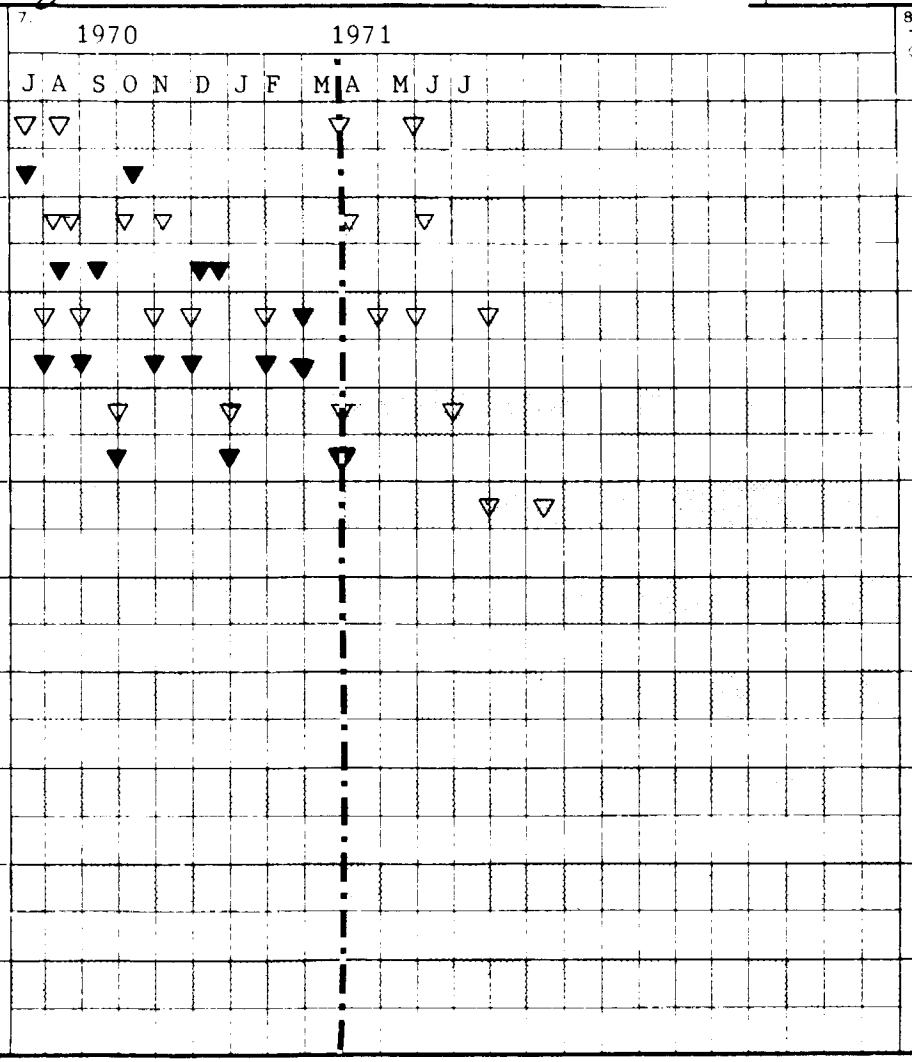

NASA-C-63 (Rev. 1-68)

NASA APPROVED SCHEDULE

CONTRACTOR'S WORKING SCHEDULE